

U-BENCH: A COMPREHENSIVE UNDERSTANDING OF U-NET THROUGH 100-VARIANT BENCHMARKING

Anonymous authors
Paper under double-blind review

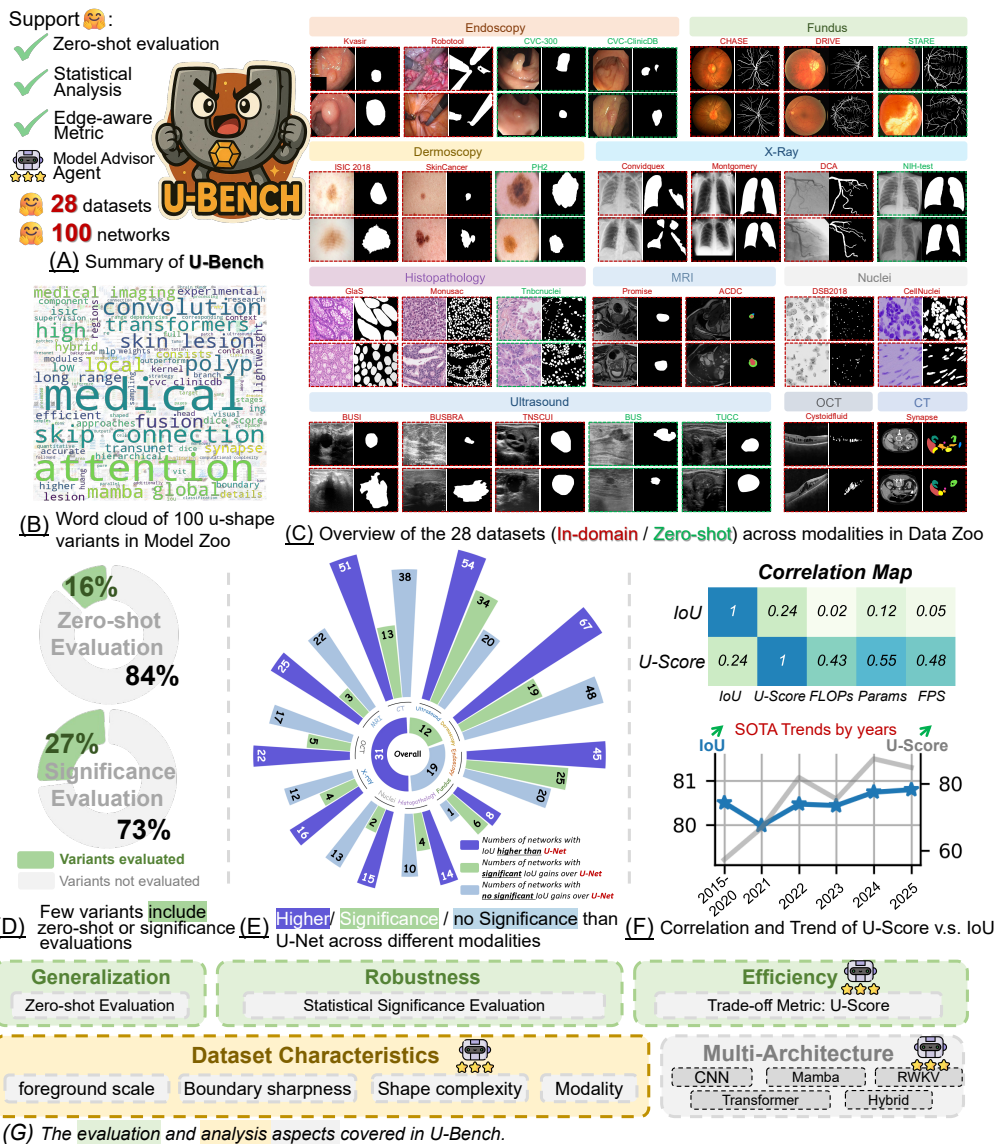


Figure 1: Overview of U-Bench. (A) The summary of U-Bench, which encompasses the most comprehensive large-scale evaluation of U-shaped architectures. (B) Word cloud of 100 published U-shaped variants in U-Bench Model Zoo. (C) Examples of the 28 datasets in U-Bench Data Zoo. The red / green box: in-domain / zero-shot split for evaluation. (D) Literature analysis. Among 100 recent works, 84% papers neglect zero-shot evaluation and 73% papers lack of statistical significance testing. (E) Significance analysis. Only a minority achieve statistically significant gains over U-Net. (F) Overview of a new metric, U-score. Top: IoU does not account for efficiency, while U-Score demonstrates a strong correlation with both segmentation performance and efficiency metrics. Bottom: while IoU shows a trend of saturation, U-Score highlights the yearly trends toward more efficient models. (G) The evaluation and analysis aspects covered in U-Bench.

ABSTRACT

Over the past decade, U-Net has been the dominant architecture in medical image segmentation, leading to the development of thousands of U-shaped variants. Despite its widespread adoption, there is still no comprehensive benchmark to systematically evaluate their performance and utility, largely because of insufficient statistical validation and limited consideration of efficiency and generalization across diverse datasets. To bridge this gap, we present U-Bench, the first large-scale, statistically rigorous 2D benchmark that evaluates 100 U-Net variants across 28 datasets and 10 imaging modalities. Our contributions are three-fold: (1) Comprehensive Evaluation: U-Bench evaluates models along three key dimensions: statistical robustness, zero-shot generalization, and computational efficiency. We introduce a novel metric, U-Score, which jointly captures the performance-efficiency trade-off, offering a deployment-oriented perspective on model progress. (2) Systematic Analysis and Model Selection Guidance: We summarize key findings from the large-scale evaluation and systematically analyze the impact of dataset characteristics and architectural paradigms on model performance. Based on these insights, we propose a model advisor agent to guide researchers in selecting the most suitable models for specific datasets and tasks. (3) Public Availability: We provide all code, models, protocols, and weights, enabling the community to reproduce our results and extend the benchmark with future methods. In summary, U-Bench not only exposes gaps in previous evaluations but also establishes a foundation for fair, reproducible, and practically relevant benchmarking in the next decade of U-Net-based segmentation models. The weights, datasets, and results will be released after the acceptance. Code is available at: <https://anonymous.4open.science/r/U-Bench>.

1 INTRODUCTION

Medical image segmentation is a critical and challenging task that can greatly enhance diagnostic efficiency by offering doctors objective and precise references for regions of interest (Zhou et al., 2017). Over the past decade, U-Net (Ronneberger et al., 2015) has become a cornerstone of medical image segmentation, thanks to its encoder-decoder structure with skip connections that effectively combine multi-scale features. Building on its promising segmentation results across diverse modalities, numerous U-shaped variants have been proposed to further improve performance, with lightweight designs (Valanarasu & Patel, 2022; Tang et al., 2024; Chen et al., 2024a; Valanarasu et al., 2021; Cao et al., 2022), attention mechanisms (Oktay et al., 2018; Tang et al., 2023), multi-scale feature fusion (Zhou et al., 2018; Huang et al., 2020), and more recently Mamba- (Liu et al., 2024a; Wu et al., 2025b), RWKV (Receptance Weighted Key Value)-based (Ye et al., 2025; Jiang et al., 2025), as well as hybrid architectures (Chen et al., 2021; Tang et al., 2025b; Dong et al., 2025; Tang et al., 2025a). Over the past decade, more than ten thousand U-Net variants have been proposed, and by 2025, nearly a thousand studies have employed U-shaped networks for medical image segmentation.

Among the vast number of U-Net variants, a central challenge remains unresolved: *How to conduct a fair and comprehensive comparison across them?* Although several benchmarks and surveys have attempted to organize this proliferation (Tab. 1), they mostly lack a large-scale, systematic evaluation. Critical aspects such as robustness of improvements, zero-shot generalization, and computational efficiency are often overlooked, and they also fail to provide complete and in-depth analyses of dataset-specific characteristics and model architectures. Despite reported gains in recent works, many studies report metrics without statistical validation (73% omit it, Fig. 1D), use incomplete baseline comparisons, or rely on limited dataset coverage. Moreover, efficiency, although vital for real-world clinical deployment (Vashist, 2017; Wenderott et al., 2024; Xu et al., 2025), is rarely considered. Compounding this issue, evaluations are typically confined to in-distribution settings (84% of work ignores zero-shot evaluation, Fig. 1D), even though clinical practice inevitably involves domain shifts across institutions and annotation protocols (Yan et al., 2019; Koch et al., 2024). These gaps leave the robustness and practicality of U-Net variants in real-world scenarios largely unverified (Niu et al., 2024).

Table 1: Comparisons between U-Bench and other medical image segmentation benchmarks. Details can be found in the Appendix B.

Category	Item	U-Bench (ours)	TorchStone (Bassi et al., 2024)	nnWNet (Zhou et al., 2025)	MedSegBench (Kuş & Aydin, 2024b)	nnU-Net Revisited (Isensee et al., 2024)
Models		100	19	20	6	19
Datasets		28	3	8	35	6
Modalities	Ultrasound	✓			✓	
	Dermoscopy	✓		✓	✓	
	Endoscopy	✓		✓	✓	
	Fundus	✓		✓	✓	
	X-Ray	✓			✓	
	Histopathology	✓			✓	
	CT	✓	✓	✓	✓	✓
	MRI	✓		✓	✓	✓
	Nuclei	✓			✓	✓
OCT	✓			✓		
Evaluation	Robustness	✓	✓	✓		✓
	Generalization	✓	✓			
	Efficiency	✓				
Architecture Analysis	CNN	✓	✓	✓	✓	✓
	Transformer	✓	✓	✓		✓
	Hybrid	✓	✓	✓	✓	✓
	Mamba	✓				✓
	RWKV	✓				✓
Dataset Analysis	Scale	✓				
	Boundary	✓				
	Shape	✓				

To systematically and comprehensively evaluate U-shaped medical image segmentation models, we introduce **U-Bench**, the first large-scale, statistically rigorous, and efficiency-oriented 2D benchmark for U-Net and its variants. U-Bench is built upon three key aspects: **(1) Broad dataset and model coverage:** we implement **100** recent U-Net variants and evaluate them on **28** benchmark datasets covering **10** diverse imaging modalities (ultrasound, dermoscopy, endoscopy, fundus photography, histopathology, nuclear imaging, X-ray, MRI, CT, and OCT; Fig. 1A, C). **(2) Rigorous and comprehensive evaluation:** all models are implemented to calculate performance gains over the baseline U-Net with statistical significance, ensuring robust and fair comparisons (Fig. 1E). To capture clinical utility, we further assess zero-shot generalization across modalities. Additionally, to address practical considerations in real-world edge deployment, we introduce the **U-Score**, a statistically grounded, large-scale metric that jointly accounts for accuracy, parameter numbers, computational cost, and inference speed (Fig. 1F). **(3) Public availability and reproducibility:** U-Bench implements models using official code implementations, pre-trained weights, and deep supervision strategies (if available). At the same time, U-Bench is released with all code, models, and protocols, enabling the community to reproduce our results and extend the benchmark with future methods.

Building on this large-scale evaluation, we identify key findings that challenge common assumptions. Traditional metrics like IoU show signs of saturation, offering a limited discriminative power (Fig. 1F). Additionally, reported improvements are often inconsistent or statistically insignificant (Fig. 1E). At the same time, an increasing focus on storage and computational cost is reflected in the rising trajectory of U-Score (Fig. 1F). To explore these dynamics, we conduct a systematic analysis of U-Net variants, examining the influence of dataset and architectural factors on model performance across different modalities, architectures, and computational resource limitations (Fig. 1G). Building on these analyses, we introduce a model advisor agent that suggests suitable architectures based on dataset and task attributes, turning an actionable guidance for practitioners in clinical and research contexts.

Our contribution can be summarized as:

- We provide a comprehensive evaluation benchmark of 100 U-shaped variants across 28 datasets from 10 modalities with a rigorous assessment across statistical robustness, zero-shot generalization, and computational efficiency. To better capture the trade-off between accuracy and efficiency, we introduce U-Score, a novel metric grounded in large-scale statistical analysis that enables fair and holistic evaluation.
- We summarize the observations over large-scale evaluation: Most variants show performance gains, but few show in-domain statistical significance over the original U-Net. Zero-shot performances show significant and promising improvements. U-Score shows

an increasing trajectory, indicating the shift from purely pursuing accuracy to balancing accuracy with efficiency.

- We disentangle different aspects, including dataset characteristics and architectural designs, revealing their impact on performance and efficiency, and further build a model recommender that helps researchers identify well-suited architectures under diverse data and resource conditions.
- We open-source U-Bench and all the pretrained weights, providing a large-scale benchmark with comprehensive evaluation for medical image segmentation, to foster fair, robust, generalizable, and efficient research in the community.

2 U-BENCH CONSTRUCTION

2.1 PRELIMINARIES: U-SHAPED DESIGN

A U-shaped model generally comprises four components: hierarchical encoder, decoder, bottleneck, and skip-connection. Given an input image $x \in \mathbb{R}^{3 \times H \times W}$, $\text{Encoder}(\cdot)$ extracts multi-scale features f_i by N stages from up-bottom, denoted as $\{f_i\}_{i=1}^N, f_i \in \mathbb{R}^{C_i \times \frac{H}{2^{(i-1)}} \times \frac{W}{2^{(i-1)}}}$. $\text{Bottleneck}(\cdot)$ processes the last output feature, and $\text{Decoder}(\cdot)$ is composed of $N - 1$ stages for upsampling decoder features d_j from bottom-up, each stage comprises $\text{Skip-connection}(\cdot)$ for feature fusion. Final prediction \hat{x} is produced by the segmentation head after the top decoder stage. The differences across variants are illustrated in Fig. 2: **Convolutional Neural Networks (CNNs) and related architectures (Attention, Mamba, RWKV) form the core building blocks, which can be organized in pure CNN / Attention, parallel, or sequential configurations for both encoding and decoding. Detailed categorization can be found in the Appendix B and D.**

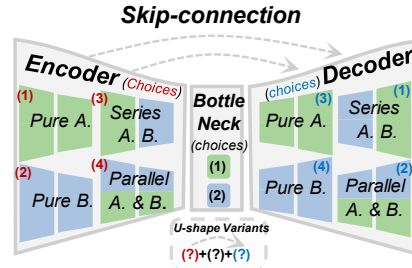


Figure 2: **Summary of U-shaped networks.** The network comprises an encoder, a bottleneck, and a decoder with skip-connection, each of which can integrate attention gates and multi-scale fusion. The blue and green blocks represent different core building blocks, which can be integrated sequentially, in parallel, or used individually.

2.2 DATASET AND MODEL ZOO

Dataset Zoo. As shown in Fig. 1(C), the U-Bench dataset zoo consists of 28 diverse publicly available 2D medical image segmentation datasets spanning a wide range of imaging modalities, including ultrasound, dermoscopy, endoscopy, fundus photography, histopathology, nuclear imaging, X-ray, MRI, CT, and OCT. We train on 20 datasets and evaluate zero-shot generalization on 8 additional ones. Following prior work (Chen et al., 2021; Tang et al., 2025b; Valanarasu & Patel, 2022; Jiang et al., 2025; Wang et al., 2022a), all datasets are resized to 256×256 and augmented by random rotation and flipping; for models with fixed input size, we keep their original resolution (typically 224×224). Official splits are used when available; otherwise, a 7/3 split is applied. All details on datasets and preprocessing are provided in the Appendix C.

Model Zoo. We curate a collection of 100 publicly available and widely adopted U-Net variants, covering CNN-, Transformer-, Mamba-, and RWKV-based architectures, as well as their hybrid designs (Fig. 1(B)). To ensure strict reproducibility and fair comparison, we follow the official implementations for all models, adopting their predefined settings, pretrained weights, and deep supervision strategies when available. All model details are provided in the Appendix D.

2.3 EVALUATION PROTOCOL

Evaluation Metrics. Following previous works (Luo et al., 2025; Jiang et al., 2025; Tang et al., 2025b; Valanarasu & Patel, 2022; Tang et al., 2024), we evaluate segmentation performance using Intersection over Union (IoU). We also report the commonly used performance metrics, including Dice coefficient, and boundary evaluation metrics HD95 and Boundary-F1 in Appendix. To evaluate the statistical significance of performance differences between models, we conduct paired sample

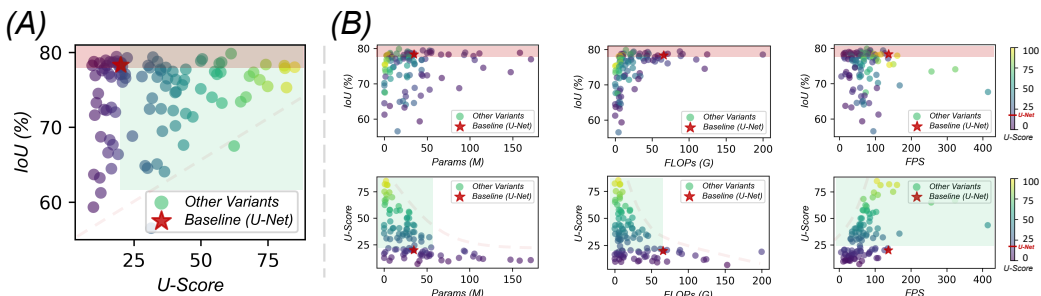


Figure 3: **Comparison between IoU and U-Score.** Red rectangle indicates the models perform better than U-Net in IoU, and green rectangle indicates the models perform better than U-Net in U-Score. (A) Across 100 variants, few methods show better IoU compared to baseline U-Net, while more than half of the methods show better U-Score. (B) The relationship between performance (IoU) and the increase in computational resources (FLOPs, parameters, FPS) is complex, whereas U-Score offers a clear distribution that effectively distinguishes favorable and unfavorable accuracy-efficiency trade-off.

t-tests, comparing each variant to the baseline U-Net. U-Bench also considers computational efficiency metrics, including Parameters (M), FLOPs (G), and FPS. All result details are provided in the Appendix D.

Zero-shot Evaluation. To evaluate the generalization capability of each model beyond the training distribution, we conduct zero-shot inference on unseen datasets within the same modality and task. Specifically, models are trained on source datasets and then directly evaluated on unseen datasets that share the same modality but differ in acquisition domain. Detailed dataset split can be found in Fig. 1(C). This approach aligns with clinical demands, where domain shifts frequently occur in real-world applications due to variations in devices, institutions, and patient populations.

U-Score. To assess real-world deployability, we propose U-Score, a unified metric that jointly accounts for accuracy and efficiency. For each model i , we compute segmentation accuracy evaluated by IoU A_i , parameter P_i , FLOPs G_i , and FPS S_i , which are percentile-normalized into $a_i, p_i, g_i, s_i \in [0, 1]$ using the 10-th/90-th quantiles across the model zoo. Given a harmonic mean function $\mathcal{H}(\cdot)$ with equal weights for each input, an efficiency subscore $\text{Eff}_i = \mathcal{H}(p_i, g_i, s_i)$ is obtained, ensuring that no single factor dominates. The final U-Score is defined as $\text{U-Score}_i = \mathcal{H}(a_i, \text{Eff}_i)$ to incorporate segmentation accuracy and computational efficiency equally. This combination rewards models that achieve favorable accuracy-efficiency trade-offs and provides a deployment-oriented alternative to IoU. For example, although some models surpass U-Net in segmentation accuracy, they require substantially different levels of computational overhead, making direct comparisons with the baseline difficult. Additionally, we conduct extensive sensitivity analysis of U-Score covering the accuracy-efficiency trade-off, efficiency component weights, and normalization percentiles. More details of U-Score and sensitivity analysis can be found in Appendix E.

3 U-BENCH RESULTS & DISCUSSION

In this section, we present the results of the U-Bench benchmark across multiple dimensions, including accuracy, efficiency, and generalization. We organize the results as follows: In 3.1, we present and discuss retrospective analysis of the develop trends and statistical findings over 100 variants spanning different architectures and publication years. In 3.2, we disentangle influence factors into two aspects: dataset and architecture, and analyze how these factors impact model performance. In 3.3, we propose our ranking-based advisor agent, offering practical guidance for selecting optimal models based on dataset characteristics and resource constraints.

3.1 RETROSPECTIVE ANALYSIS OF THE PAST DECADE

Finding 1: In-domain Top-1 performance has marginal gains in segmentation accuracy, while zero-shot improves more pronouncedly. We analyzed 100 variants across different architectures

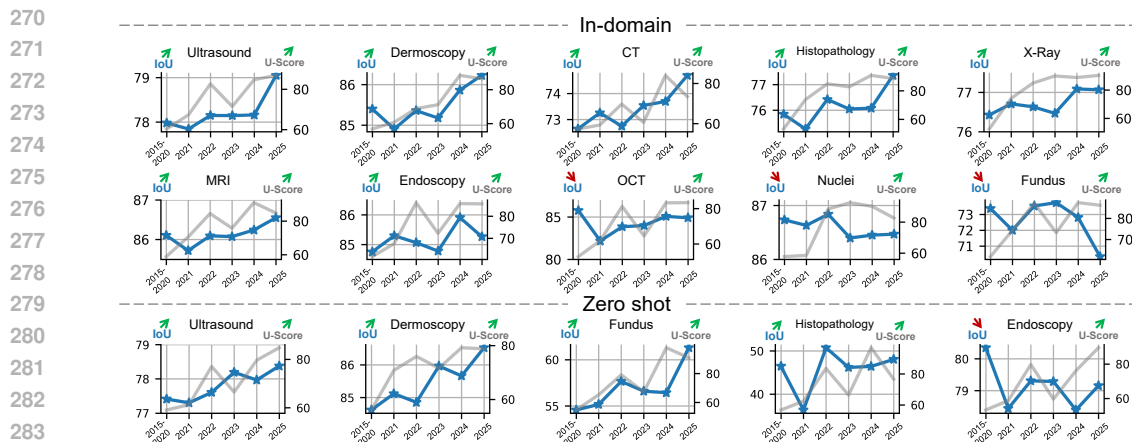


Figure 4: Performance trends of SOTA models over the past decade. The x-axis indicates publication year, with each point marking the yearly best result. The y-axes report two evaluation metrics: IoU (left axis) and U-Score (right axis). The trend’s summary is shown as arrows at the top of the y-axis, with green ones highlighting improvements and red ones indicating stagnation. Source domain performance is shown at the top, and zero-shot performance is shown at the bottom.

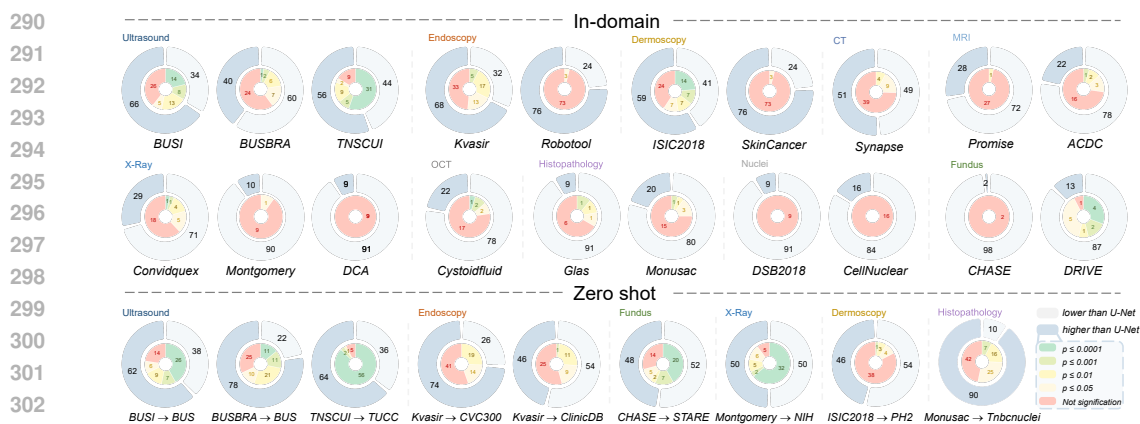


Figure 5: Statistical significance analysis on the IoU against U-Net across 28 datasets across 10 modalities. The outer blue pie represents the number of variants surpassing U-Net; the inner pie quantifies the statistical significance of the methods with improvements, annotated by non-significant to highly significant, with the number of works annotated in the middle. In general, in-domain improvements show limited statistical significance, while zero-shot performances show more significant improvements.

and publication years (the detailed list can be found in the Appendix B of Fig. 9), reporting the best-performing variant for each year, as shown in Fig. 4. Over the past decade, 70% of modalities have demonstrated steady progress of segmentation accuracy in both source and target domains, as reflected in IoU. However, IoU gains have been marginal (on average 1%-2%) and inconsistent. Some modalities (*i.e.* OCT, Nuclei, and Fundus) even show a sign of stagnation. In comparison, when considering zero-shot performances, the improvements have been more obvious (more than 3% on average) in 80% of the modalities.

Finding 2: Although some in-domain improvements exist on average, few reach statistical significance, whereas the average zero-shot improvements remain consistently significant. To rigorously distinguish modalities with genuine improvements from those with only numerical fluctuations, we perform *t*-tests between each variant and the U-Net baseline. The results are presented in Fig. 1(E) and Fig. 5. We observe that over 80% of variants fail to achieve statistically significant improvements. Even in the most heavily studied modalities, such as Ultrasound, Endoscopy, Dermoscopy, CT, and MRI, most gains are marginal and lack significance. Only a handful of datasets (*e.g.*, BUSI, TNSCUI, Kvasir, ISIC2018, Convidquex) exhibit consistent clusters of superior vari-

Table 2: **Top-10 variants ranked by performance (IoU) and efficiency (U-Score) under in-domain and zero-shot settings.** Variants cover CNN, Transformer, Mamba, RWKV, and Hybrid architectures.

In-domain (IoU)		Zero-shot (IoU)		In-domain (U-Score)		Zero-shot (U-Score)	
Rank	Variants	Rank	Variants	Rank	Variants	Rank	Variants
#1	RWKV-UNet	#1	RWKV-UNet	#1	LGMSNet	#1	LGMSNet
#2	nnUNet	#2	G-CASCADE	#2	MBSNet	#2	LV-UNet
#3	AURA-Net	#3	Swin-umamba	#3	CMUNeXt	#3	U-KAN
#4	UTANet	#4	MADGNet	#4	LV-UNet	#4	Mobile U-ViT
#5	ResEncUNet-L	#5	CASCADE	#5	Mobile U-ViT	#5	RWKV-UNet
#6	MADGNet	#6	MFMSNet	#6	Tinyunet	#6	MBSNet
#7	Swin-umamba	#7	TransResUNet	#7	U-RWKV	#7	SwinUNETR
#8	MFMSNet	#8	DS-TransUNet	#8	U-KAN	#8	CMUNeXt
#9	TransResUNet	#9	CENet	#9	DCSAU-Net	#9	G-CASCADE
#10	EViT-UNet	#10	PraNet	#10	RWKV-UNet	#10	TA-Net
#25	U-Net	#11	ResEncUNet-L	#24	ResEncUNet-L	#32	ResEncUNet-L
		#24	nnUNet	#25	nnUNet	#33	nnUNet
		#72	U-Net	#64	U-Net	#69	U-Net

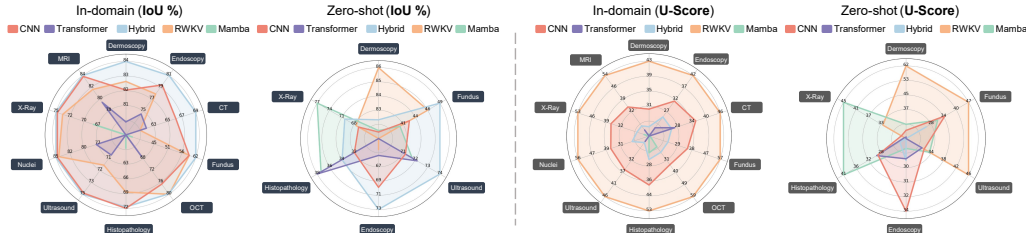


Figure 6: **Average performance of different architectures across modalities under in-domain and zero-shot settings.** Left: IoU-based comparison; Right: U-Score-based comparison of different architecture strengths in source-domain and zero-shot.

ants. In contrast, in experiments with zero-shot transfer, for variants that outperform U-Net, more than 50% of the variants are significant across 75% of the modalities.

Possible explanations for findings 1 & 2: We provide a possible explanation for these interesting observations. Considering in-domain evaluations, the improvements with statistical significance are typically associated with the lesion localization tasks which requires global semantic comparison. Specifically, lesions often exhibit significant differences from surrounding normal tissues, requiring a global context to model these distinctions (Zhou et al., 2017; Isensee et al., 2021). In recent years, with the growing adoption of long-range modeling techniques (e.g., attention-based Transformers, state-space models such as Mamba, and RNN-inspired hybrids like RWKV), architectural innovations have increasingly focused on capturing long-range dependencies, leading to more pronounced and steady improvements in these lesion segmentation tasks. On the other hand, long-range modeling techniques have been proven to be more generalizable (Jiang et al., 2024a; Harun et al., 2024; Hou et al., 2025; Gu et al., 2024), leading to improvements in zero-shot generalization ability. By contrast, modalities dominated by repetitive local patterns (e.g., Nuclei, Fundus) benefit far less from global modeling, exhibiting only marginal improvements. This underscores the complementary need for localized mechanisms to achieve precise boundary delineation.

Finding 3: Increasing attention on efficiency. We report the IoU and U-Score for all models with Parameter, FLOPs, and FPS, as shown in Fig. 3 and Fig 1(F). While IoU shows marginal improvements, suggesting a saturation point, illustrating that performance is no longer the key bottleneck in medical segmentation tasks, U-Score improvements are more pronounced, with an average increase of 33%. The increasing trend of U-Score reflects the growing emphasis and room for improvement on efficient models in the medical community, echoing the practical demand for clinical deployment beyond the lab research.

378
379
380
381
382
383
384
385
386
387
388
389
390
391
392
393
394
395
396
397
398
399
400
401
402
403
404
405
406
407
408
409
410
411
412
413
414
415
416
417
418
419
420
421
422
423
424
425
426
427
428
429
430
431

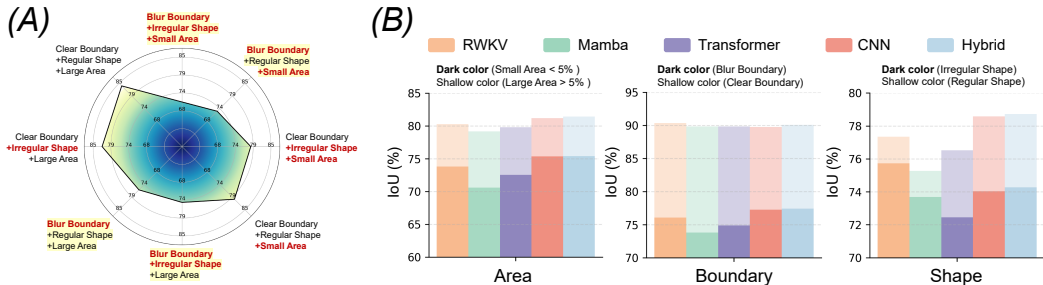


Figure 7: **Performance analysis under varying foreground properties.** (A) Foreground properties influence segmentation task difficulty. The yellow background indicates the challenge segmentation case. (B) Architectural influence on segmentation difficulty across diverse foreground properties. Dark / Shallow: hard / easy case.

3.2 INFLUENCING FACTOR ANALYSIS: ARCHITECTURES AND DATA CHARACTERISTICS

3.2.1 ARCHITECTURES

To analyze the performance regarding architectural choices, we divide 100 models into five families: **CNN**, **Transformer**, **Mamba**, **RWKV**, and **Hybrid**. The detailed descriptions are summarized in Appendix D. We present the top-10 variants across all datasets ranked by IoU and U-Score under in-domain and zero-shot settings, as shown in Tab. 2, and we calculate the average performance of each architecture family, as shown in Fig. 6.

Considering segmentation performance (IoU), **Hybrid** architectures achieve the highest accuracy by combining local priors with global attention. As shown in Tab. 2(Left), 5 of the top 10 models in both in-domain and zero-shot are hybrid, highlighting their high potential. On average, the hybrid family consistently delivers the best in-domain performance and competitive zero-shot generalization (Fig. 6(Left)), particularly excelling on lesion-centric tasks such as Ultrasound and Endoscopy. The newly proposed **RWKV** family ranks first in IoU for both in-domain and zero-shot evaluations, indicating promising potential despite limited prior research. In contrast, **Mamba** family shows weaker segmentation performance, which may be attributed to its architectural design, which, despite its strengths in certain tasks, might struggle with capturing fine-grained details or handling complex patterns in segmentation tasks.

Once computational demands are taken into account, as shown in Tab. 2(Right), the U-Score-based leaderboard is reshuffled, with the **CNN** family leading in performance, comprising 7 / 5 out of the top 10 models in in-domain / zero-shot settings, respectively. The newly proposed **RWKV** family achieves the best average in-domain results and competitive zero-shot performance (Fig. 6(Right)), further supporting its structural superiority and potential. In contrast, inefficient long-range modeling methods, including **Transformer**, and **Hybrid** architectures, face higher computational demands, leading to reduced performance when evaluated by U-Score. Although **Mamba** excels in efficiency, its inconsistent accuracy undermines the U-Score, offsetting its efficiency advantage.

3.2.2 DATA CHARACTERISTICS

We further investigate how performances vary with distinct foreground characteristics with three aspects: foreground scale, boundary sharpness, and shape complexity. The Appendix F.1 provides detailed definitions for the different scales of target area, edge, and shape regularity.

Figure 7(A) summarizes the characteristics of challenging cases: blurry boundaries are the dominant factor, with often causing substantial drops in segmentation performance, while small object size and irregular shapes further exacerbate the difficulty. When these foreground properties shift across datasets, different models exhibit varying performance patterns. As shown in Fig. 7(B), consistent with our earlier findings, hybrid architectures dominate both in easier and more challenging cases, proving that local and global fusion mechanism enables greater adaptability across diverse foreground properties, particularly for blurry boundaries. RWKV-based models show specific strength in capturing irregular but well-defined shapes, reflecting their ability to model long-range contours.

Nonetheless, boundary ambiguity, along with small and irregular targets, remains the central challenge; given its prevalence in medical images, uncertainty-aware designs are needed. Since architectural strengths are dataset-dependent, these observations highlight the importance of task-aware advising mechanisms that can match models to dataset properties.

3.3 MODEL ADVISOR AGENT

Based on our analysis, we introduce a ranking-based model advisor agent, designed to guide the community in selecting the most suitable models based on dataset characteristics and task requirements. This tool not only streamlines model selection but also helps users navigate the trade-offs between performance and efficiency, ensuring more informed, task-aware decisions.

The system overview is shown in Fig. 8. Our advisor agent system utilizes dataset-level characteristics (e.g., modality, boundary sharpness, shape complexity, and foreground scale) along with resource constraints (storage, computation, and speed) to predict the suitability of various U-shaped architectures. Rather than relying on a manual trial-and-error approach, our framework leverages XGBoost (Chen & Guestrin, 2016) as the recommended backbone and outputs candidate models and architectures that best satisfy the specified requirements. Crucially, the output is not a single “best” model but a prioritized list, offering more flexibility in choices to practitioners. Further details on the recommendation setup, dataset construction, implementation details, and evaluation metrics are provided in the Appendix F.2 and F.3.

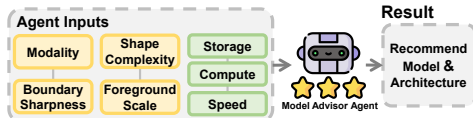


Figure 8: Our model advisor agent.

We design a set of experiments to validate the feasibility of automatic model suggestion in medical image segmentation. Our setup uses 18 in-domain datasets for training and holds out 2 datasets for validation. We use Normalized Discounted Cumulative Gain (NDCG), mean average precision (MAP) and Spearman correlation for evaluation (See Appendix F.3). As shown in Tab. 3, our experiments demonstrate that the proposed model advisor agent effectively recovers ranking orders that align with ground-truth IoU and U-Score rank in our benchmark. The results validate that our advisor agent system is able to prioritize suitable models across different task requirements, making it a reliable tool for model selection and deployment.

Table 3: NDCG, MAP, and Spearman correlation of our advisor agent.

Ranking Metric	NDCG		MAP	Spearman
	@5	@20		
IoU	0.75	0.76	0.24	0.36
U-Score	0.74	0.79	0.43	0.52

4 CONCLUSION

Conclusion. A key challenge in the field of medical image segmentation remains: How can we conduct a fair and comprehensive comparison across the numerous U-shaped variants? To address this, we introduce U-Bench, a framework that fills critical gaps in prior evaluations by offering a comprehensive, statistically rigorous, and efficiency-oriented approach. Our results challenge common assumptions in the field, revealing that while many variants show performance gains, few achieve statistical significance in-domain. In contrast, zero-shot generalization demonstrates substantial improvements, highlighting the potential for better model generalization across domains. Additionally, the newly proposed U-Score metric, which emphasizes efficiency alongside performance, signals a paradigm shift from models focused solely on accuracy to those that balance both performance and computational efficiency. Leveraging insights from our analysis of model architecture and dataset characteristics, we propose a ranking-based model recommender that transforms our large-scale evaluation into actionable guidance for selecting models tailored to specific tasks. By releasing U-Bench as an open-source platform, we provide the community with a robust, reproducible tool to advance research in medical image segmentation, enabling the development of models that are both accurate and computationally feasible for clinical deployment.

Future Work. In future work, we aim to incorporate clinical perspectives in evaluating the trade-off between segmentation performance and computational efficiency. This could help guide the development of a clinical-driven metric to better align with real-world clinical needs.

REFERENCES

- 486
487
488 Walid Al-Dhabyani, Mohammed Gomaa, Hussien Khaled, and Aly Fahmy. Dataset of breast ultra-
489 sound images. *Data in brief*, 28:104863, 2020.
- 490 Alyaa Amer and Xujiong Ye. Mca-unet: A multiscale context aggregation u-net for the segmentation
491 of covid-19 lesions from ct images. *Computer Methods and Programs in Biomedicine Update*, 4:
492 100114, 2023.
- 493 Reza Azad, Mohammad T Al-Antary, Moein Heidari, and Dorit Merhof. Transnorm: Transformer
494 provides a strong spatial normalization mechanism for a deep segmentation model. *IEEE Access*,
495 10:108205–108215, 2022.
- 496 Reza Azad, René Arimond, Ehsan Khodapanah Aghdam, Amirhossein Kazerouni, and Dorit Mer-
497 hof. Dae-former: Dual attention-guided efficient transformer for medical image segmentation. In
498 *International workshop on predictive intelligence in medicine*, pp. 83–95. Springer, 2023.
- 499 Pedro RAS Bassi, Wenxuan Li, Yucheng Tang, Fabian Isensee, Zifu Wang, Jieneng Chen, Yu-Cheng
500 Chou, Yannick Kirchhoff, Maximilian R Rokuss, Ziyang Huang, et al. Touchstone benchmark: Are
501 we on the right way for evaluating ai algorithms for medical segmentation? *Advances in Neural*
502 *Information Processing Systems*, 37:15184–15201, 2024.
- 503 Jorge Bernal, F Javier Sánchez, Gloria Fernández-Esparrach, Debora Gil, Cristina Rodríguez, and
504 Fernando Vilariño. Wm-dova maps for accurate polyp highlighting in colonoscopy: Validation
505 vs. saliency maps from physicians. *Computerized medical imaging and graphics*, 43:99–111,
506 2015.
- 507 Olivier Bernard, Alain Lalonde, Clement Zotti, Frederick Cervenansky, Xin Yang, Pheng-Ann Heng,
508 Irem Cetin, Karim Lekadir, Oscar Camara, Miguel Angel Gonzalez Ballester, et al. Deep learning
509 techniques for automatic mri cardiac multi-structures segmentation and diagnosis: is the problem
510 solved? *IEEE transactions on medical imaging*, 37(11):2514–2525, 2018.
- 511 Fares Bougourzi, Fadi Dornaika, Cosimo Distanti, and Abdelmalik Taleb-Ahmed. D-trattunet: To-
512 ward hybrid cnn-transformer architecture for generic and subtle segmentation in medical images.
513 *Computers in Biology and Medicine*, 176:108590, 2024.
- 514 Nhat-Tan Bui, Dinh-Hieu Hoang, Quang-Thuc Nguyen, Minh-Triet Tran, and Ngan Le. Meganet:
515 Multi-scale edge-guided attention network for weak boundary polyp segmentation. In *Proceed-*
516 *ings of the IEEE/CVF Winter Conference on Applications of Computer Vision*, pp. 7985–7994,
517 2024.
- 518 Hu Cao, Yueyue Wang, Joy Chen, Dongsheng Jiang, Xiaopeng Zhang, Qi Tian, and Manning Wang.
519 Swin-unet: Unet-like pure transformer for medical image segmentation. In *European conference*
520 *on computer vision*, pp. 205–218. Springer, 2022.
- 521 Bingzhi Chen, Yishu Liu, Yingjian Li, Zheng Zhang, Guangming Lu, and Adams Wai Kin Kong.
522 Transattunet: Multi-level attention-guided u-net with transformer for medical image segmen-
523 tation. *IEEE Transactions on Instrumentation & Measurement*, 2022.
- 524 Gongping Chen, Lu Zhou, Jianxun Zhang, Xiaotao Yin, Liang Cui, and Yu Dai. Esknet: An en-
525 hanced adaptive selection kernel convolution for ultrasound breast tumors segmentation. *Com-*
526 *puter Methods and Programs in Biomedicine*, 226:107086, 2023.
- 527 Jieneng Chen, Yongyi Lu, Qihang Yu, Xiangde Luo, Ehsan Adeli, Yan Wang, Le Lu, Alan L Yuille,
528 and Yuyin Zhou. Transunet: Transformers make strong encoders for medical image segmentation.
529 *arXiv preprint arXiv:2102.04306*, 2021.
- 530 Junren Chen, Rui Chen, Wei Wang, Junlong Cheng, Lei Zhang, and Liangyin Chen. Tinyu-net:
531 Lighter yet better u-net with cascaded multi-receptive fields. In *Medical Image Computing and*
532 *Computer-Assisted Intervention (MICCAI)*. Springer, 2024a.
- 533 Tianqi Chen and Carlos Guestrin. Xgboost: A scalable tree boosting system. In *Proceedings of the*
534 *22nd acm sigkdd international conference on knowledge discovery and data mining*, pp. 785–794,
535 2016.

- 540 Tianxiang Chen, Xudong Zhou, Zhentao Tan, Yue Wu, Ziyang Wang, Zi Ye, Tao Gong, Qi Chu,
541 Nenghai Yu, and Le Lu. Zig-rir: Zigzag rwkv-in-rwkv for efficient medical image segmentation.
542 *IEEE Transactions on Medical Imaging*, 2025.
- 543 Yifei Chen, Binfeng Zou, Zhaoxin Guo, Yiyu Huang, Yifan Huang, Feiwei Qin, Qin Hai Li, and
544 Changmiao Wang. Scunet++: Swin-unet and cnn bottleneck hybrid architecture with multi-fusion
545 dense skip connection for pulmonary embolism ct image segmentation. In *Proceedings of the*
546 *IEEE/CVF winter conference on applications of computer vision*, pp. 7759–7767, 2024b.
- 547 Noel CF Codella, David Gutman, M Emre Celebi, Brian Helba, Michael A Marchetti, Stephen W
548 Dusza, Aadi Kalloo, Konstantinos Liopyris, Nabin Mishra, Harald Kittler, et al. Skin lesion anal-
549 ysis toward melanoma detection: A challenge at the 2017 international symposium on biomedical
550 imaging (isbi), hosted by the international skin imaging collaboration (isic). In *ISBI 2018*, pp.
551 168–172. IEEE, 2018.
- 552 Ethan Cohen and Virginie Uhlmann. aura-net: Robust segmentation of phase-contrast microscopy
553 images with few annotations. In *2021 IEEE 18th International Symposium on Biomedical Imag-*
554 *ing (ISBI)*, pp. 640–644. IEEE, 2021.
- 555 Yunjiao Deng, Hui Wang, Yulei Hou, Shunpan Liang, and Daxing Zeng. Lfu-net: A lightweight
556 u-net with full skip connections for medical image segmentation. *Current Medical Imaging*, 19:
557 347–360, 2023.
- 558 Binh-Duong Dinh, Thanh-Thu Nguyen, Thi-Thao Tran, and Van-Truong Pham. 1m parameters are
559 enough? a lightweight cnn-based model for medical image segmentation. In *2023 Asia Pacific*
560 *Signal and Information Processing Association Annual Summit and Conference (APSIPA ASC)*,
561 pp. 1279–1284. IEEE, 2023.
- 562 Bo Dong, Wenhai Wang, Deng-Ping Fan, Jinpeng Li, Huazhu Fu, and Ling Shao. Polyp-pvt: Polyp
563 segmentation with pyramid vision transformers. *arXiv preprint arXiv:2108.06932*, 2021.
- 564 Chengqi Dong, Fenghe Tang, Rongge Mao, Xinpei Gao, and S Kevin Zhou. Lgmsnet: Thin-
565 ning a medical image segmentation model via dual-level multiscale fusion. *arXiv preprint*
566 *arXiv:2508.15476*, 2025.
- 567 Alexey Dosovitskiy, Lucas Beyer, Alexander Kolesnikov, Dirk Weissenborn, Xiaohua Zhai, Thomas
568 Unterthiner, Mostafa Dehghani, Matthias Minderer, Georg Heigold, Sylvain Gelly, et al. An
569 image is worth 16x16 words: Transformers for image recognition at scale. *arXiv preprint*
570 *arXiv:2010.11929*, 2020.
- 571 Deng-Ping Fan, Ge-Peng Ji, Tao Zhou, Geng Chen, Huazhu Fu, Jianbing Shen, and Ling Shao.
572 Pranel: Parallel reverse attention network for polyp segmentation. In *Medical Image Computing*
573 *and Computer-Assisted Intervention*, pp. 263–273. Springer, 2020.
- 574 Muhammad Moazam Fraz, Paolo Remagnino, Andreas Hoppe, Bunyarit Uyyanonvara, Alicja R.
575 Rudnicka, Christopher G. Owen, and Sarah A. Barman. Chase db1: Retinal vessel reference
576 dataset, 2012. URL <https://researchdata.kingston.ac.uk/96/>.
- 577 Yunhe Gao, Mu Zhou, and Dimitris N Metaxas. Utnet: a hybrid transformer architecture for medical
578 image segmentation. In *International conference on medical image computing and computer-*
579 *assisted intervention*, pp. 61–71. Springer, 2021.
- 580 Yunhe Gao, Mu Zhou, Di Liu, Zhennan Yan, Shaoting Zhang, and Dimitris N. Metaxas. A data-
581 scalable transformer for medical image segmentation: Architecture, model efficiency, and bench-
582 mark. *arXiv preprint arXiv:2203.00131*, 2023.
- 583 Wilfrido Gómez-Flores, Maria Julia Gregorio-Calas, and Wagner Coelho de Albuquerque Pereira.
584 Bus-bra: a breast ultrasound dataset for assessing computer-aided diagnosis systems. *Medical*
585 *Physics*, 51(4):3110–3123, 2024.
- 586 Albert Gu and Tri Dao. Mamba: Linear-time sequence modeling with selective state spaces. *arXiv*
587 *preprint arXiv:2312.00752*, 2023.

- 594 Ran Gu, Guotai Wang, Tao Song, Rui Huang, Michael Aertsen, Jan Deprest, Sébastien Ourselin,
595 Tom Vercauteren, and Shaoting Zhang. Ca-net: Comprehensive attention convolutional neural
596 networks for explainable medical image segmentation. *IEEE transactions on medical imaging*,
597 40(2):699–711, 2020.
- 598
599 Tiancheng Gu, Kaicheng Yang, Xiang An, Ziyong Feng, Dongnan Liu, Weidong Cai, and Jiankang
600 Deng. Rwkv-clip: A robust vision-language representation learner. In *Proceedings of the 2024*
601 *Conference on Empirical Methods in Natural Language Processing*, pp. 4799–4812, 2024.
- 602 Zaiwang Gu, Jun Cheng, Huazhu Fu, Kang Zhou, Huaying Hao, Yitian Zhao, Tianyang Zhang,
603 Shenghua Gao, and Jiang Liu. Ce-net: Context encoder network for 2d medical image segmenta-
604 tion. *IEEE transactions on medical imaging*, 38(10):2281–2292, 2019a.
- 605
606 Zaiwang Gu, Jun Cheng, Huazhu Fu, Kang Zhou, Huaying Hao, Yitian Zhao, Tianyang Zhang,
607 Shenghua Gao, and Jiang Liu. Ce-net: Context encoder network for 2d medical image segmenta-
608 tion. *IEEE transactions on medical imaging*, 38(10):2281–2292, 2019b.
- 609
610 Changlu Guo, Márton Szemenyei, Yugen Yi, Wenle Wang, Buer Chen, and Changqi Fan. Sa-unet:
611 Spatial attention u-net for retinal vessel segmentation. In *2020 25th International Conference on*
612 *Pattern Recognition (ICPR)*, pp. 1236–1242. IEEE, 2021.
- 613
614 B Hamilton. Kaggle data science bowl: Find the nuclei in divergent images to advance medical
615 discovery, 2018.
- 616
617 Yousuf Harun, Kyungbok Lee, Jhair Gallardo, Giri Krishnan, and Christopher Kanan. What vari-
618 ables affect out-of-distribution generalization in pretrained models? *Advances in Neural Infor-*
mation Processing Systems, 37:56479–56525, 2024.
- 619
620 Ali Hatamizadeh, Vishwesh Nath, Yucheng Tang, Dong Yang, Holger R Roth, and Daguang Xu.
621 Swin unetr: Swin transformers for semantic segmentation of brain tumors in mri images. In
622 *International MICCAI Brainlesion Workshop*, pp. 272–284, 2021.
- 623
624 Ali Hatamizadeh, Vishwesh Nath, Yucheng Tang, Dong Yang, Holger R. Roth, Bennett A. Land-
625 man, Daguang Xu, Shashank Nath, Tong Zhao, and Ali Gholipour. Unetr: Transformers for 3d
626 medical image segmentation. In *2022 IEEE Winter Conference on Applications of Computer*
Vision (WACV), pp. 574–584. IEEE, 2022.
- 627
628 Along He, Kai Wang, Tao Li, Chengkun Du, Shuang Xia, and Huazhu Fu. H2former: An efficient
629 hierarchical hybrid transformer for medical image segmentation. *IEEE Transactions on Medical*
Imaging, 42(9):2763–2776, 2023.
- 630
631 Moein Heidari, Amirhossein Kazerouni, Milad Soltany, Reza Azad, Ehsan Khodapanah Aghdam,
632 Julien Cohen-Adad, and Dorit Merhof. Hiformer: Hierarchical multi-scale representations using
633 transformers for medical image segmentation. In *Proceedings of the IEEE/CVF Winter Confer-*
634 *ence on Applications of Computer Vision (WACV)*, pp. 6202–6212, 2023.
- 635
636 AD Hoover, Valentina Kouznetsova, and Michael Goldbaum. Locating blood vessels in retinal im-
637 ages by piecewise threshold probing of a matched filter response. *IEEE Transactions on Medical*
imaging, 19(3):203–210, 2000.
- 638
639 Wenjin Hou, Dingjie Fu, Kun Li, Shiming Chen, Hehe Fan, and Yi Yang. Zeromamba: Explor-
640 ing visual state space model for zero-shot learning. In *Proceedings of the AAAI Conference on*
641 *Artificial Intelligence*, volume 39, pp. 3527–3535, 2025.
- 642
643 Jintong Hu, Siyan Chen, Zhiyi Pan, Sen Zeng, and Wenming Yang. Perspective+ unet: Enhancing
644 segmentation with bi-path fusion and efficient non-local attention for superior receptive fields. In
645 *International Conference on Medical Image Computing and Computer-Assisted Intervention*, pp.
646 499–509. Springer, 2024.
- 647
Hejun Huang, Zuguo Chen, Ying Zou, Ming Lu, and Chaoyang Chen. Channel prior convolutional
attention for medical image segmentation. *Current Medical Imaging*, 19:347–360, 2023a.

- 648 Huimin Huang, Lanfen Lin, Ruofeng Tong, Hongjie Hu, Qiaowei Zhang, Yutaro Iwamoto, Xianhua
649 Han, Yen-Wei Chen, and Jian Wu. Unet 3+: A full-scale connected unet for medical image
650 segmentation. In *ICASSP 2020-2020 IEEE international conference on acoustics, speech and*
651 *signal processing (ICASSP)*, pp. 1055–1059. Ieee, 2020.
- 652 Xiaohong Huang, Zhifang Deng, Dandan Li, Xueguang Yuan, and Ying Fu. Missformer: An ef-
653 fective medical image segmentation transformer. *IEEE Transactions on Medical Imaging*, 42(5):
654 1484–1494, 2023b.
- 655 Nabil Ibtehaz and M Sohel Rahman. Multiresunet: Rethinking the u-net architecture for multimodal
656 biomedical image segmentation. *Neural networks*, 121:74–87, 2020.
- 657 Fabian Isensee, Paul F Jaeger, Simon AA Kohl, Jens Petersen, and Klaus H Maier-Hein. nnu-
658 net: a self-configuring method for deep learning-based biomedical image segmentation. *Nature*
659 *methods*, 18(2):203–211, 2021.
- 660 Fabian Isensee, Tassilo Wald, Constantin Ulrich, Michael Baumgartner, Saikat Roy, Klaus Maier-
661 Hein, and Paul F Jaeger. nnu-net revisited: A call for rigorous validation in 3d medical image
662 segmentation. In *International Conference on Medical Image Computing and Computer-Assisted*
663 *Intervention*, pp. 488–498. Springer, 2024.
- 664 Stefan Jaeger, Sema Candemir, Sameer Antani, Yi-Xiáng J Wáng, Pu-Xuan Lu, and George Thoma.
665 Two public chest x-ray datasets for computer-aided screening of pulmonary diseases. *Quantitative*
666 *imaging in medicine and surgery*, 4(6):475, 2014.
- 667 Debesh Jha, Pia H Smedsrud, Michael A Riegler, Dag Johansen, Thomas De Lange, Pål Halvorsen,
668 and Håvard D Johansen. Resunet++: An advanced architecture for medical image segmentation.
669 In *2019 IEEE international symposium on multimedia (ISM)*, pp. 225–2255. IEEE, 2019.
- 670 Debesh Jha, Michael A Riegler, Dag Johansen, Pål Halvorsen, and Håvard D Johansen. Double-
671 net: A deep convolutional neural network for medical image segmentation. In *2020 IEEE 33rd In-*
672 *ternational Symposium on Computer-Based Medical Systems (CBMS)*, pp. 558–564. IEEE, 2020a.
- 673 Debesh Jha, Pia H Smedsrud, Michael A Riegler, Pål Halvorsen, Thomas De Lange, Dag Johansen,
674 and Håvard D Johansen. Kvasir-seg: A segmented polyp dataset. In *MultiMedia modeling: 26th*
675 *international conference, MMM 2020, proceedings, part II 26*, pp. 451–462. Springer, 2020b.
- 676 Debesh Jha, Sharib Ali, Nikhil Kumar Tomar, Håvard D Johansen, Dag Johansen, Jens Rittscher,
677 Michael A Riegler, and Pål Halvorsen. Real-time polyp detection, localization and segmentation
678 in colonoscopy using deep learning. *IEEE Access*, 9:40496–40510, 2021.
- 679 Jiarui Jiang, Wei Huang, Miao Zhang, Taiji Suzuki, and Liqiang Nie. Unveil benign overfitting for
680 transformer in vision: Training dynamics, convergence, and generalization. *Advances in Neural*
681 *Information Processing Systems*, 37:135464–135625, 2024a.
- 682 Juntao Jiang, Mengmeng Wang, Huizhong Tian, Lingbo Cheng, and Yong Liu. Lv-unet: a
683 lightweight and vanilla model for medical image segmentation. In *2024 IEEE International Con-*
684 *ference on Bioinformatics and Biomedicine (BIBM)*, pp. 4240–4246. IEEE, 2024b.
- 685 Juntao Jiang, Jiangning Zhang, Weixuan Liu, Muxuan Gao, Xiaobin Hu, Xiaoxiao Yan, Feiyue
686 Huang, and Yong Liu. Rwkv-unet: Improving unet with long-range cooperation for effective
687 medical image segmentation. *CoRR*, 2025.
- 688 Taehun Kim, Hyemin Lee, and Daijin Kim. Uacanet: Uncertainty augmented context attention for
689 polyp segmentation. In *Proceedings of the 29th ACM International Conference on Multimedia*
690 *(MM '21)*, pp. 1–9. ACM, 2021.
- 691 Lisa M Koch, Christian F Baumgartner, and Philipp Berens. Distribution shift detection for
692 the postmarket surveillance of medical ai algorithms: a retrospective simulation study. *NPJ Digital*
693 *Medicine*, 7(1):120, 2024.
- 694 Zeki Kuş and Musa Aydın. Medsegbench: A comprehensive benchmark for medical image segmen-
695 tation in diverse data modalities. *Scientific Data*, 11(1):1283, 2024a.

- 702 Zeki Kuş and Musa Aydın. Medsegbench: A comprehensive benchmark for medical image segmen-
703 tation in diverse data modalities. *Scientific Data*, 11(1):1283, 2024b.
- 704
- 705 Libin Lan, Yanxin Li, Xiaojuan Liu, Juan Zhou, Jianxun Zhang, Nannan Huang, and Yudong Zhang.
706 Mslau-net: A hybrid cnn-transformer network for medical image segmentation. *arXiv preprint*
707 *arXiv:2505.18823*, 2025.
- 708 Chenxin Li, Xinyu Liu, Wuyang Li, Cheng Wang, Hengyu Liu, Yifan Liu, Zhen Chen, and Yixuan
709 Yuan. U-kan makes strong backbone for medical image segmentation and generation. In *The*
710 *Thirty-Ninth AAAI Conference on Artificial Intelligence (AAAI-25)*, 2025a.
- 711 Hao Li, Di-Hua Zhai, and Yuanqing Xia. Erdunet: An efficient residual double-coding unet for
712 medical image segmentation. *IEEE Transactions on Circuits and Systems for Video Technology*,
713 34(4):2083–2096, 2024a.
- 714
- 715 Jiaxuan Li, Qing Xu, Xiangjian He, Ziyu Liu, Daokun Zhang, Ruili Wang, Rong Qu, and Guoping
716 Qiu. Cfformer: Cross cnn-transformer channel attention and spatial feature fusion for improved
717 segmentation of heterogeneous medical images. *Expert Systems with Applications*, 2025b.
- 718 Xiang Li, Chong Fu, Qun Wang, Wenchao Zhang, Chen Ye, Junxin Chen, and Chui-Wing Sham.
719 Multi-scale dynamic sparse attention unet for medical image segmentation. *IEEE Journal of*
720 *Biomedical and Health Informatics*, 2025c.
- 721
- 722 Xin Li, Wenhui Zhu, Xuanzhao Dong, Oana M Dumitrescu, and Yalin Wang. Evit-unet: U-net like
723 efficient vision transformer for medical image segmentation on mobile and edge devices. In *2025*
724 *IEEE 22nd International Symposium on Biomedical Imaging (ISBI)*, pp. 1–5. IEEE, 2025d.
- 725 Zihan Li, Yuan Zheng, Dandan Shan, Shuzhou Yang, Qingde Li, Beizhan Wang, Yuanting Zhang,
726 Qingqi Hong, and Dinggang Shen. Scribformer: Transformer makes cnn work better for scribble-
727 based medical image segmentation. *IEEE Transactions on Medical Imaging*, 2024b.
- 728
- 729 Ailiang Lin, Bingzhi Chen, Jiayu Xu, Zheng Zhang, and Guangming Lu. Ds-transunet: Dual swin
730 transformer u-net for medical image segmentation. *IEEE Transactions on Instrumentation &*
731 *Measurement*, 2022.
- 732 Xian Lin, Zengqiang Yan, Xianbo Deng, Chuansheng Zheng, and Li Yu. Convformer: Plug-and-play
733 cnn-style transformers for improving medical image segmentation. In *International Conference*
734 *on Medical Image Computing and Computer-Assisted Intervention*, pp. 642–651. Springer, 2023.
- 735 Jiarun Liu, Hao Yang, Hong-Yu Zhou, Yan Xi, Lequan Yu, Cheng Li, Yong Liang, Guangming
736 Shi, Yizhou Yu, Shaoting Zhang, et al. Swin-umamba: Mamba-based unet with imagenet-based
737 pretraining. In *International conference on medical image computing and computer-assisted in-*
738 *tervention*, pp. 615–625. Springer, 2024a.
- 739 Jiarun Liu, Hao Yang, Hong-Yu Zhou, Lequan Yu, Yong Liang, Yizhou Yu, Shaoting Zhang,
740 Hairong Zheng, and Shanshan Wang. Swin-umamba†: Adapting mamba-based vision founda-
741 tion models for medical image segmentation. *IEEE Transactions on Medical Imaging*, 2024b.
- 742
- 743 Xiao Liu, Peng Gao, Tao Yu, Fei Wang, and Ru-Yue Yuan. Cswin-unet: Transformer unet with
744 cross-shaped windows for medical image segmentation. *Information Fusion*, 113(102634), 2025.
- 745 Yutong Liu, Haijiang Zhu, Mengting Liu, Huaiyuan Yu, Zihan Chen, and Jie Gao. Rolling-unet:
746 Revitalizing mlp’s ability to efficiently extract long-distance dependencies for medical image
747 segmentation. In *Proceedings of the Thirty-Eighth AAAI Conference on Artificial Intelligence*
748 *(AAAI-24)*, pp. 3819–3827, 2024c.
- 749
- 750 Ze Liu, Yutong Lin, Yue Cao, Han Hu, Yixuan Wei, Zheng Zhang, Stephen Lin, and Baining Guo.
751 Swin transformer: Hierarchical vision transformer using shifted windows. In *Proceedings of the*
752 *IEEE/CVF international conference on computer vision*, pp. 10012–10022, 2021.
- 753 Ange Lou, Shuyue Guan, and Murray Loew. Cfpnet-m: A light-weight encoder-decoder based
754 network for multimodal biomedical image real-time segmentation. In *Medical Imaging 2021:*
755 *Image Processing*, volume 11596, pp. 115962T. International Society for Optics and Photonics,
2021.

- 756 Ange Lou, Shuyue Guan, Hanseok Ko, and Murray Loew. Caranet: Context axial reverse attention
757 network for segmentation of small medical objects. In *Medical Imaging 2022: Image Processing*,
758 volume 12032, pp. 81–92. SPIE, 2022.
- 759
- 760 Zichen Luo, Xinshan Zhu, Lan Zhang, and Biao Sun. Rethinking u-net: Task-adaptive mixture of
761 skip connections for enhanced medical image segmentation. In *The Thirty-Ninth AAAI Confer-*
762 *ence on Artificial Intelligence (AAAI-25)*, 2025.
- 763 Omid Nejati Manzari, Javad Mirzapour Kaleybar, Hooman Saadat, and Shahin Maleki. Befunet:
764 A hybrid cnn-transformer architecture for precise medical image segmentation. *arXiv preprint*
765 *arXiv:2402.08793*, 2024.
- 766
- 767 Teresa Mendonça, Pedro M Ferreira, Jorge S Marques, André RS Marcal, and Jorge Rozeira. Ph
768 2-a dermoscopic image database for research and benchmarking. In *2013 35th EMBC*, pp. 5437–
769 5440. IEEE, 2013.
- 770
- 771 Viet-Thanh Nguyen, Van-Truong Pham, and Thi-Thao Tran. Ac-mambaseg: An adaptive convo-
772 lution and mamba-based architecture for enhanced skin lesion segmentation. In *International*
773 *Conference on Green Technology and Sustainable Development*, pp. 13–26. Springer, 2024.
- 774 Ke Niu, Jiacheng Han, and Jiuyun Cai. Cfm-unet: coupling local and global feature extraction
775 networks for medical image segmentation. *Scientific Reports*, 15(22236), 2025.
- 776
- 777 Ziwei Niu, Shuyi Ouyang, Shiao Xie, Yen-wei Chen, and Lanfen Lin. A survey on domain general-
778 ization for medical image analysis. *arXiv preprint arXiv:2402.05035*, 2024.
- 779
- 780 Ozan Oktay, Jo Schlemper, Loic Le Folgoc, Matthew Lee, Mattias Heinrich, Kazunari Misawa,
781 Kensaku Mori, Steven McDonagh, Nils Y Hammerla, and Bernhard et al. Kainz. Attention u-net:
782 Learning where to look for the pancreas. In *Medical Imaging with Deep Learning*, 2018.
- 783 Yanchi Ou, Yufeng Chen, Yuzhi Zhang, Shukai Yang, Xiaoqian Zhang, Ying Zhou, Siyu Chen, and
784 Lifan Peng. Enhanced medical image segmentation via deep dynamic self-adjusting u-net with
785 multi-scale attention and semantic mitigation. *The Visual Computer*, pp. 1–17, 2025.
- 786
- 787 Bo Peng, Eric Alcaide, Quentin Anthony, Alon Albalak, Samuel Arcadinho, Stella Biderman,
788 Huanqi Cao, Xin Cheng, Michael Chung, Matteo Grella, et al. Rwkv: Reinventing rnns for
789 the transformer era. *arXiv preprint arXiv:2305.13048*, 2023.
- 790
- 791 Yaopeng Peng, Danny Z Chen, and Milan Sonka. U-net v2: Rethinking the skip connections of u-
792 net for medical image segmentation. In *2025 IEEE 22nd International Symposium on Biomedical*
793 *Imaging (ISBI)*, pp. 1–5. IEEE, 2025.
- 794
- 795 Payel Pramanik, Ayush Roy, Erik Cuevas, Marco Perez-Cisneros, and Ram Sarkar. Dau-net:
796 Dual attention-aided u-net for segmenting tumor in breast ultrasound images. *Plos one*, 19(5):
e0303670, 2024.
- 797
- 798 Md Mostafijur Rahman and Radu Marculescu. Medical image segmentation via cascaded attention
799 decoding. In *Proceedings of the IEEE/CVF Winter Conference on Applications of Computer*
800 *Vision (WACV)*, pp. 6222–6231, 2023a.
- 801
- 802 Md Mostafijur Rahman and Radu Marculescu. G-cascade: Efficient cascaded graph convolutional
803 decoding for 2d medical image segmentation. In *Proceedings of the IEEE/CVF Winter Conference*
804 *on Applications of Computer Vision (WACV)*, pp. 7728–7737, 2023b.
- 805
- 806 Md Mostafijur Rahman and Radu Marculescu. Multi-scale hierarchical vision transformer with cas-
807 caded attention decoding for medical image segmentation. In *Proceedings of Machine Learning*
808 *Research (MIDL 2023)*, volume 165, pp. 1–19, 2023c.
- 809
- 808 Md Mostafijur Rahman, Mustafa Munir, and Radu Marculescu. Emcad: Efficient multi-scale con-
809 volutional attention decoding for medical image segmentation. In *Proceedings of the IEEE/CVF*
Conference on Computer Vision and Pattern Recognition, pp. 11769–11779, 2024.

- 810 Olaf Ronneberger, Philipp Fischer, and Thomas Brox. U-net: Convolutional networks for biomedical
811 image segmentation. In *Medical Image Computing and Computer-Assisted Intervention*, pp.
812 234–241. Springer, 2015.
- 813
- 814 Jiacheng Ruan and Suncheng Xiang. Vm-unet: Vision mamba unet for medical image segmentation.
815 *CoRR*, 2024.
- 816 Jiacheng Ruan, Suncheng Xiang, Mingye Xie, Ting Liu, and Yuzhuo Fu. Malunet: A multi-attention
817 and light-weight unet for skin lesion segmentation. In *2022 IEEE International Conference on*
818 *Bioinformatics and Biomedicine (BIBM)*, pp. 1150–1156. IEEE, 2022.
- 819
- 820 Edward Sanderson and Bogdan J Matuszewski. Fcn-transformer feature fusion for polyp segmenta-
821 tion. In *Medical Image Computing and Computer-Assisted Intervention Workshop*, pp. 644–654.
822 Springer, 2022.
- 823 Xin Shu, Jiashu Wang, Aoping Zhang, Jinlong Shi, and Xiao-Jun Wu. Csca u-net: A channel
824 and space compound attention cnn for medical image segmentation. *Artificial Intelligence In*
825 *Medicine*, 150:102800, 2024.
- 826
- 827 K Sirinukunwattana, JP Pluim, H Chen, X Qi, and PAG Heng. Glas@ miccai’2015: Gland segmen-
828 tation challenge contest, 2015.
- 829
- 830 Abhishek Srivastava, Debesh Jha, Sukalpa Chanda, Umapada Pal, Håvard D Johansen, Dag Jo-
831 hansen, Michael A Riegler, Sharib Ali, and Pål Halvorsen. Msrf-net: A multi-scale residual
832 fusion network for biomedical image segmentation. *IEEE Journal of Biomedical and Health*
833 *Informatics*, 26(5):2252–2263, 2021.
- 834 Joes Staal, Michael D Abramoff, Meindert Niemeijer, Max A Viergever, and Bram Van Ginneken.
835 Ridge-based vessel segmentation in color images of the retina. *IEEE transactions on medical*
836 *imaging*, 23(4):501–509, 2004.
- 837
- 838 Guanqun Sun, Yizhi Pan, Weikun Kong, Zichang Xu, Jianhua Ma, Teeradaj Racharak, Le-Minh
839 Nguyen, and Junyi Xin. Da-transunet: integrating spatial and channel dual attention with trans-
840 former u-net for medical image segmentation. *Frontiers in Bioengineering and Biotechnology*,
841 12:1398237, 2024.
- 842 Fenghe Tang, Lingtao Wang, Chunping Ning, Min Xian, and Jianrui Ding. Cmu-net: a strong
843 convmixer-based medical ultrasound image segmentation network. In *2023 IEEE 20th interna-*
844 *tional symposium on biomedical imaging (ISBI)*, pp. 1–5. IEEE, 2023.
- 845 Fenghe Tang, Jianrui Ding, Quan Quan, Lingtao Wang, Chunping Ning, and S Kevin Zhou.
846 Cmunext: An efficient medical image segmentation network based on large kernel and skip fu-
847 sion. In *ISBI*, 2024.
- 848
- 849 Fenghe Tang, Wenxin Ma, Zhiyang He, Xiaodong Tao, Zihang Jiang, and S Kevin Zhou.
850 Pre-trained llm is a semantic-aware and generalizable segmentation booster. *arXiv preprint*
851 *arXiv:2506.18034*, 2025a.
- 852 Fenghe Tang, Bingkun Nian, Jianrui Ding, Wenxin Ma, Quan Quan, Chengqi Dong, Jie Yang, Wei
853 Liu, and S Kevin Zhou. Mobile u-vit: Revisiting large kernel and u-shaped vit for efficient medical
854 image segmentation. *arXiv preprint arXiv:2508.01064*, 2025b.
- 855
- 856 Youbao Tang, Yuxing Tang, Jing Xiao, and Ronald M Summers. Xlsor: A robust and accurate lung
857 segmentor on chest x-rays using criss-cross attention and customized radiorealistic abnormalities
858 generation. In *International Conference on Medical Imaging with Deep Learning (MIDL)*, 2019.
- 859 Nikhil Kumar Tomar, Annie Shergill, Brandon Rieders, Ulas Bagci, and Debesh Jha. Transresu-net:
860 Transformer based resu-net for real-time colonoscopy polyp segmentation. *CoRR*, 2022.
- 861
- 862 Jeya Maria Jose Valanarasu and Vishal M Patel. Unext: Mlp-based rapid medical image segmen-
863 tation network. In *International conference on medical image computing and computer-assisted*
intervention, pp. 23–33. Springer, 2022.

- 864 Jeya Maria Jose Valanarasu, Poojan Oza, Ilker Hacihaliloglu, and Vishal M Patel. Medical trans-
865 former: Gated axial-attention for medical image segmentation. In *Medical Image Computing and*
866 *Computer-Assisted Intervention*, pp. 36–46. Springer, 2021.
- 867 Sandeep Kumar Vashist. Point-of-care diagnostics: Recent advances and trends. *Biosensors*, 7(4):
868 62, 2017.
- 869 David Vázquez, Jorge Bernal, F Javier Sánchez, Gloria Fernández-Esparrach, Antonio M López,
870 Adriana Romero, Michal Drozdal, and Aaron Courville. A benchmark for endoluminal scene
871 segmentation of colonoscopy images. *Journal of healthcare engineering*, 2017(1):4037190, 2017.
- 872 Haibin Wang, Zhenfeng Zhao, Qi Liu, and Shenwen Wang. Resu-kan: a medical image segmenta-
873 tion model integrating residual convolutional attention and atrous spatial pyramid pooling. *Ap-
874 plied Intelligence*, 55(568), 2025a.
- 875 Haonan Wang, Peng Cao, Jiaqi Wang, and Osmar R Zaiane. Uctransnet: Rethinking the skip con-
876 nections in u-net from a channel-wise perspective with transformer. In *The Thirty-Sixth AAAI
877 Conference on Artificial Intelligence (AAAI-22)*, 2022a.
- 880 Haotian Wang, Min Xian, and Aleksandar Vakanski. Ta-net: Topology-aware network for gland
881 segmentation. In *Proceedings of the IEEE/CVF winter conference on applications of computer
882 vision*, pp. 1556–1564, 2022b.
- 883 Hongyi Wang, Shiao Xie, Lanfen Lin, Yutaro Iwamoto, Xian-Hua Han, Yen-Wei Chen, and Ruofeng
884 Tong. Mixed transformer u-net for medical image segmentation. In *ICASSP 2022-2022 IEEE
885 International Conference on Acoustics, Speech and Signal Processing (ICASSP)*, pp. 2390–2394.
886 IEEE, 2022c.
- 887 Shengxiang Wang, Ge Li, Min Gao, Linlin Zhuo, Mingzhe Liu, Zhizhong Ma, Wei Zhao, and
888 Xiangzheng Fu. Gh-unet: group-wise hybrid convolution-vit for robust medical image segmenta-
889 tion. *npj Digital Medicine*, 8(426), 2025b.
- 891 Ziyang Wang, Jian-Qing Zheng, Yichi Zhang, Ge Cui, and Lei Li. Mamba-unet: Unet-like pure
892 visual mamba for medical image segmentation. *CoRR*, abs/2402.05079, 2024. URL <https://doi.org/10.48550/arXiv.2402.05079>.
- 893 Katharina Wenderott, Jim Krups, Fiona Zaruchas, and Matthias Weigl. Effects of artificial intelli-
894 gence implementation on efficiency in medical imaging—a systematic literature review and meta-
895 analysis. *NPJ Digital Medicine*, 7(1):265, 2024.
- 896 Huisi Wu, Shihuai Chen, Guilian Chen, Wei Wang, Baiying Lei, and Zhenkun Wen. Fat-net: Fea-
897 ture adaptive transformers for automated skin lesion segmentation. *Medical Image Analysis*, 76:
898 102327, 2022.
- 899 Renkai Wu, Yinghao Liu, Pengchen Liang, and Qing Chang. H-vmunet: High-order vision mamba
900 unet for medical image segmentation. *Neurocomputing*, 624:129447, 2025a.
- 901 Renkai Wu, Yinghao Liu, Guochen Ning, Pengchen Liang, and Qing Chang. Ultralight vm-unet:
902 Parallel vision mamba significantly reduces parameters for skin lesion segmentation. *Patterns*, 6
903 (101298), 2025b.
- 904 Ruichao Wu, Zihuan Yao, Xiangyu Lu, and Yide Ma. Mfmsnet: A multi-frequency and multi-scale
905 interactive cnn-transformer hybrid network for breast ultrasound image segmentation. *Ultrasound
906 in Medicine & Biology*, 2023.
- 907 Guoping Xu, Xuan Zhang, Xinwei He, and Xinglong Wu. Levit-unet: Make faster encoders with
908 transformer for medical image segmentation. In *Chinese Conference on Pattern Recognition and
909 Computer Vision (PRCV)*, pp. 42–53. Springer, 2023a.
- 910 Qing Xu, Zhicheng Ma, Wenting Duan, et al. Dcsau-net: A deeper and more compact split-attention
911 u-net for medical image segmentation. *Computers in Biology and Medicine*, 154:106626, 2023b.
- 912 Yiwen Xu, Tariq M Khan, Yang Song, and Erik Meijering. Edge deep learning in computer vision
913 and medical diagnostics: a comprehensive survey. *Artificial Intelligence Review*, 58(3):93, 2025.

- 918 Wenjun Yan, Yuanyuan Wang, Shengjia Gu, Lu Huang, Fuhua Yan, Liming Xia, and Qian Tao.
919 The domain shift problem of medical image segmentation and vendor-adaptation by unet-gan. In
920 *International Conference on Medical Image Computing and Computer-Assisted Intervention*, pp.
921 623–631. Springer, 2019.
- 922 Hongbo Ye, Fenghe Tang, Peiang Zhao, Zhen Huang, Dexin Zhao, Minghao Bian, and S Kevin
923 Zhou. U-rwkv: Lightweight medical image segmentation with direction-adaptive rwkv. *arXiv*
924 *preprint arXiv:2507.11415*, 2025.
- 926 Yunguang Ye, Ping Huang, Yu Sun, and Dachuan Shi. Mbsnet: A deep learning model for multibody
927 dynamics simulation and its application to a vehicle-track system. *Mechanical Systems and Signal*
928 *Processing*, 157:107716, 2021.
- 929 Xiang Yu, Yayan Chen, Guannan He, Qing Zeng, Yue Qin, Meiling Liang, Dandan Luo, Yimei Liao,
930 Zeyu Ren, and Cheng et al. Kang. Simple is what you need for efficient and accurate medical
931 image segmentation. *arXiv preprint arXiv:2506.13415*, 2025.
- 933 Chunyu Yuan, Dongfang Zhao, and Sos S Agaian. Mucm-net: A mamba powered ucm-net for skin
934 lesion segmentation. *CoRR*, 2024a.
- 935 Haojun Yuan, Lingna Chen, and Xiaofeng He. Mmunet: Morphological feature enhancement net-
936 work for colon cancer segmentation in pathological images. *Biomedical Signal Processing and*
937 *Control*, 91:105927, 2024b.
- 939 Hanxiao Zhang, Yifan Zhou, and Guo-Hua Wang. Dense vision transformer compression with few
940 samples. In *Proceedings of the IEEE/CVF conference on computer vision and pattern recognition*,
941 pp. 15825–15834, 2024a.
- 942 Mingya Zhang, Yue Yu, Sun Jin, Limei Gu, Tingsheng Ling, and Xianping Tao. Vm-unet-v2:
943 rethinking vision mamba unet for medical image segmentation. In *International symposium on*
944 *bioinformatics research and applications*, pp. 335–346. Springer, 2024b.
- 946 Yingtao Zhang, Min Xian, Heng-Da Cheng, Bryar Shareef, Jianrui Ding, Fei Xu, Kuan Huang,
947 Boyu Zhang, Chunping Ning, and Ying Wang. Busis: a benchmark for breast ultrasound image
948 segmentation. In *Healthcare*, volume 10, pp. 729. MDPI, 2022.
- 949 Yundong Zhang, Huiye Liu, and Qiang Hu. Transfuse: Fusing transformers and cnns for medical
950 image segmentation. In *International conference on medical image computing and computer-*
951 *assisted intervention*, pp. 14–24. Springer, 2021.
- 952 Kevin Zhou, Hayit Greenspan, and Dinggang Shen. *Deep learning for medical image analysis*.
953 Academic Press, 2017.
- 955 Yanfeng Zhou, Lingrui Li, Le Lu, and Minfeng Xu. nnwnet: Rethinking the use of transformers in
956 biomedical image segmentation and calling for a unified evaluation benchmark. In *Proceedings*
957 *of the Computer Vision and Pattern Recognition Conference*, pp. 20852–20862, 2025.
- 958 Zongwei Zhou, Md Mahfuzur Rahman Siddiquee, Nima Tajbakhsh, and Jianming Liang. Unet++:
959 A nested u-net architecture for medical image segmentation. In *International workshop on deep*
960 *learning in medical image analysis*, pp. 3–11. Springer, 2018.
- 962 Hancan Zhu, Jinhao Chen, and Guanghua He. Medvkan: Efficient feature extraction with mamba
963 and kan for medical image segmentation. *arXiv preprint arXiv:2505.11797*, 2025.
- 964
965
966
967
968
969
970
971

972
973
974
975
976
977
978
979
980
981
982
983
984
985
986
987
988
989
990
991
992
993
994
995
996
997
998
999
1000
1001
1002
1003
1004
1005
1006
1007
1008
1009
1010
1011
1012
1013
1014
1015
1016
1017
1018
1019
1020
1021
1022
1023
1024
1025

A APPENDIX

In this appendix, we provide additional details and results to complement the main paper. The content is organized as follows:

Appendix B: Related Work.

Appendix C: Details of U-Bench Data Zoo.

Appendix D: Details of U-Bench Model Zoo.

Appendix E: Details of U-Score.

Appendix F: Implementation and Evaluation Details.

Appendix G: Additional Results.

Appendix J: Reproducibility Checklist.

B RELATED WORK

In Appendix B, we present a broad view of the variations of U-shape networks, including the architecture of the network and existing medical segmentation benchmarks.

B.1 MODEL ARCHITECTURE

As the core architecture for medical image segmentation, the U-Net has evolved into numerous variants in recent years, driven by advancements in feature representation capabilities, long-range dependency modeling techniques, and the trade-off between efficiency and accuracy. This section categorizes and organizes these U-Net variants based on their core paradigms and design motivations, systematically tracing their evolutionary path from foundational construction to integrated innovation. Fig. 9 summarizes the evolution of U-Net variants over time.

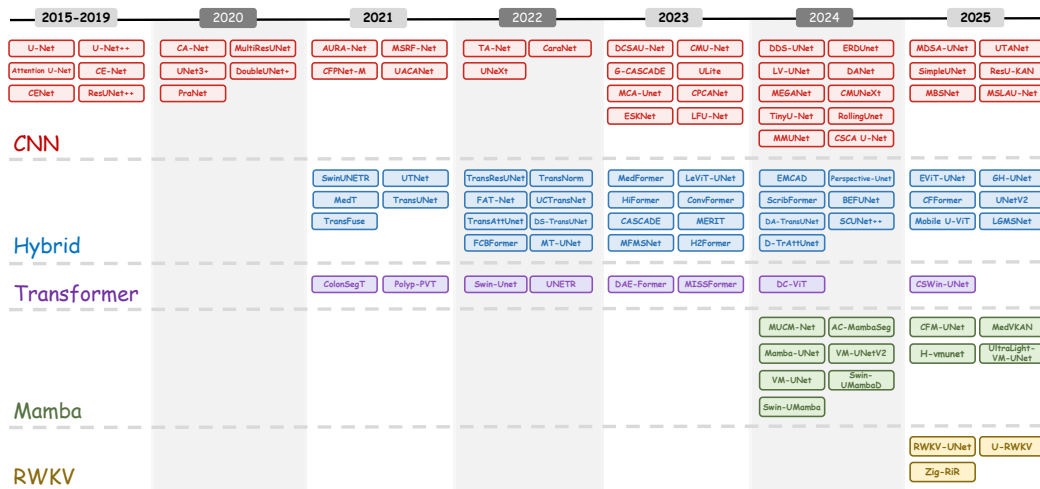


Figure 9: Time and architecture distribution of all evaluated models.

1. U-shaped Networks Dominated by Convolutional Neural Networks (CNNs) (2015-2021: Foundational Laying)

U-shaped networks, using convolutional neural networks as their sole backbone, extract local features through convolution operations and utilize fixed skip connections to fuse multi-scale information, laying the foundation for the "encoder-decoder" paradigm in medical image segmentation. Their advantages lie in their ability to accurately capture local details (such as textures and edges), their relatively lightweight architecture, and their stable training process, providing a solid design baseline for subsequent complex variants. However, the local receptive field of convolutional operations limits the ability to model global semantic information, and fixed skip connections easily lead to a semantic gap between the encoder and decoder, limiting performance.

2. Transformer-driven U-Networks (2021-2023: Paradigm Shift)

This variant introduces the Transformer architecture (including variants such as Vision Transformer (Dosovitskiy et al., 2020) and Swin Transformer (Liu et al., 2021)) to replace or enhance the traditional CNN backbone, leveraging the self-attention mechanism to effectively model long-range dependencies. However, the computational complexity of the self-attention mechanism grows quadratically with sequence length, resulting in low inference efficiency. Furthermore, this type of model is poorly adaptable to small-scale medical datasets and is prone to overfitting due to insufficient data, making it difficult to meet the stringent real-time requirements of clinical edge devices.

3. U-Networks Based on State-Space Models (SSMs) and Recurrent Paradigms (2023-2025: Efficiency-Oriented)

Recent research explores replacing the quadratic-cost self-attention with linear-time alternatives. One line leverages state-space models (e.g., Mamba (Gu & Dao, 2023)) that adopt selective state updates to capture long-range dependencies while achieving linear complexity, markedly improving inference efficiency and adaptability to small sample sizes. Another complementary line introduces RWKV (Peng et al., 2023), a recurrent-inspired model that combines Transformer-like expressiveness with RNN-style recurrence, enabling efficient sequential processing and stronger generalization across varying input lengths. Together, these paradigms alleviate the computational and data-dependency limitations of Transformers.

4. Multi-Paradigm Fusion U-Networks (Hybrid Networks) (2020-2025: Fusion and Innovation)

This phase aims to integrate the advantages of CNNs in local feature extraction, the global semantic modeling capabilities of Transformers. The goal is to achieve a balance between accuracy, efficiency, and generalization by fusing different architectures. This type of network variant can adapt to complex clinical scenarios such as multimodal imaging and cross-center data heterogeneity, significantly improving the practical value of segmentation results. However, the architectural design complexity increases significantly, and the coordination mechanisms between modules of different paradigms (such as the timing of feature interactions and weight distribution) still need further optimization.

The development of the four types of U-shaped network variants follows a technological evolutionary path of "local refinement → global correlation → efficiency considerations → multi-paradigm collaboration," reflecting the shift in clinical needs from static, single-scenario segmentation toward more efficient, generalized solutions adaptable across diverse conditions.

B.2 MEDICAL SEGMENTATION BENCHMARKS

To fill the research gap in the evaluation of U-net systems, we comprehensively compare previous segmentation evaluation benchmarks with the U-Bench proposed in this paper, thereby clarifying the innovative positioning of U-Bench.

B.2.1 RELATED WORK

Medical image segmentation has seen rapid progress, driven by deep learning architectures and large-scale datasets. However, the validity and reproducibility of many reported advances have been challenged due to inconsistent evaluation protocols, limited dataset diversity, and insufficient consideration of deployment constraints.

TorchStone (Bassi et al., 2024) addressed some of these limitations by introducing a large-scale collaborative benchmark for abdominal organ segmentation, leveraging diverse CT scans from multiple hospitals worldwide. While it emphasized out-of-distribution generalization and standardized evaluation, its scope was limited to a single anatomical region and modality, making it less suitable for assessing broader architectural capabilities. MedSegBench (Kuş & Aydin, 2024b) expanded coverage across modalities, incorporating 35 datasets from ultrasound, MRI, X-ray, and others. It provided standardized splits and evaluated multiple encoder-decoder variants, aiming to foster universal segmentation models. However, its focus remained on a smaller set of architectures and lacked comprehensive analysis of robustness, efficiency, and cross-paradigm comparisons. nnWNet (Zhou et al., 2025) proposed architectural modifications to integrate convolutions and transformers within a U-Net framework, addressing the need for continuous transmission of local and global features. Although it benchmarked on multiple 2D and 3D datasets, its evaluation was limited to a small number of models and lacked systematic efficiency analysis. nnU-Net Revisited (Isensee et al., 2024) critically examined recent architectural claims, showing that properly configured CNN-based U-Nets could still match or outperform newer transformer and Mamba-based models when trained with sufficient resources. This study highlighted the importance of rigorous baselines and computational reproducibility, yet it did not provide a multi-modal, multi-dataset framework for comparing a large number of variants. Collectively, these efforts underscore the need for a unified, statistically rigorous, and comprehensive benchmark that systematically evaluates a broad spectrum of U-Net variants across diverse modalities, datasets, and deployment metrics.

1134 B.2.2 TARGETED IMPROVEMENTS OF U-BENCH

1135
1136 As summarized in Tab. 1, existing medical image segmentation benchmarks suffer from limited
1137 modality coverage, insufficient evaluation diversity, narrow architectural scope, and lack of dataset-
1138 specific analysis-all of which hinder comprehensive assessment of model generalization. To address
1139 these gaps, U-Bench is designed with three targeted innovations, establishing a more comprehensive
1140 and clinically relevant evaluation framework while aligning with its core goals: evaluating 100 U-
1141 Net variants across 28 datasets and 10 modalities, introducing the performance-efficiency balanced
1142 U-Score, and enabling fair, reproducible benchmarking.

1143 1. Multimodality and Full Task Coverage

1144 U-Bench encompasses 10 major medical imaging modalities (ultrasound, dermoscopy, en-
1145 doscopy, fundus, histopathology, nuclei, X-Ray, MRI, CT, OCT) and integrates 28 datasets
1146 (sample sizes: 20-17,000). It covers tasks from macroscopic organ segmentation (e.g.,
1147 lung CT, cardiac MRI) to microscopic structure segmentation (e.g., histopathological nu-
1148 clei, retinal microvasculature), with standardized train/test splits. This design tests cross-
1149 modality adaptability of models, matching real-world clinical multimodal diagnostic work-
1150 flows.

1151 2. Multi-Dimensional Evaluation System

1152 Beyond traditional accuracy metrics (IoU, Dice), U-Bench introduces three critical eval-
1153 uation dimensions and a unified U-Score to quantify clinical utility: *Computational Effi-
1154 ciency*: Standardized reporting of model parameters (M), inference FLOPs (G), and FPS to
1155 reflect deployability on resource-constrained devices. *Generalization Performance*: Zero-
1156 shot transfer tests on 8 unseen target datasets (distinct from 20 training source datasets) to
1157 assess robustness to domain shifts (e.g., cross-center ultrasound, unseen dermoscopic le-
1158 sions). *Statistical Significance*: Paired t-tests between each variant and the original U-Net
1159 ($p < 0.05$ as significant) to validate reliable performance gains. *U-Score*: A comprehensive
1160 metric using quantile normalization and weighted harmonic mean to balance accuracy and
1161 efficiency, bridging academic performance and clinical deployment value.

1162 3. Large-Scale Reproducible Validation

1163 U-Bench includes 100 publicly available U-Net variants, covering mainstream architectures
1164 from 2015 to 2025 (CNN, Transformer, Mamba, RWKV, hybrid designs). To ensure repro-
1165 ducibility, all models adopt official implementations, pre-trained weights (if available), and
1166 deep supervision strategies (if applicable).

1167 C DETAILS OF DATA ZOO

1168 We summarize the dataset statistics used in this paper in Table 4. This table details the datasets used
1169 for experimental evaluation, covering 10 core imaging modalities, including ultrasound (e.g., BUSI),
1170 dermoscopy (e.g., ISIC2018), endoscopy (e.g., Kvasir-SEG), fundus (e.g., CHASE), histopathology
1171 (e.g., Glas), nuclear (e.g., DSB2018), X-ray (e.g., Montgomery), MRI (e.g., ACDC), CT (e.g.,
1172 Synapse), and OCT (e.g., Cystoidfluid). For each dataset, we provide key information such as the
1173 segmentation class (binary or multiclass), the number of samples, the year of publication, and a
1174 basic description. All datasets used are publicly available. Therefore, we provide access links in the
1175 relevant references and supplementary tables. The details are available in Tab. 4. A brief description
1176 of the dataset is as follows:

1177
1178 **BUSI.** The Breast Ultrasound Images (BUSI) dataset (Al-Dhabyani et al., 2020), collected from
1179 600 female patients in 2018, contains 133 normal, 487 benign, and 210 malignant cases with corre-
1180 sponding ground truth labels. The data labels are obtained using ultrasound scans to examine breast
1181 cancer lesion areas.

1182 **BUS.** The Breast UltraSound (BUS) public dataset (Zhang et al., 2022) includes 562 images (306
1183 benign, 256 malignant) collected via five ultrasound devices, used for generalization experiments.
1184 The data labels are obtained using ultrasound scans to examine breast cancer lesion (or non-lesion)
1185 areas.

1186 **BUSBRA.** The BUS-BRA dataset (Gómez-Flores et al., 2024) comprises 1875 anonymized images
1187 from 1064 patients (corresponding to 722 benign and 342 malignant cases) acquired via four ultra-

1188 sound scanners. The data labels are obtained using ultrasound scans to examine breast cancer lesion
1189 (or non-lesion) areas.

1190 **TNSCUI.** The Thyroid Nodule Segmentation and Classification in Ultrasound Images 2020 dataset¹
1191 includes 3644 cases from the Chinese Artificial Intelligence Alliance for Thyroid and Breast Ultra-
1192 sound. The data label is the thyroid nodule area obtained by thyroid ultrasound.

1193 **TUCC.** The Thyroid Ultrasound (TUCC) dataset² collects data from 167 patients, including 192
1194 biopsy-confirmed nodules. The data label is the thyroid nodule area obtained by thyroid ultrasound.

1195 **ISIC2018.** The ISIC 2018 dataset (Codella et al., 2018) is a large-scale dermoscopy dataset for
1196 lesion segmentation, containing 2594 skin lesion images. The data label is the melanoma (or non-
1197 lesion) area of the skin disease obtained by dermoscopy imaging.

1198 **PH2.** The PH² database (Mendonça et al., 2013) includes 200 dermoscopic images with manual
1199 segmentation and clinical diagnosis. The data label is the melanoma (or non-lesion) area of the skin
1200 disease obtained by dermoscopy imaging.

1201 **SkinCancer.** The SkinCancer dataset (Kuş & Aydin, 2024a) contains 206 dermoscopic samples
1202 extracted from DermIS and DermQuest. The data label is the melanoma (or non-lesion) area of the
1203 skin disease obtained by dermoscopy imaging

1204 **Covidquex.** The Covidquex dataset (Kuş & Aydin, 2024a) includes 2,913 chest X-ray images (256 ×
1205 256 pixels) for binary segmentation. The dataset is labeled with COVID-infected areas on chest X-
1206 rays.

1207 **Montgomery.** The Montgomery dataset (Jaeger et al., 2014) contains 138 chest X-rays (80 normal,
1208 58 with tuberculosis). The data label is the tuberculosis lesion (or non-lesion) area on the lung X-ray.

1209 **NIH-test.** The NIH-test dataset (Tang et al., 2019) is a manually annotated chest X-ray dataset with
1210 100 lung masks. The data labels are lung segmentations from chest X-rays.

1211 **DCA.** The DCA dataset (Kuş & Aydin, 2024a) contains 134 fundus images (300 × 300 pixels). The
1212 data label is the blood vessel segmentation of the fundus image.

1213 **Kvasir.** The Kvasir dataset (Jha et al., 2020b) contains 1000 gastrointestinal polyp images and
1214 corresponding ground truth. The data labels are pathological areas of gastrointestinal endoscopic
1215 imaging.

1216 **CVC-300.** The CVC-300 dataset (Vázquez et al., 2017) comprises 60 colonoscopy polyp images
1217 (500 × 574 pixels). The data labels are pathological areas of gastrointestinal endoscopic imaging.

1218 **CVC-ClinicDB.** The CVC-ClinicDB dataset (Bernal et al., 2015) includes 612 images from 29
1219 colonoscopy sequences. The data labels are pathological areas of gastrointestinal endoscopic imag-
1220 ing.

1221 **Robotool.** The Robotool dataset (Kuş & Aydin, 2024a) consists of 500 images extracted from
1222 multiple surgical videos. The data label is the instrument area imaged by the endoscope.

1223 **Promise.** The Promise dataset (Kuş & Aydin, 2024a) includes 1,473 prostate MRI samples (512 ×
1224 512 pixels).

1225 **ACDC.** The ACDC dataset (Bernard et al., 2018) contains 100 cardiac MRI scans. The data labels
1226 for left ventricle (LV), right ventricle (RV), and myocardium (MYO) in heart segmentation.

1227 **CHASE.** The CHASE dataset (Fraz et al., 2012; Guo et al., 2021) includes 28 retinal images (one
1228 per eye from 14 children). The data label is the vascular area of the fundus image.

1229 **Stare.** The Stare dataset (Hoover et al., 2000) includes 20 ocular fundus vessel images with manual
1230 annotations. The data label is the vascular area of the fundus image.

1231 **DRIVE.** The DRIVE dataset (Staal et al., 2004) is collected from a Dutch diabetic retinopathy
1232 screening program. The data label is the vascular area of the fundus image.

1233 ¹Available at: <https://tn-scui2020.grand-challenge.org/Home>.

1234 ²Available at: <https://aimi.stanford.edu/datasets/thyroid-ultrasound-cine-clip>.

Table 4: Dataset information summary, where 'O' in split type represents ourself-split, and 'S' represents splitting by data source

Modal	Dataset	Category	Quantity	Year	Split type	Source
Ultrasound	BUSI	Binary	0.5k~1k	2020	O	[link]
	BUS	Binary	0.5k~1k	2022	O	[link]
	BUSBRA	Binary	1k~2k	2024	O	[link]
	TNSCUI	Binary	3k~4K	2020	O	[link]
	TUCC	Binary	10k~20k	-	O	[link]
Dermoscopy	ISIC2018	Binary	2k~3k	2018	O	[link]
	PH ²	Binary	<0.5k	2013	S	[link]
	SkinCancer	Binary	206	2024	S	[link]
X-Ray	Covidquex	Binary	2k ~ 3k	2021	S	[link]
	Montgomery	Binary	<0.5k	2014	S	[link]
	NIH-test	Binary	<0.5k	2019	S	[link]
	DCA	Binary	<0.5k	2019	S	[link]
Endoscopy	Kvasir-SEG	Binary	1k~2k	2020	S	[link]
	CVC-300	Binary	<0.5k	2017	S	[link]
	CVC-ClinicDB	Binary	0.5k~1k	2015	S	[link]
	Robotool	Binary	0.5k~1k	2021	S	[link]
MRI	Promise	Binary	1k~2k	2024	S	[link]
	ACDC	4-Class	<0.5k	2018	S	[link]
Fundus	CHASE	Binary	<0.5k	2012	S	[link]
	Stare	Binary	<0.5k	2000	S	[link]
	DRIVE	Binary	<0.5k	-	S	[link]
CT	Synapse	9-Class	3k~4k	2023	S	[link]
OCT	Cystoidfluid	Binary	1k~2k	2024	S	[link]
Nuclear	DSB2018	Binary	0.5k~1k	2018	S	[link]
	Cell	Binary	0.5k~1k	2018	S	[link]
Histopathology	Monusac	Binary	<0.5k	2016	S	[link]
	Tnbcnuclei	Binary	<0.5k	2018	S	[link]
	Glas	Binary	<0.5k	2015	S	[link]

Cell. The Cell dataset (Kuş & Aydın, 2024a) consists of 670 nuclei images with a resolution of 320×256 pixels. The data label is the cell nucleus segmentation area.

Glas. The Glas dataset (Sirinukunwattana et al., 2015) contains 165 H&E stained slide images for gland segmentation. The data label is the glandular lesion (or non-lesion) area of the Hematoxylin and Eosin image.

Monusac. The Monusac dataset (Kuş & Aydın, 2024a) includes 310 H&E stained digital tissue images. The data labels are the nucleus regions of H&E stained histology images.

Tnbcnuclei. The Tnbcnuclei dataset (Kuş & Aydın, 2024a) contains 50 pathological samples for binary segmentation. The data labels are the cell nucleus regions of Hematoxylin and Eosin stained histology images.

Synapse. The Synapse multi-organ dataset includes 30 abdominal CT scans with 8-organ segmentation. The data labels are 8 abdominal organs (aorta, gallbladder, left kidney, right kidney, liver, pancreas, spleen, stomach).

Cystoidfluid. The Cystoidfluid dataset (Kuş & Aydın, 2024a) contains 1,006 Optical Coherence Tomography images. The dataset is labeled the Cystoid Macular Edema (CME) region of the retina.

Table 5: Hybrid architecture model comparison.

Model	Deep Supervision	Pre-training	Zero-shot	P-value	Params (M)	FLOPs (G)	FPS
BEFUNet (Manzari et al., 2024)		✓		✓	42.61	7.95	69.89
CASCADE (Rahman & Marculescu, 2023a)	✓	✓			35.27	8.15	57.91
CFFormer (Li et al., 2025b)			✓	✓	158.44	71.17	30.28
DA-TransUNet (Sun et al., 2024)				✓	2.60	6.92	67.48
DS-TransUNet (Lin et al., 2022)	✓	✓	✓		171.34	51.15	24.28
D-TrAttUnet (Bougourzi et al., 2024)	✓			✓	104.16	54.00	53.85
EMCAD (Rahman et al., 2024)	✓	✓			26.76	5.60	56.17
EViT-UNet (Li et al., 2025d)		✓			54.79	8.36	16.73
FAT-Net (Wu et al., 2022)		✓			29.62	42.80	76.01
FCNFormer (Sanderson & Matuszewski, 2022)		✓	✓		52.94	40.88	25.70
GH-UNet (Wang et al., 2025b)	✓			✓	12.81	21.58	14.61
H2Former (He et al., 2023)					33.63	32.25	55.26
HiFormer (Heidari et al., 2023)		✓			34.14	17.75	68.12
LeViT-UNet (Xu et al., 2023a)		✓			17.53	27.24	102.91
LGMSNet (Dong et al., 2025)			✓	✓	2.32	4.89	105.04
MedFormer (Gao et al., 2023)					28.07	21.79	59.85
MedT (Valanarasu et al., 2021)		✓			1.37	2.41	5.15
MERIT (Rahman & Marculescu, 2023c)		✓		✓	147.68	33.28	18.69
MFMSNet (Wu et al., 2023)	✓	✓	✓		31.56	10.08	13.44
Mobile U-ViT (Tang et al., 2025b)			✓		6.21	10.43	96.80
MT-UNet (Wang et al., 2022c)				✓	75.07	57.72	11.23
Perspective-Unet (Hu et al., 2024)					111.08	124.48	41.80
ScribFormer (Li et al., 2024b)	✓			✓	47.91	44.63	35.25
SCUNet++ (Chen et al., 2024b)		✓			43.54	16.68	59.66
SwinUNETR (Hatamizadeh et al., 2021)					6.29	4.86	84.41
TransAttUnet (Chen et al., 2022)		✓			22.65	88.78	99.76
TransFuse (Zhang et al., 2021)	✓	✓			26.17	11.53	59.97
TransNorm (Azad et al., 2022)		✓			105.59	39.28	42.59
TransResUNet (Tomar et al., 2022)		✓			27.07	24.06	85.84
TransUNet (Chen et al., 2021)		✓			93.23	32.23	58.45
UCTransNet (Wang et al., 2022a)				✓	66.24	43.06	35.12
UNetV2 (Peng et al., 2025)	✓		✓	✓	25.13	5.40	60.33
UTNet (Gao et al., 2021)					14.41	20.49	76.67

DSB2018. The DSB2018 dataset (Hamilton, 2018) includes 670 Hematoxylin and Eosin (H&E)-stained nuclear images. The data label is the cell nucleus segmentation area.

D DETAILS OF MODEL ZOO

We conducted a comprehensive statistical analysis of the 100 models evaluated by U-bench, as shown in Tab. 6, 5 and 7.

Tab. 6 and Tab. 5 summarize the basic information of the single architecture and hybrid architecture respectively., quantifying critical metrics including deep supervision adoption, pre-training status, zero-shot capability, statistical significance (P-value), parameter count (Params), computational cost (FLOPs), and inference speed (FPS);

Tab. 7 further clarifies the training foundation of all evaluated models, documenting their publication year, venue, target dataset modality, and open-source repository links for reproducibility.

E DETAILS OF U-SCORE

Clinical deployment of segmentation models often requires operation under constrained resources. However, existing evaluations focus predominantly on segmentation performance, while failing to balance key computational factors such as model size, inference cost, and speed. This disconnect makes it difficult to assess real-world deployability. To bridge this gap, we introduce U-Score, a unified metric that quantifies the trade-off between performance and efficiency using quantile statistics under large-scale benchmark. Specifically, we report the 10th and 90th percentiles of IoU, Params, FLOPs, and FPS, as summarized in Tab. 8 and 9. The formulation is represented as follow.

Given model i , we compute IoU A_i across datasets, parameter P_i in millions, FLOPs G_i in GLOPs, and runtime speed S_i in FPS. We normalize each component using the 10th and 90th percentiles computed over the model zoo. Let Q_{10}^M and Q_{90}^M denote the 10th and 90th percentiles of metric M .

1350
1351
1352
1353
1354
1355
1356
1357
1358
1359
1360
1361
1362
1363
1364
1365
1366
1367
1368
1369
1370
1371
1372
1373
1374
1375
1376
1377
1378
1379
1380
1381
1382
1383
1384
1385
1386
1387
1388
1389
1390
1391
1392
1393
1394
1395
1396
1397
1398
1399
1400
1401
1402
1403

Table 6: Single-architecture model comparison.

Architecture	Model	Deep Supervision	Pre-training	Zero-shot	P-value	Params (M)	FLOPs (G)	FPS
CNN	AtU-Net (Oktay et al., 2018)				✓	34.88	66.63	126.09
	AURA-Net (Cohen & Uhlmann, 2021)					52.84	25.15	121.63
	CA-Net (Gu et al., 2020)				✓	2.79	5.99	31.71
	CaraNet (Lou et al., 2022)	✓	✓			44.59	11.50	26.82
	CENet (Gu et al., 2019b)					33.36	10.64	23.63
	CE-Net (Gu et al., 2019a)					29.00	8.90	103.22
	CFPN-Net (Lou et al., 2021)			✓		0.76	3.47	73.13
	CMU-Net (Tang et al., 2023)					49.93	91.25	83.28
	CMUNet (Tang et al., 2024)					3.15	7.42	161.14
	CPCANet (Huang et al., 2023a)					43.39	13.36	16.23
	CSCA U-Net (Shu et al., 2024)	✓				35.27	13.74	44.99
	DANet (Pramanik et al., 2024)	✓			✓	94.51	33.24	48.18
	DCSAU-Net (Xu et al., 2023b)					10.81	23.83	56.84
	DDS-UNet (Ou et al., 2025)					43.62	17.40	36.87
	DoubleUNetPlus (Jha et al., 2020a)	✓		✓		29.29	53.96	100.99
	ERDUnet (Li et al., 2024a)			✓		10.21	10.29	43.18
	ESKNet (Chen et al., 2023)				✓	26.71	45.28	75.38
	G-CASCADE (Rahman & Marculescu, 2023b)	✓	✓			26.63	5.54	62.77
	LFU-Net (Deng et al., 2023)					0.05	0.76	167.91
	LV-UNet (Jiang et al., 2024b)					0.92	0.21	139.30
	MALUNet (Ruan et al., 2022)					0.18	0.08	108.64
	MBSNet (Ye et al., 2021)					3.98	6.86	115.10
	MCA-Unet (Amer & Ye, 2023)	✓				8.66	58.02	12.26
	MDSA-UNet (Li et al., 2025c)					6.58	5.65	77.36
	MEGANet (Bui et al., 2024)	✓				29.27	11.71	59.62
	MMUNet (Yuan et al., 2024b)					17.73	24.04	46.93
	MSLAU-Net (Lan et al., 2025)			✓		21.88	6.27	35.34
	MSRF-Net (Srivastava et al., 2021)	✓			✓	22.50	109.73	33.16
	MultiResUNet (Ibtehaz & Rahman, 2020)					7.25	18.76	84.31
	PraNet (Fan et al., 2020)	✓	✓	✓	✓	50.01	11.96	27.55
	ResNet34UnetPlus (Zhou et al., 2018)				✓	26.90	37.63	84.54
	ResU-KAN (Wang et al., 2025a)					18.59	7.78	67.56
	ResUNetPlusPlus (Jha et al., 2019)					14.48	70.99	91.72
	RollingUnet (Liu et al., 2024c)					7.10	8.28	31.85
SimpleUNet (Yu et al., 2025)					0.06	0.74	414.31	
TA-Net (Wang et al., 2022b)					29.57	9.32	94.43	
TinyU-Net (Chen et al., 2024a)					0.48	1.66	150.32	
UACANet (Kim et al., 2021)	✓	✓	✓	✓	67.11	31.55	27.79	
U-KAN (Li et al., 2025a)					9.38	6.89	93.47	
ULite (Dinh et al., 2023)					0.88	0.76	323.06	
U-Net (Ronneberger et al., 2015)					34.53	65.52	137.05	
UNet3+ (Huang et al., 2020)					26.97	199.74	50.70	
UNetXt (Valanarasu & Patel, 2022)				✓	1.47	0.57	256.68	
UTANet (Luo et al., 2025)				✓	45.03	87.59	85.63	
nnUNet (Isensee et al., 2021)	✓			✓	92.46	115.79	314.56	
ResEncUNet-L (Isensee et al., 2024)	✓			✓	393.06	435.17	124.54	
Mamba	AC-MambaSeg (Nguyen et al., 2024)			✓	✓	7.42	6.27	35.64
	CFM-UNet (Niu et al., 2025)			✓	✓	52.96	6.17	38.08
	H-vmunet (Wu et al., 2025a)					6.44	0.74	16.30
	Mamba-UNet (Wang et al., 2024)		✓			15.48	4.60	94.47
	MedVKAN (Zhu et al., 2025)					43.58	14.13	45.91
	MUCM-Net (Yuan et al., 2024a)					0.08	0.06	107.24
	Swin-UMamba (Liu et al., 2024a)		✓			55.06	43.93	58.52
	Swin-UMambaD (Liu et al., 2024b)		✓			21.74	6.20	65.48
	UltraLight-VM-UNet (Wu et al., 2025b)			✓		0.04	0.06	82.45
	VM-UNet (Ruan & Xiang, 2024)			✓	✓	34.62	7.56	48.08
VM-UNetV2 (Zhang et al., 2024b)			✓		17.91	4.40	62.85	
RWKV	RWKV-UNet (Jiang et al., 2025)		✓			17.10	14.58	76.14
	U-RWKV (Ye et al., 2025)					2.82	6.90	107.52
	Zig-RiR (Chen et al., 2025)				✓	24.25	3.31	35.59
Transformer	DC-ViT (Zhang et al., 2024a)			✓		6.84	20.87	65.34
	ColonSegT (Jha et al., 2021)					5.01	62.16	135.43
	ConvFormer (Lin et al., 2023)		✓			115.61	121.13	43.05
	CSWin-UNet (Liu et al., 2025)		✓			23.57	6.14	33.05
	DAE-Former (Azad et al., 2023)		✓		✓	29.69	34.10	55.23
	MISSFormer (Huang et al., 2023b)		✓		✓	35.45	7.25	57.68
	Polyp-PVT (Dong et al., 2021)	✓	✓	✓	✓	25.11	5.30	67.64
	SwinUnet (Cao et al., 2022)		✓			41.34	8.69	63.25
UNETR (Hatamizadeh et al., 2022)				✓	87.51	26.41	104.25	

Table 7: Training modal information of all evaluation models.

Architecture	Model	Year	Publication	Modality	GitHub
	AttU-Net	2018	MIDL	CT	[link]
	AURA-Net	2021	ISBI	Microscopy	[link]
	CA-Net	2020	TMI	Dermoscopy, MRI	[link]
	CaraNet	2022	SPIE Medical Imaging	Colonoscopy, MRI	[link]
	CENet	2025	MICCAI	Dermoscopy, CT, MRI	[link]
	CE-Net	2019	TMI	Fundus, CT, Microscopy, OCT	[link]
	CFPNet-M	2021	Medical Imaging	Thermography, Microscopy, Colonoscopy, Dermoscopy, Fundus	[link]
	CMU-Net	2023	ISBI	Ultrasound	[link]
	CMUNetXt	2024	ISBI	Ultrasound	[link]
	CPCANet	2023	CMI	MRI, Dermoscopy	[link]
	CSCA U-Net	2024	AIIM	Colonoscopy, Pathology, Ultrasound	[link]
	DANet	2024	Plos one	Ultrasound	[link]
	DCSAU-Net	2023	CBM	Colonoscopy, Microscopy, Dermoscopy	[link]
	DDS-UNet	2025	The Visual Computer	Ultrasound, Dermoscopy, Colonoscopy	[link]
	DoubleUNetPlus	2020	IEEE CBMS	Colonoscopy, Dermoscopy, Microscopy	[link]
	ERDUNet	2024	TCSVT	Microscopy, Dermoscopy, Colonoscopy, Pathology, MRI	[link]
	ESKNet	2023	CMPB	Ultrasound	[link]
	G-CASCADE	2023	WACV	CT, MRI, Dermoscopy, Colonoscopy	[link]
	LFU-Net	2023	CMI	CT, MRI	[link]
	LV-UNet	2024	BIBM	Dermoscopy, Ultrasound, Colonoscopy	[link]
	MALUNet	2022	BIBM	Dermoscopy	[link]
	MBSNet	2021	MSSP	Dermoscopy, Ultrasound, Colonoscopy	[link]
CNN	MCA-UNet	2023	CMPBU	CT	[link]
	MDSA-UNet	2025	JBHI	Ultrasound, CT, Dermoscopy	[link]
	MEGANet	2024	WACV	Colonoscopy	[link]
	MMUNet	2024	BSPC	Histological image	[link]
	MSLAU-Net	2025	arXiv (cs.CV)	CT, MRI, Colonoscopy	[link]
	MSRF-Net	2021	JBHI	Colonoscopy, Microscopy, Dermoscopy	[link]
	MultiResUNet	2020	Neural networks	Microscopy, Dermoscopy, Colonoscopy, MRI	[link]
	PraNet	2020	MICCAI	Colonoscopy	[link]
	ResNet34UNetPlus	2018	TMI	Microscopy, CT, MRI	[link]
	ResUNetPlusPlus	2019	ISM	Colonoscopy	[link]
	RollingUNet	2024	AAAI	Ultrasound, Histological image, Dermoscopy, Fundus	[link]
	SimpleUNet	2025	arXiv	Ultrasound, Dermoscopy, Colonoscopy	[link]
	TA-Net	2022	WACV	Histological image	[link]
	TinyU-Net	2024	MICCAI	Dermoscopy, CT	[link]
	UACANet	2021	ACM MM	Colonoscopy	[link]
	ULite	2023	APSIPA	Dermoscopy, Microscopy, Histological image	[link]
	U-Net	2015	MICCAI	Microscopy, Microscopy	[link]
	UNet3+	2020	ICASSP	CT	[link]
	UNetXt	2022	MICCAI	Dermoscopy, Ultrasound	[link]
	UTANet	2025	AAAI	Histology Image, Microscopy, Abdominal CT, Dermoscopy	[link]
	ResU-KAN	2025	Applied Intelligence	Ultrasound, Histological, Colonoscopy	[link]
	U-KAN	2025	AAAI	Ultrasound, Histological image, Colonoscopy	[link]
	Mamba-UNet	2024	CoRR	MRI, CT	[link]
	MedVKAN	2025	arxiv	Microscopy, MRI, Ultrasound, CT	[link]
	Swin-UMambaD	2024	TMI	MRI, Endoscopy, Microscopy	[link]
	UltraLight-VM-UNet	2025	Patterns	Dermoscopy	[link]
	VM-UNet	2024	CoRR	Dermoscopy, CT	[link]
Mamba	VM-UNetV2	2024	ISBRA	Dermoscopy, Colonoscopy	[link]
	AC-MambaSeg	2024	ICGTSD	Dermoscopy	[link]
	CFM-UNet	2025	Scientific Reports	CT, MRI, Colonoscopy, MRI	[link]
	MUCM-Net	2024	CoRR	Dermoscopy	[link]
	Swin-UMamba	2024	MICCAI	MRI, Endoscopy, Microscopy	[link]
	H-vmunet	2024	arxiv	Colonoscopy, Dermoscopy, CT, MRI	[link]
	Zig-RiR	2025	TMI	Dermoscopy, CT, MRI, Microscopy	[link]
	RWKV-UNet	2025	CoRR	CT, MRI, Ultrasound, Colonoscopy, Dermoscopy, Histological image	[link]
	U-RWKV	2025	MICCAI	Ultrasound, Colonoscopy, Dermoscopy, CT	[link]
	DC-ViT	2024	CVPR	Natural images	[link]
	ColonSegT	2021	IEEE ACCESS	Colonoscopy	[link]
	CSWin-UNet	2025	Information Fusion	CT, MRI, Dermoscopy	[link]
	DAE-Former	2023	IWPIM	CT, Dermoscopy	[link]
	MISSFormer	2023	TMI	CT, MRI	[link]
	Polyp-PVT	2021	arXiv	Colonoscopy	[link]
	SwinUNet	2022	ECCVW	CT, MRI	[link]
	UNETR	2022	WACV	CT, MRI	[link]
	BEFNet	2024	arXiv	CT, Microscopy, Dermoscopy	[link]
	CASCADE	2023	WACV	CT, MRI, Colonoscopy	[link]
	CFFormer	2025	ESA	Ultrasound, Dermoscopy, Colonoscopy, CT, MRI	[link]
	ConvFormer	2023	MICCAI	Ultrasound, Dermoscopy, CT	[link]
	DA-TransUNet	2024	FBB	CT, Colonoscopy, X-ray, Dermoscopy, Endoscopy	[link]
	DS-TransUNet	2022	TIM	Colonoscopy, Dermoscopy, Histology, Microscopy	[link]
	D-TrAttUnet	2024	CBM	CT, Histology Image, Microscopy	[link]
	EMCAD	2024	CVPR	Colonoscopy, Dermoscopy, Ultrasound, CT, MRI	[link]
	EVIT-UNet	2025	ISBI	CT, Histology Image, Microscopy	[link]
	FAT-Net	2022	MIA	Dermoscopy	[link]
	FCNFormer	2022	MICCAI	Colonoscopy	[link]
	GH-UNet	2025	Digital Medicine	Dermoscopy, Colonoscopy, Fundus, MRI, CT	[link]
	H2Former	2023	TMI	Fundus, Colonoscopy, Dermoscopy, MRI, CT	[link]
	HiFormer	2023	WACV	CT, Dermoscopy, Microscopy	[link]
	LeViT-UNet	2023	PRCV	CT, MRI	[link]
	LGMSNet	2025	ECAI	Ultrasound, Dermoscopy, Colonoscopy, CT	[link]
	MADGNet	2024	CVPR	Ultrasound, Dermoscopy, Colonoscopy, Microscopy, CT	[link]
	MedFormer	2023	arXiv	MRI, CT	[link]
	MedT	2021	MICCAI	Ultrasound, Histology Image, Microscopy	[link]
	MERT	2023	MIDL	CT, MRI	[link]
	MFMSNet	2023	UMB	Ultrasound	[link]
	Mobile U-ViT	2025	ACM MM	Ultrasound, Dermoscopy, Colonoscopy, CT	[link]
	MT-UNet	2022	ICASSP	CT, MRI	[link]
	Perspective-UNet	2024	MICCAI	CT, MRI	[link]
	ScribFormer	2024	TMI	MRI, CT	[link]
	SCUNet++	2024	WACV	CT	[link]
	SwinUNETR	2021	MICCAI	MRI	[link]
	TransAttUnet	2022	TIM	Dermoscopy, X-ray, CT, Biological Image, Histology Image	[link]
	TransFuse	2021	MICCAI	Colonoscopy, Dermoscopy, X-ray, MRI	[link]
	TransNorm	2022	IEEE Access	CT, Dermoscopy, Microscopy	[link]
	TransResUNet	2022	CoRR	Colonoscopy	[link]
	TransUNet	2021	arXiv	Abdominal CT, MRI	[link]
	UCTransNet	2022	AAAI	Histology Image, Microscopy, CT	[link]
	UNetV2	2025	ISBI	Dermoscopy, Colonoscopy	[link]
	UTNet	2021	MICCAI	MRI	[link]

Table 8: In-domain per-dataset 10th and 90th percentiles of IoU, Params, FLOPs, and FPS.

Modality	Dataset	IoU (%)		Params (M)		FLOPs (G)		FPS	
		Q_{10}^A	Q_{90}^A	Q_{10}^P	Q_{90}^P	Q_{10}^G	Q_{90}^G	Q_{10}^S	Q_{90}^S
Ultrasound	BUSI	0.58	0.71	0.39	4.32	0.88	4.20	24.28	121.63
	BUSBRA	0.78	0.84	0.39	4.32	0.88	4.20	24.28	121.63
	TNSCUI	0.66	0.78	0.39	4.32	0.88	4.20	24.28	121.63
Dermoscopy	ISIC2018	0.81	0.84	0.39	4.32	0.88	4.20	24.28	121.63
	SkinCancer	0.79	0.85	0.39	4.32	0.88	4.20	24.28	121.63
Endoscopy	Kvasir	0.75	0.84	0.39	4.32	0.88	4.20	24.28	121.63
	Robotool	0.69	0.85	0.39	4.32	0.88	4.20	24.28	121.63
Fundus	CHASE	0.47	0.81	0.39	4.32	0.88	4.20	24.28	121.63
	DRIVE	0.15	0.62	0.39	4.32	0.88	4.20	24.28	121.63
Nuclei	DSB2018	0.85	0.88	0.39	4.32	0.88	4.20	24.28	121.63
	CellNuclear	0.78	0.84	0.39	4.32	0.88	4.20	24.28	121.63
Histopathology	Glas	0.63	0.83	0.39	4.32	0.88	4.20	24.28	121.63
	Monusac	0.53	0.67	0.39	4.32	0.88	4.20	24.28	121.63
X-Ray	Covidquex	0.63	0.70	0.39	4.32	0.88	4.20	24.28	121.63
	Montgomery	0.92	0.96	0.39	4.32	0.88	4.20	24.28	121.63
	DCA	0.51	0.63	0.39	4.32	0.88	4.20	24.28	121.63
MRI	ACDC	0.73	0.85	0.39	4.32	0.88	4.20	24.28	121.63
	Promise	0.78	0.87	0.39	4.32	0.88	4.20	24.28	121.63
CT	Synapse	0.55	0.72	0.39	4.32	0.88	4.20	24.28	121.63
OCT	Cystoidfluid	0.63	0.83	0.39	4.32	0.88	4.20	24.28	121.63

Table 9: Zero-shot per-dataset 10th and 90th percentiles of IoU, Params, FLOPs, and FPS.

Source	Target	IoU (%)		Params (M)		FLOPs (G)		FPS	
		Q_{10}^A	Q_{90}^A	Q_{10}^P	Q_{90}^P	Q_{10}^G	Q_{90}^G	Q_{10}^S	Q_{90}^S
BUSI	BUS	0.60	0.81	0.39	4.32	0.88	4.20	24.28	121.63
BUSBRA	BUS	0.78	0.85	0.39	4.32	0.88	4.20	24.28	121.63
TNSCUI	TUCC	0.56	0.64	0.39	4.32	0.88	4.20	24.28	121.63
ISIC2018	PH2	0.82	0.85	0.39	4.32	0.88	4.20	24.28	121.63
Kvasir	CVC300	0.61	0.80	0.39	4.32	0.88	4.20	24.28	121.63
Kvasir	CVC-ClinicDB	0.60	0.75	0.39	4.32	0.88	4.20	24.28	121.63
CHASE	STARE	0.30	0.54	0.39	4.32	0.88	4.20	24.28	121.63
Monusac	Tnbcnuclei	0.25	0.44	0.39	4.32	0.88	4.20	24.28	121.63
Montgomery	NIH-test	0.58	0.82	0.39	4.32	0.88	4.20	24.28	121.63

The normalized scores are defined as:

$$\begin{aligned}
 a_i &= \text{clip} \left(\frac{A_i - Q_{10}^A}{Q_{90}^A - Q_{10}^A}, 0, 1 \right), & p_i &= \text{clip} \left(\frac{\log Q_{90}^P - \log P_i}{\log Q_{90}^P - \log Q_{10}^P}, 0, 1 \right), \\
 g_i &= \text{clip} \left(\frac{\log Q_{90}^G - \log G_i}{\log Q_{90}^G - \log Q_{10}^G}, 0, 1 \right), & s_i &= \text{clip} \left(\frac{S_i - Q_{10}^S}{Q_{90}^S - Q_{10}^S}, 0, 1 \right).
 \end{aligned} \tag{1}$$

Then, we compute an efficiency subscore via the weighted harmonic mean of p_i , g_i , and s_i . Since we regard storage, cost, and speed as equally important, we set $w_P = w_G = w_S = \frac{1}{3}$, leading to:

$$\text{Eff}_i = \frac{3}{\frac{1}{p_i} + \frac{1}{g_i} + \frac{1}{s_i}}. \tag{2}$$

Finally, we combine accuracy and efficiency via a harmonic mean. To balance the two factors equally, we set $\alpha = 0.5$, yielding:

$$\text{U-Score}_i = \frac{2}{\frac{1}{\alpha_i} + \frac{1}{\text{Eff}_i}}. \tag{3}$$

Table 10: Robustness of U-Score rankings over 105 configurations (Five choices of α , Seven efficiency weightings w , Three quantile pairs). Baseline: $\alpha = 0.5$, $(w_P, w_G, w_S) = (1, 1, 1)$, q -pair = (0.10, 0.90).

Metric	Mean	Std	Min	25%	Median	75%
Kendall- τ vs. base U-Score ranking	0.77	0.08	0.55	0.71	0.77	0.83
Spearman- ρ vs. base U-Score ranking	0.90	0.06	0.72	0.86	0.91	0.95
Kendall- τ vs. IoU	0.19	0.14	-0.07	0.06	0.19	0.30
Top-10 keep	0.86	0.12	0.60	0.80	0.90	0.90

E.1 ABLATION U-SCORE SENSITIVITY OF WEIGHTS AND PERCENTILES

We supplement the system with a comprehensive sensitivity analysis, performing a grid search over the following configurations: the accuracy–efficiency trade-off $\alpha \in \{0.25, 0.33, 0.5, 0.67, 0.75\}$, efficiency weights $(w_P, w_G, w_S) \in \{(1, 1, 1), (2, 1, 1), (1, 2, 1), (1, 1, 2), (3, 1, 1), (1, 3, 1), (1, 1, 3)\}$, and quantile pairs (10/90, 5/95, 20/80). We evaluate ranking stability using Kendall- τ , Spearman- ρ , and Top- k monotonicity. For each configuration, we compute: (I) Kendall- τ and Spearman- ρ between the resulting ranking and the baseline U-Score ranking (our default setting: $\alpha = 0.5$, $(w_P, w_G, w_S) = (1, 1, 1)$, q -pair = (0.10, 0.90)); (II) Kendall- τ against the IoU-only ranking; and (III) Top- k set stability (the overlap of the Top-10 models with the baseline Top- k under a deterministic tie-breaking scheme).

The results are summarized in Table 10. We observe that the rankings are highly stable: Kendall- τ versus the baseline has a mean of 0.77, a median of 0.77, and remains ≥ 0.55 even in the worst configuration; Spearman- ρ versus the baseline has a mean of 0.90 and a median of 0.91. The Top-10 set also exhibits strong robustness, with a mean overlap of 0.86, a median of 0.90, and never dropping below 0.60. Importantly, U-Score is distinct from pure accuracy: Kendall- τ relative to the IoU-only ranking is much lower, with a mean of 0.19 (median 0.19), demonstrating that U-Score genuinely captures the accuracy–efficiency trade-off. These results collectively underscore the robustness and stability of the proposed U-Score.

E.2 ABLATION U-SCORE SENSITIVITY OF ACCURACY-EFFICIENCY (α)

We further investigate the impact of the accuracy–efficiency trade-off parameter α on U-Score rankings, isolating α while keeping $(w_P, w_G, w_S) = (1, 1, 1)$ and q -pair = (0.10, 0.90). Table 11 shows that changing α produces stable rankings, with Kendall- τ values consistently above 0.8 across all settings, and the Top-10 overlap remains between 0.80 and 1.00. These results demonstrate that U-Score provides a robust benchmark, where users can adjust α to reflect deployment priorities without introducing significant ranking shifts.

In Table 12 and Table 13, we isolate the effect of the quantile pair (q_{pair}) and efficiency weights (w_P, w_G, w_S) . The results indicate that moderate changes in quantile ranges (e.g., (0.05, 0.95) to (0.20, 0.80)) have minimal impact on U-Score rankings, with Kendall- τ values ranging from 0.76 to 1.00. The Top-10 overlap stays high, with most configurations showing stable rankings. This shows that U-Score remains reliable even under adjustments to the quantile clipping range. Similarly, varying the efficiency weights (w_P, w_G, w_S) does not drastically alter the leaderboard. Kendall- τ values between 0.86 and 0.94 and Top-10 overlap values above 0.9. This flexibility allows users to bias U-Score towards their desired trade-offs (e.g., memory, computation, or latency).

Finally, we add a comprehensive Leave-One-Modality-Out (LOMO) evaluation using the suggested ‘closest-dataset IoU heuristic’ as a strong, label-free baseline. On IoU-only ranking (Table 14, left), this heuristic is extremely competitive because IoU is highly modality-specific, and transferring the ranking from the closest source dataset provides a near-oracle estimate. The advisor therefore does not surpass the heuristic in accuracy-only setting. However, when switching to the multi-objective U-Score (accuracy–efficiency trade-offs), the picture reverses: the advisor outperforms the heuristic in 7 out of 10 modalities, including large gains on CT (+0.056 NDCG@10) and Pathology (+0.027), demonstrating that handcrafted similarity based solely on IoU does not generalize to multi-objective optimization, while the advisor captures cross-modal architectural patterns that transfer better. Finally, our deployment-time evaluation reveals complementary strengths. The heuristic

Table 11: Sensitivity of U-Score to the accuracy–efficiency weight α . We report Kendall- τ vs. the baseline U-Score ranking ($\alpha = 0.5, w_P, w_G, w_S = (1, 1, 1), q\text{-pair} = (0.10, 0.90)$), Kendall- τ vs. IoU-only, and the median Top-10 keep.

α	τ_{base}	τ_{IoU}	Top-10 keep
0.25	0.82	-0.01	0.90
0.33	0.89	0.06	1.00
0.50	1.00	0.17	1.00
0.67	0.92	0.25	0.90
0.75	0.87	0.31	0.80

Table 12: Sensitivity of U-Score to the quantile pair ($q_{q\text{-pair}}$). We report Kendall- τ vs. the baseline U-Score ranking ($\alpha = 0.5, w_P, w_G, w_S = (1, 1, 1), q\text{-pair} = (0.10, 0.90)$), Kendall- τ vs. IoU-only, and the median Top-10 keep.

q_{pair}	τ_{base}	τ_{IoU}	Top-10 keep
(0.05, 0.95)	0.90	0.14	1.00
(0.10, 0.90)	1.00	0.17	1.00
(0.20, 0.80)	0.76	0.31	0.80

Table 13: Sensitivity of U-Score to the efficiency weight (w_P, w_G, w_S). We report Kendall- τ vs. the baseline U-Score ranking ($\alpha = 0.5, w_P, w_G, w_S = (1, 1, 1), q\text{-pair} = (0.10, 0.90)$), Kendall- τ vs. IoU-only, and the median Top-10 keep.

(w_P, w_G, w_S)	τ_{base}	τ_{IoU}	Top-10 keep
(1, 1, 1)	1.00	0.17	1.00
(1, 1, 2)	0.92	0.19	1.00
(1, 1, 3)	0.87	0.21	1.00
(1, 2, 1)	0.90	0.15	1.00
(1, 3, 1)	0.86	0.14	1.00
(2, 1, 1)	0.94	0.17	0.90
(3, 1, 1)	0.90	0.17	0.90

Table 14: Model Advisor vs. closest-dataset heuristic under Leave-One-Modality-Out (LOMO). A-NDCG and B-NDCG denote Advisor and Baseline NDCG@10, respectively. A-Trial and B-Trial report the number of trials needed to find a top-10% model. The heuristic is extremely strong for IoU-only ranking due to modality-specific performance, while the advisor generalizes better for the multi-objective U-Score and yields substantial trial reductions when no close source modality exists.

Modality	IoU LOMO				U-Score LOMO			
	A-NDCG	B-NDCG	A-Trial	B-Trial	A-NDCG	B-NDCG	A-Trial	B-Trial
Ultrasound	0.676	0.946	3.67	1.00	0.845	0.841	1.00	2.00
Dermoscopy	0.671	0.917	4.00	1.00	0.831	0.813	10.0	2.00
Endoscopy	0.616	0.861	3.00	2.50	0.837	0.855	4.00	2.50
Fundus	0.783	0.949	3.00	1.00	0.834	0.875	7.00	1.50
Histopathology	0.728	0.905	4.67	1.00	0.871	0.844	5.67	1.33
Nuclear	0.759	0.924	4.00	1.00	0.864	0.853	7.00	3.00
X-ray	0.729	0.954	3.67	1.33	0.859	0.870	5.00	1.00
MRI	0.682	0.855	3.00	1.00	0.851	0.838	4.00	2.00
CT	0.715	0.757	2.00	1.00	0.858	0.802	1.00	5.00
OCT	0.752	0.946	5.00	1.00	0.857	0.839	5.00	2.00

excels when a close source modality exists, but collapses in hard cases (e.g., CT: 5 trials), whereas the advisor reliably identifies a top-10% model in just 1 trial, highlighting its substantial practical benefit in real model-selection scenarios.

F IMPLEMENTATION AND EVALUATION DETAILS

F.1 FOREGROUND CHARACTERIZATION METRICS

We employ three metrics to characterize dataset-level foreground properties: scale, boundary sharpness, and shape regularity.

Foreground scale. Foreground scale is measured as the ratio between the foreground area A_f and the total image area A_t .

$$A = \frac{A_f}{A_t}. \quad (4)$$

We categorize samples as *small-scale* if $A < 0.05$ and *large-scale* otherwise.

Shape complexity. We quantify the sharpness of the segmented foreground boundaries using a composite score S derived from two standard geometric descriptors: *circularity* and *solidity*. We categorize samples with $S < 0.5$ as *irregular*, and those with $S \geq 0.5$ as *regular*. The boundary sharpness score S is defined as:

$$S = 0.5 \times \text{Circularity} + 0.5 \times \text{Solidity}. \quad (5)$$

Circularity measures how close the shape is to a perfect circle. It is defined as: $\text{Circularity} = \frac{4\pi A_f}{P^2}$, where A_f is the foreground area and P is the perimeter of the contour. Solidity evaluates the extent to which a shape fills its convex hull. It is given by: $\text{Solidity} = \frac{A_f}{A_c}$, where A_f is the foreground area and A_c is the area of its convex hull.

Boundary Sharpness. We assess boundary sharpness using two complementary measures: *boundary width* and *boundary contrast*. Given a binary mask m , we first construct a narrow boundary ring by applying morphological dilation and erosion. The boundary width is then computed as the ratio between the area of this ring and the contour perimeter: $w = \frac{\text{Area}(\text{Ring})}{P + \epsilon}$, where P denotes the sum of contour perimeters. A larger w indicates blurrier boundaries, while a smaller w corresponds to sharper edges. To evaluate intensity separation across the boundary, we form two narrow bands: one inside the mask and one outside, each of width t pixels. Let (μ_{in}, σ_{in}) and $(\mu_{out}, \sigma_{out})$ denote the mean and standard deviation of pixel intensities inside and outside the boundary band. The boundary contrast is defined as $\text{CNR} = \frac{|\mu_{in} - \mu_{out}|}{\sigma_{in} + \sigma_{out} + \epsilon}$. To obtain a unified measure of boundary clarity, we normalize both w and CNR to $[0, 1]$ across the dataset. A composite blur score is then computed as:

$$B = \frac{w_{norm}}{w_{norm} + c_{norm} + \epsilon}, \quad (6)$$

where w_{norm} and c_{norm} are the normalized boundary width and contrast, respectively. We categorize samples with $b < 0.6$ as *clear*, and those with $b \geq 0.6$ as *blur*.

F.2 MODEL ADVISOR AGENT SETTINGS

We construct a comprehensive feature space that integrates both continuous and discretized descriptors from models and datasets. For model-level attributes, we discretize storage (parameter) into four scales (Tiny: 0-10M, Small: 10-50M, Medium: 50-200M, Large: >200M), computation cost (FLOPs) into three levels (Low: 0-10 GFLOPs, Medium: 10-100 GFLOPs, High: >100 GFLOPs), and inference speed (FPS) into three categories (Slow: <15 FPS, Medium: 15-60 FPS, Fast: >60 FPS). On the data characteristics side, we discretize foreground-related properties: foreground scale (< 0.05 vs. ≥ 0.05 , denoting small vs. large targets), shape complexity (< 0.5 vs. ≥ 0.5 , irregular vs. regular), and boundary sharpness (< 0.6 vs. ≥ 0.6 , clear vs. blurry). We train an XGBRanker with the rank:pairwise objective on 18 in-domain datasets, reserving 2 datasets (BUSI and Skin-Cancer) for testing. Scores are normalized into relevance values within each dataset, with higher relevance indicating better relative performance. Dataset-level grouping is used to enforce within-dataset ranking consistency during training. At evaluation, the ranker outputs predicted scores, which are converted into ranked lists for each dataset. Performance is assessed using NDCG@50/20 for ranking quality, MAP for precision under binary relevance, and correlation metrics (Spearman) to quantify alignment between predicted and ground-truth orderings. Finally, the agent exports the recommended models per test dataset, providing a practical reference list for downstream selection.

1674 F.2.1 DATA PREPROCESSING

1675
1676 **Experimental Data Split.** For all experiments on the unified dataset, we used the same train-test
1677 split. For data without a clear train-test split in the dataset source, we adopted a random split; for
1678 data with a known train-test split in the dataset source, we followed the original split. The division
1679 method of each dataset is shown in Tab. 4, where 'O' denotes our self-defined division and 'S'
1680 denotes the division consistent with the referenced data source.

1681 F.2.2 RETRAINING AND INFERENCE DETAILS

1682
1683 **Training and Inference Protocol.** The experiments are utilizing eight NVIDIA H20 GPUs. A total
1684 of 100 models are trained with 6000 hours. We provide a fully reproducible description in the
1685 Table 16. All FPS values in U-Score are measured as pure forward-pass latency (no dataloader, I/O,
1686 or post-processing), using batch size 1, on our compute cluster equipped with $8 \times$ NVIDIA H20
1687 GPUs and Intel Xeon Platinum 8558 CPUs (2×48 cores, OMP/MKL threads fixed to 1). The imple-
1688 mentation is based on Python 3.9 and PyTorch 2.4.0 (CUDA 12.4, cuDNN 9.1); no torch.compile,
1689 TensorRT, graph mode, or mixed-precision inference is used (FP32 only). Before timing, each
1690 model is warmed up for 10 iterations, followed by 30 timed iterations, using torch.cuda.Event with
1691 GPU synchronization. The model structure files are primarily obtained from the open-source code
1692 of the original models, with only minor modifications (e.g. input and output channels) to some input
1693 parameters to adapt to our framework.

1694 Table 15: Hyperparameters in U-Bench

1696 Optimizer	1696 Learning Rate	1696 Epochs	1696 Random Seed	1696 Batch Size
1697 SGD (Momentum=0.9, Weight Decay=0.0001)	1697 0.01	1697 300	1697 41	1697 8

1698
1699 **Data augmentation.** Following prior works (Valanarasu & Patel, 2022; Tang et al., 2023; 2024;
1700 Chen et al., 2024a; Tang et al., 2025b; Ye et al., 2025; Jiang et al., 2025; Dong et al., 2025), we
1701 rescale all images to a resolution of 256×256 by default and apply standard data augmentation.
1702 For models that require a fixed input size (e.g., Swin Transformer variants designed for $224 \times$
1703 224 inputs), we preserve their original settings without rescaling. For 3D datasets (e.g. Synapse
1704 and ACDC), we follow the same approach as previous methods such as TransUNet Chen et al.
1705 (2021), CASCADE Rahman & Marculescu (2023a), SwinUnet Cao et al. (2022), and Mobile U-
1706 ViT Tang et al. (2025b), where we process 3D data by slicing along the axial (transverse) plane
1707 (Z-axis). Augmentations include random 90° rotations, random horizontal and vertical flips, and
1708 normalization. To ensure fair comparisons, the same preprocessing pipeline is applied consistently
1709 across all experiments. Notably, for models that adopt deep supervision, we retain their original
1710 training strategy to enable accurate performance evaluation.

1711 **Training Settings.** Following previous work (Dong et al., 2025; Tang et al., 2024; 2025b; Chen
1712 et al., 2021; Wang et al., 2024; Ye et al., 2025), we unify training settings across all models to
1713 ensure fair comparisons, as summarized in Tab. 15. Moreover, we use commonly adopted loss
1714 configurations (Dong et al., 2025; Tang et al., 2024; 2025b; Ye et al., 2025) to promote generalizable
1715 results and enable more equitable performance evaluation.

1716 **Loss Function.** Specifically, for the ground truth y and the predicted output \hat{y} , the loss function is
1717 defined as:

$$1718 \mathcal{L} = 0.5 \times BCE(\hat{y}, y) + Dice(\hat{y}, y), \quad (7)$$

1719 where BCE denotes the binary cross-entropy loss and Dice denotes the Dice loss. Note that for 3D
1720 data ACDC and Synapse, we follow CASCADE (Rahman & Marculescu, 2023a) weights $0.5 \times$
1721 $BCE(\hat{y}, y), 0.7 \times Dice(\hat{y}, y)$

1722 F.3 METRICS

1723
1724 **Intersection over Union (IoU)** IoU quantifies the overlap between two regions (predicted A and
1725 ground-truth B) as:

$$1726 IoU(\hat{Y}, Y) = \frac{|\hat{Y} \cap Y|}{|\hat{Y} \cup Y|}, \quad (8)$$

Table 16: Measurement Protocol.

<i>Inference Hardware</i>	
GPU Model	8 × NVIDIA H20 (FPS measured on a single GPU)
GPU Memory	96 GB per GPU
CPU Model	Intel Xeon Platinum 8558
CPU Cores / Threads	48 cores × 2 sockets, 2 threads/core (192 threads total)
OMP Threads	OMP_NUM_THREADS=1
MKL Threads	MKL_NUM_THREADS=1
<i>Torch & Cuda Version</i>	
Python Version	Python 3.9.0
PyTorch Version	PyTorch 2.4.0
CUDA Version	CUDA 12.4
cuDNN Version	cuDNN 9.1.0
<i>Precision & Compute Settings</i>	
Precision Mode	FP32 only
Mixed Precision	AMP / FP16 / BF16 disabled
TF32	Disabled (<code>allow_tf32=False</code>)
Acceleration Libraries	No TensorRT / no <code>torch.compile</code> / no CUDA Graphs
<i>Resolution Policy</i>	
CNN, ViT, RWKV, Hybrid Models	256 × 256
Swin-based variants	224 × 224
FLOPs Alignment	Same resolution as FPS measurement
<i>Timing Protocol</i>	
Batch Size	1
Warm-up Iterations	10
Timed Iterations	30
Timing Method	<code>torch.cuda.Event(enable_timing=True)</code>
Synchronization	Explicit <code>torch.cuda.synchronize()</code> per iteration
<i>Isolation & Clean Measurement</i>	
Dataloader	Disabled (no workers)
I/O Operations	Disabled
Post-Processing	Disabled
Model Mode	<code>model.eval()</code> , dropout disabled
GPU Usage Policy	Single-GPU measurement, no concurrent jobs

where $|\hat{Y} \cap Y|$ is the area of intersection, and $|\hat{Y} \cup Y|$ is the area of union.

U-Score. To address the limitation that existing evaluations primarily focus on segmentation performance while failing to balance key computational factors such as model size, inference cost, and speed-making it difficult to assess practical deployment capabilities-we construct the U-Score based on quantile statistics. A detailed description is provided in Appendix E.

Normalized Discounted Cumulative Gain (NDCG)

NDCG evaluates the “usefulness” of a ranked list by accounting for two key factors: (1) the *relevance* of each item, and (2) the *position* of relevant items (penalizing lower-ranked relevant items via discounting). It is normalized to a range of $[0, 1]$ to enable cross-task comparisons.

First, the *Discounted Cumulative Gain (DCG)* is defined to measure the cumulative relevance of a ranked list up to position k (denoted as $DCG@k$):

$$DCG@k = \sum_{i=1}^k \frac{rel_i}{\log_2(i+1)} \quad (9)$$

where:

- k : The cutoff position (e.g., $k = 10$ for $NDCG@10$, focusing on top-10 results).
- rel_i : The *relevance score* of the i -th item in the ranked list. For binary relevance (relevant/irrelevant).
- $\log_2(i+1)$: The discount factor, which reduces the contribution of items ranked later (since users are less likely to inspect lower positions).

To normalize DCG across different queries/tasks (where the maximum possible relevance varies), the *Ideal DCG (IDCG)*-the maximum possible $DCG@k$ for a given set of items-is computed by

1782 ranking all relevant items in descending order of rel_i :

$$1783 \text{IDCG}@k = \sum_{i=1}^{\min(k, |R|)} \frac{rel'_i}{\log_2(i+1)} \quad (10)$$

1786 where:

- 1788 • R : The set of all relevant items for the query/task.
- 1789 • $|R|$: The total number of relevant items.
- 1790 • rel'_i : The i -th highest relevance score among all items in R (i.e., the ideal ranking).

1792 NDCG@k is defined as the ratio of DCG@k to IDCG@k. To avoid division by zero (when no
1793 relevant items exist, $\text{IDCG}@k = 0$), NDCG@k is set to 0 in this edge case:

$$1794 \text{NDCG}@k = \begin{cases} 0 & \text{if } \text{IDCG}@k = 0, \\ \frac{\text{DCG}@k}{\text{IDCG}@k} & \text{otherwise.} \end{cases} \quad (11)$$

1797 For experiments with multiple queries/tasks (e.g., a retrieval dataset with 1k queries), the *mean*
1798 *NDCG@k*-the average of NDCG@k across all queries-is reported. In Table 3, NDCG@k values for
1799 $k = 5$ and $k = 20$ are provided.

1801 Mean Average Precision (MAP)

1802 MAP quantifies the average precision of relevant items in a ranked list, aggregated across all
1803 queries/tasks. It is particularly useful for scenarios where "early relevant items" (high precision
1804 at top positions) are critical (e.g., information retrieval, recommendation systems).

1805 First, *Average Precision (AP)* for a single query q is defined as the average of the precision of the
1806 ranked list at the position of each relevant item:

$$1807 \text{AP}(q) = \frac{1}{|R_q|} \sum_{r \in R_q} \text{Prec}(k_r) \quad (12)$$

1810 where:

- 1812 • q : A single query (or task instance) from the query set Q ;
- 1813 • R_q : The set of all relevant items for query q (if $|R_q| = 0$, $\text{AP}(q) = 0$ by convention);
- 1814 • k_r : The position of relevant item r in the ranked list for q ;
- 1815 • $\text{Prec}(k_r)$: The precision at position k_r , defined as $\text{Prec}(k_r) = \frac{\text{numRel}(k_r)}{k_r}$, where $\text{numRel}(k_r)$ is
1816 the number of relevant items in the top- k_r positions.

1818 For a set of $|Q|$ queries, MAP is the average of AP scores across all queries:

$$1819 \text{MAP} = \frac{1}{|Q|} \sum_{q \in Q} \text{AP}(q) \quad (13)$$

1822 Similar to NDCG, MAP ranges from $[0, 1]$: a value of 1 indicates all relevant items are ranked first
1823 (perfect precision at every relevant position), while 0 indicates no relevant items are retrieved.

1824 Spearman's Rank Correlation Coefficient

1825 Spearman's rank correlation coefficient quantifies the *monotonic relationship* between two ranked
1826 variables. It is particularly useful for evaluating how well the order of items (e.g., predicted rankings
1827 by a model and ground-truth rankings) aligns, making it relevant for tasks where the consistency of
1828 relative ordering matters (e.g., comparing ranked recommendations or human judgments).

1830 Formally, Spearman's rank correlation coefficient ρ between two variables X (e.g., model-generated
1831 ranks) and Y (e.g., ground-truth ranks) (each with n paired observations) is defined as:

$$1832 \rho = 1 - \frac{6 \sum_{i=1}^n d_i^2}{n(n^2 - 1)} \quad (14)$$

1833 where:

Table 17: Top-10 performing variants across each dataset on source domains. Baseline U-Net is highlighted (gray background), and statistical significance of p-value is highlighted: $p < 0.0001$, $p < 0.001$, $p < 0.05$, $p < 0.05$, and $P > 0.05$ (Not significant).

Rank	Ultrasound					Endoscopy			Dermoscopy					
	BUSI	BUSBRA	TNSCUI	Kvasir	Robotool	ISIC2018	SkinCancer							
1	RWKV-UNet	72.32	RWKV-UNet	84.76	RWKV-UNet	80.06	Swin-umamba	85.56	MEGANet	86.25	RWKV-UNet	84.97	RWKV-UNet	87.48
2	PraNet	71.63	EVIT-UNet	84.36	MEGANet	79.01	VMUNet	84.90	RWKV-UNet	85.95	CFFormer	84.89	DA-TransUNet	87.22
3	Mobile U-ViT	71.59	CaraNet	84.31	MADGNet	78.91	UACANet	84.81	AURA-Net	85.78	MEGANet	84.50	MSLAU-Net	86.80
4	DA-TransUNet	71.47	MADGNet	84.27	TA-Net	78.85	CFFormer	84.57	TA-Net	85.62	Swin-umamba	84.49	PraNet	86.38
5	MEGANet	71.47	TA-Net	84.17	UACANet	78.83	RWKV-UNet	84.53	EVIT-UNet	85.39	PraNet	84.42	FCBFormer	86.33
6	TransResUNet	71.27	FAT-Net	84.15	EVIT-UNet	78.75	FCBFormer	84.50	TransResUNet	85.30	TransResUNet	84.38	EMCAD	86.20
7	MADGNet	71.24	UACANet	84.07	CaraNet	78.69	PraNet	84.39	MADGNet	85.21	TA-Net	84.34	MCA-UNet	86.17
8	CFFormer	70.91	FCBFormer	84.00	Swin-umamba	78.64	CASCADE	84.34	CE-Net	85.11	CE-Net	84.32	CaraNet	86.01
9	ESKNet	70.88	MEGANet	83.99	FAT-Net	78.57	CE-Net	84.32	PraNet	85.10	CaraNet	84.26	TransNorm	85.86
10	CASCADE	70.81	AURA-Net	83.95	UTANet	78.51	MADGNet	84.32	UACANet	84.65	AURA-Net	84.25	AURA-Net	85.56
	U-Net (#68)	65.58	U-Net (#41)	82.91	U-Net (#58)	75.99	U-Net (#70)	80.11	U-Net (#23)	81.24	U-Net (#61)	82.78	U-Net (#77)	80.94

Rank	X-Ray				MRI			Fundus						
	Covidqex	Montgomery	DCA	Promise	ACDC	CHASE	DRIVE							
1	AURA-Net	70.85	RWKV-UNet	96.21	DA-TransUNet	64.90	RWKV-UNet	87.56	CENet	85.54	CMU-Net	84.33	FCBFormer	64.25
2	RWKV-UNet	70.75	DA-TransUNet	96.17	UTANet	64.23	FCBFormer	87.29	Swin-umambaD	85.45	AntU-Net	84.20	MTUNet	63.21
3	CaraNet	70.61	MEGANet	96.12	EVIT-UNet	63.81	MADGNet	87.26	DoubleUNet	85.33	U-Net	84.07	ColonSegNet	63.19
4	EVIT-UNet	70.33	TransAttUNet	96.03	MADGNet	63.81	EVIT-UNet	87.05	RWKV-UNet	85.20	UNet3plus	83.69	UTNet	63.17
5	TA-Net	70.20	RollingUNet	96.01	MEGANet	63.77	Perspective-UNet	87.03	DDANet	85.11	Perspective-UNet	82.86	ESKNet	63.15
6	MEGANet	70.19	DDANet	95.97	ESKNet	63.69	MEGANet	87.00	AntU-Net	85.01	UCTransNet	82.82	CMU-Net	62.85
7	PraNet	70.09	MT-UNet	95.90	DDANet	63.65	TransResUNet	86.95	EVIT-UNet	84.91	ESKNet	82.69	Swin-umamba	62.75
8	CE-Net	70.04	TransResUNet	95.89	RWKV-UNet	63.61	U-KAN	86.89	FCBFormer	84.90	ColonSegNet	82.20	UNet3plus	62.54
9	TransResUNet	69.81	Mobile U-ViT	95.89	UTNet	63.54	PraNet	86.88	G-CASCADE	84.89	MTUNet	82.00	RollingUNet	62.49
10	MADGNet	69.77	UNet3plus	95.88	U-Net	63.30	CMU-Net	86.87	MSRFNet	84.78	Swin-umamba	81.65	D-TransUNet	62.48
	U-Net (#31)	68.52	U-Net (#11)	95.87			U-Net (#29)	86.30	U-Net (#23)	84.32			U-Net (#14)	61.81

Rank	Histopathology			Nuclear			CT			OCT		
	EMCAD	GLAS	Monusac	DSB2018	CellNuclear	Synapse	Cystoidfluid					
1	EMCAD	85.85	MT-UNet	69.27	MT-UNet	88.74	MT-UNet	84.93	CENet	74.70	UNet3plus	85.76
2	RWKV-UNet	85.75	RWKV-UNet	68.96	DoubleUNet	88.61	TransAttUNet	84.88	Perspective-UNet	73.69	Swin-umamba	85.06
3	CASCADE	85.17	UTANet	68.39	TransAttUNet	88.49	AURA-Net	84.87	G-CASCADE	73.54	UTANet	84.89
4	MSLAU-Net	84.38	CA-Net	68.39	DCSAU-Net	88.44	CA-Net	84.85	CASCADE	73.30	MMUNet	84.21
5	UTANet	84.22	DDANet	68.38	UTNet	88.39	UTANet	84.77	AURA-Net	73.25	H2Former	83.99
6	DDANet	83.78	TransAttUNet	68.25	D-TrAttUNet	88.27	ColonSegNet	84.70	MEGANet	73.18	Perspective-UNet	83.90
7	MERIT	83.77	UTNet	67.76	ESKNet	88.23	DA-TransUNet	84.63	DS-TransUNet	72.74	FCBFormer	83.84
8	MBSNet	83.57	EVIT-UNet	67.61	AURA-Net	88.23	RollingUNet	84.62	DoubleUNet	72.63	D-TrAttUNet	83.74
9	CENet	83.47	D-TrAttUNet	66.96	LGMSNet	88.16	RWKV-UNet	84.56	MSLAU-Net	72.60	MedFormer	83.58
10	U-Net	83.30	AttU-Net	66.96	DDANet	88.16	FCBFormer	84.54	RWKV-UNet	72.56	EVIT-UNet	83.54
			U-Net (#21)	66.44	U-Net (#16)	88.05	U-Net (#17)	84.33	U-Net (#52)	67.90	U-Net (#23)	82.39

Table 18: Top-10 performing variants across each dataset on target domains. Baseline U-Net is highlighted (gray background), and statistical significance of p-value is highlighted: $p < 0.0001$, $p < 0.001$, $p < 0.05$, $p < 0.05$, and $P > 0.05$ (Not significant).

Rank	Ultrasound (Source → Target)				Rank	Endoscopy (Source → Target)				
	BUSI → BUS	BUSBRA → BUS	TNSCUI → TUCC	Kvasir → CVC300		Kvasir → CVC-ClinicDB				
1	Swin-umamba	82.91	MEGANet	86.62	MSLAU-Net	66.15	PraNet	83.31	PraNet	77.39
2	EMCAD	82.83	DoubleUNet	86.51	MERIT	66.00	RWKV-UNet	82.14	DS-TransUNet	77.38
3	CENet	82.70	CENet	86.29	EVIT-UNet	65.83	UACANet	81.72	CASCADE	77.19
4	G-CASCADE	82.61	FCBFormer	86.10	Polyp-PVT	65.23	MERIT	81.39	Swin-umambaD	76.83
5	DA-TransUNet	82.32	CASCADE	85.96	LGMSNet	65.16	MADGNet	81.24	EMCAD	76.56
6	PraNet	82.13	Polyp-PVT	85.65	G-CASCADE	65.10	TA-Net	81.24	TransResUNet	76.42
7	CASCADE	82.11	TransResUNet	85.62	CaraNet	64.61	EVIT-UNet	81.11	MADGNet	76.33
8	TransNorm	82.11	ResNet34UnetPlus	85.46	H2Former	64.48	UTANet	80.78	CFFormer	76.18
9	MCA-UNet	81.88	MCA-UNet	85.28	MEGANet	64.37	DS-TransUNet	80.58	DoubleUNet	75.72
10	CaraNet	81.32	G-CASCADE	85.27	Swin-umamba	64.00	CASCADE	80.57	MEGANet	75.64
	U-Net (#63)	72.44	U-Net (#79)	81.37	U-Net (#65)	60.50	U-Net (#75)	70.33	U-Net (#47)	69.87

Rank	Dermoscopy		Rank	Fundus		Rank	X-Ray		Rank	Histopathology	
	ISIC2018 → PH2	CHASE → DRIVE		Montgomery → NIH-test	Monusac → Tnbcnuclei						
1	MSLAU-Net	86.52	MSRFNet	55.60	MEGANet	88.19	TA-Net	50.74			
2	RWKV-UNet	86.00	DS-TransUNet	55.52	TransResUNet	87.69	CENet	48.03			
3	G-CASCADE	85.96	MBSNet	54.66	CaraNet	86.22	ResNet34UnetPlus	46.44			
4	MERIT	85.94	RWKV-UNet	54.27	DA-TransUNet	85.87	EMCAD	46.41			
5	MMUNet	85.66	CENet	53.78	PraNet	84.58	G-CASCADE	46.18			
6	H2Former	85.39	CSCAUNet	52.80	MADGNet	83.67	UNetV2	45.32			
7	CMUNeXt	85.32	MCA-UNet	52.69	Swin-umambaD	83.13	CSWin-UNet	45.18			
8	UACANet	85.12	EVIT-UNet	52.49	TransUNet	83.03	DAEFormer	45.16			
9	MADGNet	85.08	Tinyunet	52.26	TransNorm	82.90	DA-TransUNet	44.53			
10	MCA-UNet	85.08	TransResUNet	52.00	RWKV-UNet	82.41	MedVKAN	44.42			
	U-Net (#47)	84.00	U-Net (#57)	39.64	U-Net (#51)	71.33	U-Net (#91)	26.05			

- d_i : The difference between the rank of X_i and the rank of Y_i (i.e., $d_i = \text{rank}(X_i) - \text{rank}(Y_i)$).
- n : The total number of paired observations.

G ADDITIONAL RESULTS

G.1 PER-DATASET TOP-10 AND U-NET COMPARISON

We report the top-10 performing methods across each dataset, evaluated on both source and target domains. As shown in Tab. 17 and Tab. 18. For reference, the position of the vanilla U-Net is highlighted with a gray background, and we also compute the statistical significance of each variant relative to U-Net.

Top10 performance on source domain. On widely studied datasets and modalities-such as ultrasound, polyp segmentation, ISIC2018 (Dermoscopy), Synapse (CT), Drive (Fundus), ACDC (MRI), and Covidquex (X-ray)-most top-10 variants achieve significant improvements over U-Net. This trend is consistent with the increasing popularity of these datasets and 'novelty design' for long-range dependency modeling, such as incorporating Transformers, Mamba, RWKV, and hybrid designs. In contrast, on other datasets and modalities the improvements remain marginal. For example, in Montgomery (X-ray lung segmentation), DCA, Chase (Fundus), nuclear segmentation, and Histopathology, the relative gains over U-Net are not significant. This suggests that progress in these modalities has been limited, because they rely on stable local patterns rather than long-range context. These observations highlight an important direction for future research: designing models that are modality-aware, particularly tailored for domains dominated by local and repetitive structures.

Top10 performance on target domain. On the target-domain datasets, nearly all top-10 methods achieve substantial improvements, highlighting the superior generalization ability of recent variants. These gains are primarily driven by two factors: the adoption of long-range dependency modeling and the increased model complexity. Together, these characteristics enhance the representational capacity and adaptability of the variants, which aligns with the prevailing trend toward more novel and increasingly complex model architectures.

In addition, we provide the visualization results of the top 5 models and U-net of the dataset for visualization analysis. The results are shown in Fig. 15 and 16.

G.2 GPU-HOURS OF VARIANTS TO ACHIEVE OPTIMAL PERFORMANCE

We calculate the GPU hours required to achieve optimal performance for each variants and architecture family. The results are shown in Table 19 and Table 26. The Transformer family has the highest median GPU hours (1.22) and a large IQR (1.78), indicating high computational demands and variability. The Mamba family also requires significant resources (median = 1.19), but with more consistent performance (IQR = 0.47). The RWKV family is the most efficient, with the lowest median (0.63) and IQR (0.30), reflecting lightweight models with minimal variation. The CNN and Hybrid families show moderate GPU hours (0.92 and 0.90) and similar IQRs (0.67), offering a balance between performance and efficiency.

Table 19: GPU Hours for Achieving Optimal Performance by Model Family

Architecture	Median	IQR
CNN	0.92	0.67
Hybrid	0.90	0.67
Transformer	1.22	1.78
RWKV	0.63	0.30
Mamba	1.19	0.47

H RELIABLE CROSS-ARCHITECTURE EVALUATION

We add a Δ IoU column in Table 20 comparing our reproduced in-domain results with the original papers' reported metrics. The results show that our unified recipe reproduces prior performance faithfully: most Δ IoU values lie within a small and symmetric range around zero (typically $\pm 3-5\%$), and the few larger gaps correspond to architectures originally tailored to narrow modalities rather than evidence of training failure. Notably, several models even achieve higher IoU under our unified pipeline (e.g., RWKV-UNet, DA-TransUNet, U-KAN and DDANet), demonstrating that our implementation does not systematically disadvantage any architecture. To further validate the unified recipe, we conduct a controlled reproduction study on BUSI across 100 variants, using both (i) each

paper’s official hyperparameters and (ii) our unified U-Bench recipe. The results are shown Fig. 10. The unified recipe yields higher median IoU and fewer collapsed low-tail cases, confirming that the U-Bench implementation is reliable as the official pipelines.

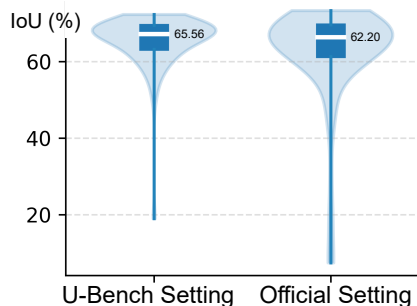


Figure 10: Comparison between official and U-Bench settings, showing higher median IoU and fewer low-tail failures with the unified recipe on BUSI.

I SCALING ANALYSIS OF DATASET SIZE WITH DIFFERENT VARIANTS FAMILIES

We present the results of a comprehensive scaling analysis examining the relationship between dataset size and model performance. We conduct experiments using dataset subsampling at 25%, 50%, 75%, and 100%, exploring both compute efficiency and data efficiency across different architectures. To ensure the analysis is representative, we select the top 3 variants from each model family (Mamba, CNN, Hybrid, RWKV, and Transformer) as representatives. The total and architecture-specific scaling results are shown in Fig. 11, where we observe consistent improvements in performance as dataset size increases, indicating predictable scaling behavior across architectures. Additionally, we examine performance across multiple modality families (shown in Fig. 12), where similar trends are observed. As dataset size increases, we consistently observe performance gains, as exemplified by the Ultrasound modality, where performance improves from 0.6928 at 25% to 0.7463 at 100%. These findings suggest the strong relationship between dataset scaling and model performance, reinforcing the predictability of scaling behavior across both architectures and modalities.

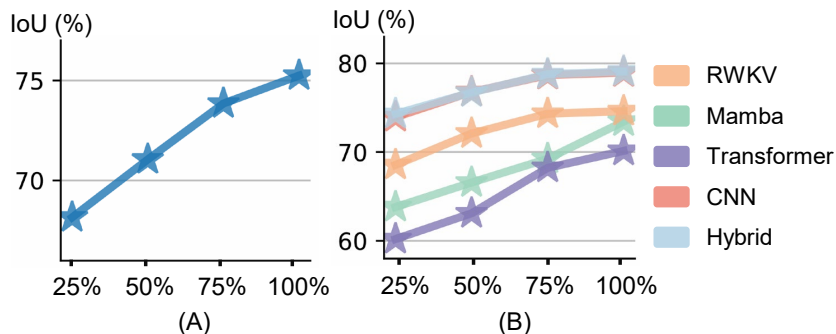


Figure 11: Overall Scaling Behavior (A) and Architecture-Specific Scaling Trends (B) with increasing dataset size (25%, 50%, 75%, and 100%) across different architectures (Mamba, CNN, Hybrid, RWKV, Transformer). The left figure shows the overall scaling trend, while the right figure displays the scaling behavior for each architecture family, highlighting the predictable improvement in performance as dataset scaling grows.

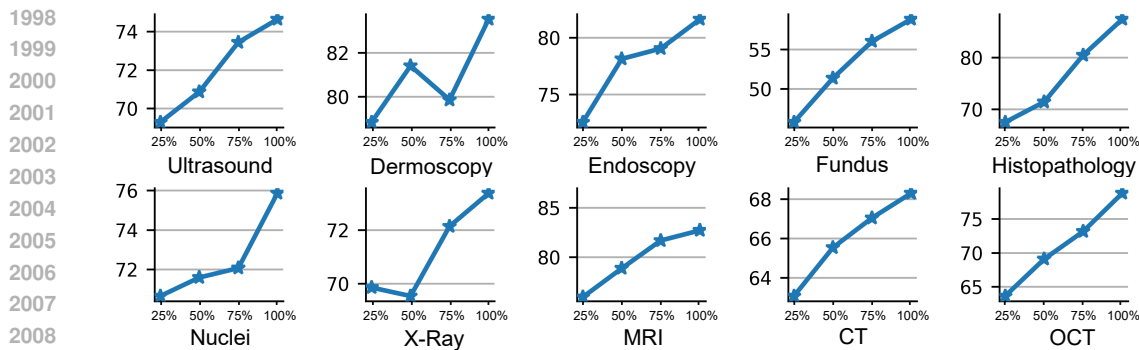


Figure 12: Modality-Specific Scaling Trends. The x-axis indicates increasing dataset size (25%, 50%, 75%, and 100%). The y-axes report IoU (%) performance.

J INCORPORATE NEW DATASETS AND ALGORITHMS IN U-BENCH

We implement U-bench using the PyTorch framework. Figure 13 illustrates the comprehensive workflow of U-bench, a system tailored for medical image analysis. It features a versatile 2D/3D Dataloader that seamlessly accommodates multiple medical imaging modalities, including MRI, CT, X-Ray, Dermoscopy, and Fundus and so on. A rich assortment of models with diverse architectural designs—spanning CNN, Transformer, RWKV, Mamba, and Hybrid—are registered via a Model JSON configuration and then leveraged by the Trainer module for 2D/3D slice-wise training. The evaluation pipeline encompasses in-domain testing, zero-shot inference, statistical significance assessments and custom assessments of U-score. Finally, results are systematically logged and visualized using tools such as Weight & Biases (wandb), ensuring thorough tracking of metrics and checkpoints. We demonstrate how to integrate new datasets and algorithms through example pseudocode Figure 14.

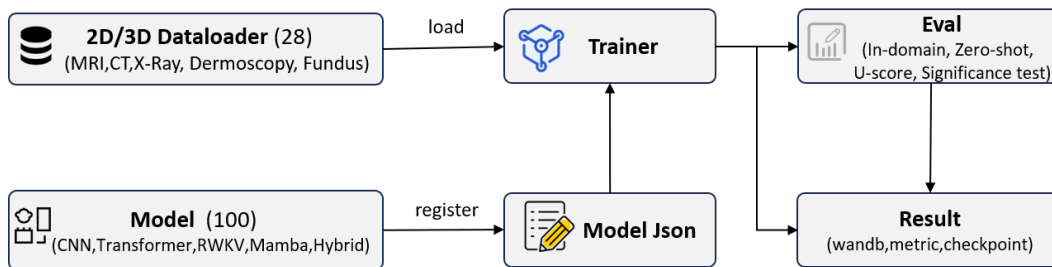


Figure 13: Overall workflow of U-bench. The Dataloader supports multiple medical imaging modalities (e.g., MRI, CT, X-Ray, Dermoscopy, Fundus). Models (with diverse architectures like CNN, Transformer, RWKV, Mamba, Hybrid) are registered and used by the Trainer for 2D/3D slice training. Evaluation covers In-domain/Zero-shot tasks, with results logged via tools like wandb.

J.1 ADDING A NEW DATASET

If the existing Dataset classes cannot meet your processing requirements, you can implement your own dataset with the structure shown as in Figure 14 (a).

Additionally, you need to add your dataset name and loading method in the Dataloader file, as shown in the Figure 14 (b).

J.2 ADDING A NEW ALGORITHM

1. First, define your model in the models directory, ensuring the first two parameters are input_channel and num_classes to adapt to our project (as shown in Figure 14 (c)).
2. Then, properly import your "modelname" in the __init__.py file under the models directory.

2052
 2053
 2054
 2055
 2056
 2057
 2058
 2059
 2060
 2061
 2062
 2063
 2064
 2065
 2066
 2067
 2068
 2069
 2070
 2071
 2072
 2073
 2074
 2075
 2076
 2077
 2078
 2079
 2080
 2081
 2082
 2083
 2084
 2085
 2086
 2087
 2088
 2089
 2090
 2091
 2092
 2093
 2094
 2095
 2096
 2097
 2098
 2099
 2100
 2101
 2102
 2103
 2104
 2105

```
class CustomDataset(data.Dataset):
    def __init__(self):
        # TODO
        # 1. Initialize file path or list of file names.
        pass
    def __getitem__(self, index):
        # TODO
        # 1. Read one data from file (e.g. using numpy.fromfile, PIL.Image.open).
        # 2. Preprocess the data (e.g. torchvision.Transform).
        # 3. Return a data pair (e.g. image and label).

        pass
    def __len__(self):
        # You should change 0 to the total size of your dataset.
        return num
```

```
if "X" in args.base_dir: # for XDataset xxxx;
    db_train = XDataset(dataset_dir=args.base_dir, mode="train", transform=
                        train_transform)
    db_val = XDataset(dataset_dir=args.base_dir, mode="test", transform=val_transform)
```

```
def modelname(input_channel=3, num_classes=2, base_channels=64):
    # Model implementation
    pass
```

```
{
    "modelname": "XXXX",
    "id": X,
    "state": "XXX",
    "deep_supervision": 0 or 1,
    "filename": "XXXX"
}
```

Figure 14: Pseudocode display. (a) Pseudocode for datasets; (b) Pseudocode for data loading; (c) Pseudocode for model definition and input parameters; (d) Example of model registration using a JSON file

2106 3. Finally, register your model in the `model_id.json` file with the format shown in Figure 14
2107 (d). Note that `modelname`, `id`, and `deep_supervision` are required fields, and `modelname`
2108 serves as the unique identifier for the model.
2109

2110 K DATASET AVAILABILITY AND ETHICAL COMPLIANCE 2111

2112 All datasets used in this benchmark, except for TNSCUI and TUCC, are publicly available. These
2113 datasets are listed in the manuscript along with appropriate citations and links for access. We have
2114 ensured that the use of each dataset complies with the respective ethical guidelines and regulations.
2115 Detailed information regarding the ethical considerations for each dataset can be found in the dataset
2116 documentation provided by the respective authors.
2117

2118 L EXPLANATION OF THE USE OF LLM 2119

2120 Large language models (LLMs) are employed solely to improve the clarity and readability of the
2121 manuscript.
2122
2123
2124
2125
2126
2127
2128
2129
2130
2131
2132
2133
2134
2135
2136
2137
2138
2139
2140
2141
2142
2143
2144
2145
2146
2147
2148
2149
2150
2151
2152
2153
2154
2155
2156
2157
2158
2159

2160
2161
2162
2163
2164
2165
2166
2167
2168
2169
2170
2171
2172
2173
2174
2175
2176
2177
2178
2179
2180
2181
2182
2183
2184
2185
2186
2187
2188
2189
2190
2191
2192
2193
2194
2195
2196
2197
2198
2199
2200
2201
2202
2203
2204
2205
2206
2207
2208
2209
2210
2211
2212
2213

Table 20: Reproduction-gap analysis across 100 U-shape segmentation models. For each dataset, we report our reproduced IoU and the corresponding Δ IoU relative to the original papers’ reported metrics. Background denotes that the original paper adopts the same split ratio as our evaluation, while the specific partition may differ. A small and symmetric Δ IoU distribution indicates strong implementation fidelity and shows that the unified U-Bench recipe neither systematically benefits nor harms specific model families.

Rank	Network	BIUI	Ultrasound Δ	TNSCU Δ	Dermoscopy Δ	Endoscopy Δ	Fundus Δ	CHASE Δ	DRIVE Δ	DSB2018 Δ	Histopathology Δ	Glas Δ	Nuclear Δ	Cell Δ	Montgomery Δ	X-Ray Δ	MRI Δ	ACDC Δ	Synapse Δ	CT Δ
#1	RWKVUnet	72.32	+2.95	80.06	84.97	84.53	+0.61	70.85	59.75	88.10	85.75	-0.03	84.56	96.21	85.20	-0.28	72.56	+0.11		
#2	UTNet	69.00		78.51	83.84	83.06		79.81	60.86	87.70	84.22		84.77	95.76	84.73		69.73		-9.21	
#3	AURA-Net	70.63		78.32	84.25	83.53		80.08	58.22	88.23	82.77		84.87	95.67	84.35		73.25			
#4	Swin-umamba	70.04		78.64	84.49	85.56		81.65	62.75	87.81	79.06		84.49	95.56	84.51		71.69			
#5	TransRefNet	71.27		78.04	84.38	83.38	+1.24	81.01	58.85	87.69	82.55		83.78	95.89	83.79		69.65			
#6	FCBFormer	68.24		78.10	83.60	84.50	-4.53	81.17	64.25	88.08	79.81		84.54	95.05	84.54		72.06			
#7	MEGANet	71.47		79.01	84.50	84.29	-2.01	73.27	52.76	87.33	82.92		84.37	96.12	83.99		73.18			+3.76
#8	Da-TransUnet	71.47		77.65	84.50	84.50	+1.17	82.89	58.45	87.65	84.63		84.63	95.87	84.63		74.30			
#9	ESKNet	70.88	+0.68	78.29	83.34	82.11		82.69	63.15	88.25	82.48		84.35	95.65	84.06		70.78			
#10	CFFormer	70.91	-4.88	78.44	84.89	84.57	-0.49	76.61	60.05	87.57	82.17		84.41	95.87	83.99		70.89		-0.99	
#11	EVFVUnet	70.50		78.55	82.73	83.53		74.06	57.45	85.53	84.31	-5.97	84.61	95.71	84.91		67.17		-0.72	
#12	CMU-Net	69.25	-4.02	77.28	82.74	83.07		84.33	62.85	87.87	81.88		84.13	95.54	84.29		68.42			
#13	DDNet	68.33		77.53	83.20	83.06	+5.06	78.94	61.40	88.16	83.78		84.17	95.97	85.11		71.83			
#14	MADNet	71.24	-3.96	78.01	84.18	83.04		81.18	57.52	83.03	84.18		84.55	95.69	83.20		72.20			
#15	Perpective-Unet	67.00		78.20	82.78	82.70		82.86	60.47	87.29	81.53		82.99	95.20	83.80	-2.31	73.69		+0.34	
#16	ArtU-Net	65.74		76.30	82.60	79.25		84.20	62.27	87.94	83.06		84.49	95.73	85.01		71.19			
#17	UNET+	65.06		74.61	82.80	78.83		83.69	60.87	87.59	82.79		84.19	95.88	84.27		70.41			
#18	UTNet	69.60		77.42	83.56	80.92		80.83	63.17	88.39	80.42		84.47	95.73	84.07		69.16			-4.32
#19	Mobile U-ViT	71.59	-2.32	78.12	83.88	82.21	-5.86	77.58	60.69	87.67	79.05		83.91	95.89	83.79		70.84			
#20	E-Net	65.58		75.99	82.78	80.11		84.07	60.81	88.05	83.30		84.53	95.87	84.72		67.90			
#21	MT-Unet	67.01		72.66	82.84	80.08		82.00	63.21	88.74	80.31		84.93	95.90	83.68	-1.15	69.81		+5.08	
#22	RollingUnet	67.68	-0.13	76.17	83.07	-1.07	81.50	78.51	+8.11	88.14	82.54	-5.48	84.62	96.01	83.88		70.12			
#23	GH-Unet	68.01		75.42	83.10	80.34		82.82	60.38	81.39	81.72		84.18	95.70	84.21		69.62		+5.38	
#24	MBSNet	68.82		76.78	83.09	81.44		77.57	61.61	87.78	83.57		83.97	95.79	84.20		69.66			
#25	CA-Net	69.62		77.61	83.51	80.93		79.87	59.76	87.26	79.53		84.17	95.72	83.80		70.11		+2.06	
#26	TransArtUnet	68.46		77.65	83.04	-0.76	81.53	75.63	62.45	88.49	81.04	-0.09	84.58	96.03	84.68	-1.79	70.46		+7.46	
#27	LQMSNet	69.45	-3.95	77.71	83.68	+0.22	81.77	-6.37	77.64	80.06	88.16	81.92	84.32	95.56	83.08		69.35			
#28	CE-Net	69.16		77.34	83.89	84.32		70.80	58.38	88.06	83.47		83.57	94.46	85.54	+0.04	74.70		+0.73	
#29	H2Former	69.80		77.84	83.31	81.88	-4.41	74.91	57.93	86.58	82.16		83.51	95.82	84.72	-1.16	70.90		+16.43	
#30	CA-Net	68.96		77.34	82.87	-2.45	80.58	74.04	61.97	88.12	81.63		84.85	95.62	84.68		70.14			
#31	CMUNet	68.68		77.18	82.80	80.21		78.25	60.99	87.62	82.12		84.80	95.54	83.33		68.05			
#32	D-TransUnet	65.38		75.21	83.06	80.78		79.19	62.48	88.27	79.38	-6.58	84.15	95.13	83.05		70.25			
#33	MeoFormer	67.08		77.81	82.59	82.06		79.90	61.77	87.64	77.93		83.61	94.87	83.30	-2.12	67.21			
#34	FoU-Net	70.17		78.57	83.91	+1.89	83.39	75.39	50.03	86.07	82.81		82.76	95.43	84.78		64.45			
#35	MCA-Unet	69.49		78.26	83.72	82.25		75.56	59.20	87.52	79.85		83.87	95.22	84.30		58.69			
#36	MSLU-Net	68.69		78.18	83.56	83.83		70.05	49.20	85.98	84.38		82.70	94.83	84.49	-1.02	72.60		+1.39	
#37	UNet++	66.44		76.87	82.59	81.83		70.77	54.45	84.43	80.43		83.56	95.30	83.25		67.43			
#38	TA-Net	69.89		78.85	84.34	83.33		71.68	50.20	86.95	81.60	-1.04	83.60	94.76	82.78		63.54			
#39	ResU-KAN	67.38	-0.36	77.39	83.36	82.70		76.12	57.84	86.86	79.44	-8.55	83.89	94.83	81.95		69.60			
#40	U-KAN	67.10	+3.72	77.15	82.73	82.11		75.80	57.21	82.13	79.75	-7.89	83.55	94.99	82.44		69.82			
#41	MSRFNet	65.81		77.30	82.86	-0.87	80.60	-8.54	69.36	87.27	88.01	+2.67	81.12	93.82	85.54		70.16			
#42	ColonSegNet	67.77		71.03	82.06		79.81	+7.42	82.20	63.19	89.01		80.56	84.70	83.76		68.07		+7.58	
#43	GH-Unet	66.20		76.69	82.55	-5.83	70.27	54.21	57.92	81.11	80.43		82.71	95.01	83.21		71.08			
#44	CE-Net	69.99		78.21	84.32	82.11		70.23	60.31	86.35	83.19		83.19	95.13	82.89		64.67			
#45	ScribFormer	66.37		76.55	83.13	79.33		74.34	60.58	87.93	77.57		84.13	95.63	83.52	-3.67	70.96			
#46	DS-TransUnet	65.91		73.09	83.30	-1.93	84.02	-1.88	72.97	85.46	81.46	+3.01	83.01	94.68	84.68		72.74			
#47	DCAU-Net	67.37		78.00	83.47	-0.63	81.07	70.08	60.31	88.44	77.00		83.86	95.48	82.65		66.33			
#48	DDS-Unet	67.63		76.19	83.67	-0.22	81.86	+3.76	74.09	54.06	86.38		79.88	83.32	84.13		80.49			
#49	TransUnet	69.43		77.72	83.47	+2.56	81.28	76.08	57.25	86.25	82.73		83.66	95.15	84.11		61.95		-2.53	
#50	MedVKA	66.71	-4.19	77.26	83.01	81.93		67.95	57.50	87.20	78.18		83.47	95.00	81.36	-3.57	66.17			
#51	DoubleUnet	66.56		74.95	81.07	-1.05	84.09	69.01	60.29	88.61	77.13		80.26	95.33	85.33		72.63			
#52	CA-MambaSeg	66.56		74.96	81.07	-1.00	81.48	68.34	60.29	88.61	77.13		80.26	95.33	85.33		72.63			
#53	MMUnet	67.40		77.60	83.13	82.79		76.15	58.40	86.65	73.61	-12.88	83.09	93.96	80.32		65.87			
#54	U-RW-KV	65.72	-5.29	72.70	82.68	+5.29	78.28	-1.30	77.13	59.50	87.98		78.14	84.00	81.13		64.59			
#55	HRFormer	67.28		73.71	83.96	+0.45	83.36	66.14	47.23	85.69	79.74		82.22	93.09	83.25		69.18		+1.54	
#56	ResUNet++	62.36		73.01	82.30	78.36	-0.91	79.93	61.55	87.15	76.16		83.75	94.86	81.45		62.47			
#57	CASCADE	70.81		77.49	83.53	84.34	-3.42	59.33	33.42	86.20	83.17		81.76	94.38	84.43		-0.12	73.30		+2.83
#58	CSCAUNet	67.19		77.52	82.79	-3.12	82.25	-2.35	70.20	86.87	81.58		82.99	95.13	82.19		71.09			
#59																				

Table 21: Average performance of 100 u-shape medical image segmentation networks with IoU. Baseline U-Net is highlighted (gray background), and statistical significance of p-value is highlighted: $p < 0.0001$, $p < 0.001$, $p < 0.05$, $p \leq 0.05$, and $P > 0.05$ (Not significant).

Rank	Network	Ultrasound	Dermoscopy	Endoscopy	ChUS	Histopathology	Nuclear	X-Ray	MR	CT	OCT	Avg										
		BUS1	BUSBRA	TNSUC1	ISK2018	SkinCancer	Kvasir	Robotest	FLARE DRIVE	DSE2018	Glas	Muscare	Cell	Covidcap	Montgomery	DCA	ACDC	Promise	CF	SVT	OCCT	
2214	U-Net	69.00	83.93	78.51	83.84	84.48	83.06	84.62	79.81	60.86	87.70	84.22	68.39	84.77	69.29	95.76	64.23	84.73	66.87	69.73	69.73	79.43
2215	ALRA-Net	70.63	83.95	78.32	84.25	85.56	85.53	85.78	80.08	58.22	88.23	82.77	66.56	84.87	70.85	95.67	63.25	84.35	86.66	73.25	73.25	79.37
2216	Swim-umamba	70.04	83.88	78.64	84.49	83.92	85.56	84.04	81.65	62.75	87.81	79.06	64.12	84.49	69.48	95.56	62.73	84.51	86.29	71.69	71.69	79.27
2217	TransUC-Net	71.27	83.86	78.04	84.38	84.79	83.38	85.30	81.01	68.83	87.09	82.35	66.86	83.78	69.81	95.89	63.25	83.79	86.95	69.65	69.65	79.13
2218	FCBFormer	68.24	84.00	78.10	83.60	86.33	84.50	77.58	81.17	64.25	88.08	79.81	66.29	84.54	67.60	95.05	61.70	84.90	87.29	72.06	72.06	78.95
2219	MEG-Net	71.47	83.99	79.01	84.20	85.23	84.29	86.25	73.27	52.76	87.33	82.92	65.86	84.37	70.19	96.12	63.77	83.99	87.00	73.18	73.18	78.85
2220	DA-TransUNet	68.45	83.95	77.95	83.95	87.22	82.20	83.09	82.69	60.47	87.48	82.89	64.26	84.63	69.61	96.17	64.90	84.30	85.84	70.15	70.15	78.82
2221	ESKNet	70.88	83.77	78.29	83.34	81.93	82.11	81.36	82.65	63.15	88.23	82.48	66.92	84.35	68.62	95.65	63.69	84.06	86.34	70.78	70.78	78.78
2222	CFFormer	70.91	82.42	78.44	84.89	83.87	84.57	83.80	76.61	60.05	87.57	82.17	64.51	84.41	68.40	95.87	62.17	83.99	86.58	70.89	70.89	78.76
2223	EMU-Net	69.25	83.39	77.28	82.74	81.90	83.07	80.25	84.33	62.85	87.87	81.88	66.48	84.13	68.28	95.54	62.64	84.24	86.87	67.42	67.42	78.70
2224	DDNet	68.33	83.36	77.53	83.20	80.91	83.06	80.35	78.94	61.40	88.16	83.78	65.38	84.17	68.32	95.97	63.65	85.11	86.20	71.83	71.83	78.69
2225	MADNet	71.24	84.27	78.91	84.18	84.67	84.32	85.21	71.18	54.35	86.92	83.03	64.66	84.14	67.77	95.69	63.80	84.32	87.26	72.20	72.20	78.62
2226	Perspective-Net	67.00	83.53	78.20	82.78	84.29	82.70	79.77	82.86	60.47	87.29	81.53	64.66	82.99	67.54	95.20	62.35	83.80	87.03	73.69	73.69	78.88
2227	MU-Net	65.74	82.43	76.30	82.60	81.74	79.23	84.20	84.20	67.20	87.94	82.96	65.32	84.49	68.03	95.73	63.14	83.09	86.69	71.19	71.19	78.87
2228	UNE3+	65.06	82.92	75.61	82.80	81.85	78.83	81.13	83.08	62.54	87.99	82.79	66.36	84.19	68.69	95.88	63.27	84.27	86.68	70.41	70.41	78.54
2229	UTNet	69.60	83.09	77.42	83.56	82.08	80.92	79.66	80.83	63.17	88.39	80.42	67.76	84.47	68.31	95.73	63.54	84.07	86.04	69.16	69.16	78.52
2230	Mobile U-Net	71.59	83.64	78.12	83.88	83.64	83.11	80.31	77.58	60.69	87.88	79.05	68.57	84.01	68.87	95.81	63.91	84.29	86.74	70.84	70.84	78.84
2231	U-Net	65.58	82.91	75.99	82.78	80.94	80.11	81.24	84.07	61.81	88.05	83.30	66.44	84.33	68.52	95.87	63.30	84.32	86.30	67.90	67.90	82.39
2232	MFA-Net	67.01	81.80	72.66	82.84	84.41	80.08	80.82	82.00	63.21	88.74	80.11	69.27	84.93	67.50	95.90	63.23	83.68	85.63	69.81	69.81	81.46
2233	Rolling-Net	67.68	83.94	78.17	83.97	82.40	81.59	78.34	78.51	62.49	87.84	82.14	68.52	84.62	68.83	95.73	63.14	83.09	83.88	85.87	85.87	81.25
2234	UCTransNet	68.01	82.51	75.42	83.10	82.77	80.34	81.23	82.82	60.38	87.72	81.39	66.59	84.18	68.34	95.70	62.25	84.21	86.01	69.62	69.62	82.05
2235	MISNet	68.82	83.60	76.76	83.09	82.86	81.44	82.85	82.25	69.25	87.78	83.57	66.81	83.97	68.54	95.79	62.95	84.20	86.29	69.66	69.66	81.28
2236	TransNet	69.62	82.84	77.61	83.51	84.85	80.93	78.30	79.87	59.76	87.26	79.33	65.24	84.17	68.95	95.72	62.85	83.40	86.01	70.70	70.70	78.54
2237	TransArtNet	68.46	83.28	77.65	83.04	79.11	81.53	80.01	75.63	62.45	88.49	81.04	68.25	84.88	69.34	96.03	63.04	83.88	85.54	70.11	70.11	80.83
2238	LGMNet	69.45	82.22	77.71	82.68	85.22	81.77	78.45	77.64	60.05	88.16	81.62	64.88	84.32	68.14	95.56	62.01	83.08	86.02	69.35	69.35	79.82
2239	CENet	69.16	82.83	77.34	83.89	84.13	84.32	80.07	70.80	58.38	88.06	83.47	64.12	83.57	67.65	94.46	61.63	84.54	83.62	74.10	74.10	82.24
2240	H2Former	69.80	83.41	77.84	83.31	83.02	81.88	78.40	74.94	57.93	86.58	82.16	65.58	83.51	67.45	95.82	62.18	84.72	86.35	70.90	70.90	83.99
2241	CA-Net	68.96	82.87	77.34	82.87	82.48	80.58	77.64	74.01	59.97	88.12	81.63	68.39	84.85	68.59	94.82	62.05	84.66	86.35	69.60	69.60	81.88
2242	CMUNet	69.88	83.63	77.18	82.80	85.39	80.21	77.83	78.25	60.99	87.62	82.12	65.35	84.00	68.08	95.54	62.99	83.13	85.57	70.85	70.85	77.99
2243	D-TransUNet	65.38	82.03	75.21	82.56	83.82	80.78	78.93	79.19	62.48	88.27	79.38	66.96	84.15	67.07	95.13	62.67	83.05	85.87	70.25	70.25	77.85
2244	MedFormer	67.08	82.43	77.81	83.09	82.16	82.06	77.61	79.00	61.77	87.64	77.93	65.52	83.61	67.29	94.87	62.43	83.30	86.53	67.21	67.21	77.74
2245	FAT-Net	67.17	84.15	78.57	83.91	84.11	83.39	84.34	73.59	59.00	86.07	82.81	64.82	82.76	69.48	95.43	63.15	84.78	86.06	64.45	64.45	80.88
2246	MCA-UNet	69.49	83.78	78.26	83.72	86.17	82.25	79.97	75.56	58.90	87.52	79.85	65.09	83.87	67.63	95.22	62.13	84.40	85.84	68.69	68.69	83.07
2247	MCLAU-Net	68.69	82.69	78.18	83.56	86.80	83.83	82.93	70.05	49.20	83.98	84.38	62.82	82.70	68.30	94.83	61.94	84.99	84.84	72.60	72.60	82.27
2248	UNE++	66.44	82.10	76.87	82.59	83.16	81.83	79.08	79.72	58.40	87.11	80.43	64.63	83.56	67.74	95.30	61.41	83.25	86.40	57.43	57.43	82.58
2249	TA-Net	69.89	84.17	78.85	84.34	83.32	83.33	85.62	71.68	59.29	86.95	81.60	64.34	83.60	70.20	94.76	62.51	82.78	86.39	65.54	65.54	77.45
2250	ReSU-KAN	67.38	83.01	77.39	82.82	82.12	82.70	77.54	76.12	67.84	86.86	79.44	64.16	83.89	67.75	94.83	62.05	81.95	86.35	69.60	69.60	81.88
2251	UKAN	67.10	82.81	77.15	82.73	84.94	80.11	77.77	77.88	59.71	86.68	79.75	63.29	83.55	64.99	94.91	62.34	84.44	86.89	69.82	69.82	82.92
2252	MSPNet	65.81	83.16	77.30	82.86	80.87	80.60	78.32	69.36	57.27	88.01	81.12	66.29	83.82	67.64	95.54	62.25	84.78	85.81	70.16	70.16	80.74
2253	ColorSegNet	62.77	82.47	77.33	82.95	82.12	79.81	83.87	82.20	63.19	88.01	80.56	65.74	84.70	66.92	95.63	62.56	83.56	86.38	69.81	69.81	77.14
2254	GH-UNet	66.20	82.86	76.69	82.55	84.98	81.36	77.58	80.21	57.92	86.01	81.91	63.09	83.01	67.16	95.01	62.17	83.21	86.19	71.08	71.08	82.60
2255	CE-Net	69.99	83.14	78.21	83.22	83.64	82.11	85.11	70.23	49.23	86.35	81.20	62.25	83.19	70.04	95.13	62.14	82.89	85.96	64.67	64.67	81.17
2256	ScinFormer	66.37	82.02	76.55	83.13	80.01	79.33	75.38	74.34	60.58	87.93	77.57	66.84	84.13	67.02	95.63	62.83	84.89	70.86	80.97	80.97	77.02
2257	DS-TransUNet	63.91	81.29	73.09	83.30	83.74	84.02	82.80	72.97	55.46	87.82	81.46	64.05	83.10	66.44	94.37	60.83	84.68	83.10	72.74	72.74	76.91
2258	DCSUNet	67.37	83.21	78.00	83.47	81.47	81.07	77.78	70.08	60.31	88.44	77.60	64.48	83.86	68.51	94.98	62.40	82.65	85.42	67.12	67.12	76.83
2259	DDS-UNet	67.63	82.74	76.19	83.67	83.58	81.86	78.22	74.09	54.06	86.38	79.88	62.80	83.32	67.45	95.14	61.94	80.49	85.78	67.80	67.80	82.55
2260																						

2268
2269
2270
2271
2272
2273
2274
2275
2276
2277
2278
2279
2280
2281
2282
2283
2284
2285
2286
2287
2288
2289
2290
2291
2292
2293
2294
2295
2296
2297
2298
2299
2300
2301
2302
2303
2304
2305
2306
2307
2308
2309
2310
2311
2312
2313
2314
2315
2316
2317
2318
2319
2320
2321

Table 22: Baseline U-Net is highlighted (gray background), and statistical significance (calculated by IoU) of p-value is highlighted: $p < 0.0001$, $p < 0.001$, $p < 0.05$, $p \leq 0.05$, and $P > 0.05$ (Not significant).

Rank	Network	Ultrasound			Dermoscopy		Endoscopy		Fundus		Histopathology			Nuclear		X-Ray		MRI		CT		QCT	Avg
		BUSI	BUSBRA	TNSCU1	ISIC2018	SkinCancer	RVIS4	Robotool	CHASE	DRIVE	DSB2018	Glas	Monsuc	Cell	Covidquex	DCA	ACDC	ACDC	Promise	Synapse	Ct	Cystofibroid	
1	LiGMSNet	86.60	85.79	88.20	83.21	89.72	77.54	69.33	86.33	88.65	90.80	88.31	84.05	89.78	80.45	87.70	86.33	84.55	86.55	83.36	82.59	84.99	84.99
2	LV-UNet	78.85	82.62	85.86	87.93	83.00	84.97	83.02	68.19	79.63	71.97	87.64	82.50	82.15	91.70	79.68	90.90	78.00	86.67	69.73	84.68	81.96	81.96
3	CMUNet	81.96	86.88	84.44	64.46	88.85	83.05	65.44	85.35	87.62	82.70	86.90	83.98	85.96	78.45	85.68	86.61	83.05	82.44	77.97	82.98	81.37	81.37
4	MBSNet	81.21	85.22	81.57	70.00	67.66	73.03	66.41	83.10	86.64	83.32	87.32	87.02	84.37	80.48	86.60	86.31	85.46	83.19	81.24	83.02	81.16	81.16
5	Timonet	45.28	81.90	81.53	47.59	54.63	37.62	54.37	82.24	96.30	77.54	90.03	70.35	91.56	73.91	80.27	83.80	84.65	81.65	83.25	90.12	74.93	74.93
6	Mobile UNet	77.81	76.35	77.00	74.58	67.76	73.98	67.44	74.46	76.66	73.54	70.83	77.17	75.13	72.49	77.81	77.60	75.20	71.62	75.33	72.18	74.25	74.25
7	U-RWVU	67.91	72.99	62.42	60.99	39.91	48.14	51.99	82.99	85.32	86.03	76.72	84.80	84.96	63.88	80.96	86.37	73.79	81.88	65.36	82.54	72.00	72.00
8	UCAN	66.86	71.29	73.84	58.88	75.10	60.02	58.72	72.17	74.12	61.24	71.74	67.77	72.92	61.75	70.32	72.14	70.77	77.30	72.83	76.59	69.67	69.67
9	DCSAU-Net	66.85	74.27	74.96	68.11	46.94	63.17	58.03	64.49	72.47	76.06	65.18	70.21	73.28	70.64	69.12	73.92	70.36	70.67	63.66	70.13	68.15	68.15
10	ULite	62.66	65.19	52.52	52.91	74.11	18.95	41.97	70.39	95.19	89.40	72.50	72.85	90.39	50.16	77.77	78.81	80.76	74.12	64.52	92.51	66.83	66.83
11	UNetV	46.75	61.09	55.94	58.30	46.96	11.45	58.13	70.75	79.78	65.60	79.51	71.93	86.46	60.55	85.18	80.66	56.34	86.75	46.86	88.44	64.87	64.87
12	CFPNet-M	63.23	66.18	72.40	64.41	52.24	55.62	66.18	66.76	80.90	71.09	76.17	72.31	77.07	65.61	70.76	70.72	67.12	61.82	61.88	9.36	62.40	62.40
13	RWVUNet	61.72	61.72	61.72	61.72	61.72	61.72	61.72	61.72	61.72	61.72	61.72	61.72	61.72	61.72	61.72	61.72	61.72	61.72	61.72	61.72	61.14	61.14
14	MISA-UNet	68.42	62.93	71.66	62.01	88.11	52.72	57.40	30.24	54.31	41.12	68.64	59.67	59.60	66.64	58.63	68.16	61.97	59.19	59.19	57.84	57.84	57.84
15	DDNet	56.79	58.05	59.28	52.96	35.00	58.05	54.34	59.52	60.36	60.77	60.77	60.77	59.88	56.60	60.77	60.77	59.28	60.77	59.28	60.77	58.60	58.60
16	ResU-Net	58.11	59.24	60.59	55.84	46.81	58.61	49.07	59.25	60.38	53.31	58.34	57.81	60.63	55.76	56.75	60.35	56.99	61.21	59.16	62.21	57.42	57.42
17	UTNet	58.08	57.02	58.06	55.41	44.84	49.08	52.14	49.49	49.69	59.67	57.04	59.67	59.60	56.11	59.68	59.67	58.59	57.85	56.11	58.52	56.11	
18	CE-Net	58.93	59.33	59.54	59.90	53.74	54.81	59.90	52.61	53.68	46.36	58.08	51.78	56.06	59.90	56.39	59.13	56.75	57.87	48.69	57.72	56.01	56.01
19	TA-Net	57.20	58.27	58.27	58.27	51.03	56.36	58.27	52.49	52.95	50.96	56.94	54.56	55.90	58.27	52.86	57.18	55.11	57.30	45.15	55.82	55.16	55.16
20	SwimUNet	44.82	43.28	43.28	43.28	47.03	39.57	24.69	47.66	47.66	70.15	46.68	63.75	76.58	31.48	64.59	74.15	10.26	66.82	48.36	73.38	54.15	54.15
21	TransResUNet	51.29	51.13	50.84	51.29	49.95	49.89	51.29	51.23	50.23	44.22	50.80	51.24	49.84	51.29	51.29	51.27	50.16	51.29	49.12	50.47	50.52	50.52
22	MEGANet	50.68	50.68	50.68	50.68	50.35	50.68	50.68	47.14	47.58	47.58	47.58	47.58	47.58	50.44	50.68	50.68	49.80	50.68	49.38	49.38	49.38	49.38
23	G-CASCADE	55.18	50.86	54.54	52.17	53.69	54.97	47.41	31.28	41.32	49.10	55.99	44.82	46.18	51.48	49.99	51.00	56.29	48.38	56.29	47.19	49.96	49.96
24	MultiResUNet	54.42	62.15	59.75	46.61	50.21	54.76	51.51	9.10	14.90	9.10	64.61	59.08	58.68	62.00	30.04	20.35	61.06	62.39	52.87	56.12	46.99	46.99
25	EMCAD	50.79	49.16	36.03	52.71	53.54	53.41	43.37	35.65	46.12	47.44	53.54	47.25	48.53	50.80	44.62	52.59	9.01	51.23	8.80	47.80	47.80	
26	MedFormer	43.84	43.96	46.61	41.60	37.91	43.92	39.29	46.80	40.76	45.49	43.63	46.88	45.66	42.06	44.06	46.42	45.73	46.77	43.11	47.22	44.36	44.36
27	HiFormer	47.32	46.40	46.45	46.30	46.25	45.95	45.83	39.93	42.43	31.62	45.03	41.87	42.37	44.76	44.80	43.50	45.61	45.94	44.93	43.05	43.82	43.82
28	SimpleUNet	9.52	9.52	9.52	9.52	9.52	9.52	9.52	9.52	9.52	9.52	9.52	9.52	9.52	9.52	9.52	9.52	9.52	9.52	9.52	9.52	9.52	9.52
29	CASCADE	43.32	44.00	46.37	44.44	46.96	47.32	43.32	36.67	34.42	37.14	47.32	33.45	41.09	44.54	47.32	43.32	43.32	46.99	47.42	42.12	42.12	42.12
30	DC-UNet	28.87	39.02	43.88	8.79	8.79	26.53	40.05	45.99	51.91	42.40	51.83	50.81	49.32	51.35	50.51	42.02	52.03	47.84	47.38	35.90	40.76	40.76
31	MMUNet	41.80	43.76	44.42	40.31	29.06	43.28	35.64	43.51	49.44	39.00	37.52	20.70	32.76	39.10	38.28	42.02	39.91	42.47	39.99	49.52	43.82	43.82
32	ML-UNet	37.64	44.13	29.61	41.94	69.92	9.50	9.50	46.00	70.37	17.77	65.37	59.99	45.25	9.50	63.43	73.16	11.65	44.34	9.50	56.28	40.50	40.50
33	ERDNet	45.10	45.34	47.41	37.87	10.27	15.87	29.01	42.01	48.23	47.47	39.68	47.92	46.76	41.26	38.96	47.88	42.08	45.80	40.87	47.07	40.37	40.37
34	TransFuse	51.82	51.09	52.08	52.55	54.85	54.97	50.90	41.12	42.08	23.48	44.83	40.98	41.19	52.07	35.46	47.8	47.12	51.70	44.40	32.99	39.67	39.67
35	U-Net++	37.94	38.71	40.79	34.03	37.76	39.08	37.55	41.69	41.27	47.37	38.83	40.76	40.36	46.46	47.88	45.88	40.84	41.58	38.97	41.71	39.52	39.52
36	AG-MambaSeg	36.31	37.59	39.01	37.05	37.17	37.52	31.33	40.25	29.21	33.41	36.23	37.47	37.19	38.56	36.69	39.44	36.72	40.32	39.68	40.75	37.54	37.54
37	HiFormer	37.89	37.76	38.03	33.65	34.46	35.98	33.92	36.87	37.66	33.53	38.07	37.63	37.25	35.23	38.34	37.72	38.59	37.96	37.83	39.86	36.83	36.83
38	CSCA-UNet	37.08	38.27	39.32	34.08	33.37	37.82	34.70	36.57	26.63	36.08	39.33	36.18	37.90	38.38	38.37	37.09	37.91	39.36	39.43	39.32	36.87	36.87
39	Polyp-PVT	59.01	52.95	56.26	52.98	57.09	58.47	53.52	8.94	8.94	8.94	8.94	8.94	8.94	51.84	50.03	8.94	58.75	50.02	54.83	8.94	36.41	36.41
40	LFU-Net	9.52	9.52	9.52	9.52	9.52	9.52	9.52	9.52	9.52	9.52	9.52	9.52	9.52	9.52	9.52	9.52	9.52	9.52	9.52	9.52	9.52	9.52
41	LaViT-UNet	8.87	8.87	8.87	16.62	16.62	16.62	16.62	16.62	16.62	16.62	16.62	16.62	16.62	16.62	16.62	16.62	16.62	16.62	16.62	16.62	16.62	16.62
42	MSL-UNet	35.37	35.00	33.78	34.93	36.58	36.23	35.76	33.66	34.15	28.80	36.58	33.90	34.40	35.01	34.56	35.79	36.36	34.66	36.58	36.19	35.05	35.05
43	FAT-Net	35.87	36.12	36.12	35.50	34.54	35.43	35.99	34.85	33.94	29.13	36.03	34.96	34.09	35.93	35.03	36.12	35.29	34.32	35.32	35.20	34.91	34.91
44	ESVNet	34.67	34.51	34.59	32.47	28.68	32.90	33.10															

2322
2323
2324
2325
2326
2327
2328
2329
2330
2331
2332
2333
2334
2335
2336
2337
2338
2339
2340
2341
2342
2343
2344
2345
2346
2347
2348
2349
2350
2351
2352
2353
2354
2355
2356
2357
2358
2359
2360
2361
2362
2363
2364
2365
2366
2367
2368
2369
2370
2371
2372
2373
2374
2375

Table 23: Average performance of 100 u-shape medical image segmentation networks with Dice. Baseline U-Net is highlighted (gray background).

Rank	Network	Ultrasound	Dermoscopy	Endoscopy	Fundus	Histopathology	Nuclear	Covidcage	X-Ray	MRI	CT	OCCT	Avg
		BUSS	ISIC2018	ESCCancer	CHASE	DRIVE	DSB2018	GLAS	Mammia	ACDC	Promis	CT	Crossmodal
#1	RVKUNet	83.94	91.75	85.92	91.87	91.32	91.62	92.44	82.94	94.80	95.68	92.33	81.63
#2	UTANet	81.65	91.26	87.96	91.21	91.59	88.77	75.67	93.45	91.44	81.23	91.76	81.86
#3	AURA-Net	82.78	91.27	87.64	91.45	92.22	91.03	92.35	88.94	91.60	91.75	90.57	79.92
#4	Swin-umamba	81.49	91.25	88.04	91.59	91.25	92.22	91.33	89.90	91.11	93.51	88.30	78.14
#5	TransResUNet	83.23	91.22	87.66	91.53	91.77	90.94	92.06	89.51	74.09	93.10	90.32	80.14
#6	FCBFomr	81.12	91.31	87.70	91.07	92.67	91.60	87.38	89.61	78.23	93.66	88.77	79.73
#7	MEGANet	83.36	91.30	88.28	91.60	92.03	91.47	92.62	84.57	69.07	93.24	90.66	79.42
#8	DA-TransUNet	83.36	91.25	87.61	91.28	93.17	90.23	90.76	88.05	73.45	93.32	90.64	78.25
#9	ESNet	82.96	91.17	87.83	90.91	90.07	90.18	89.72	90.53	77.41	93.75	90.40	80.18
#10	CFFormer	82.98	90.36	87.92	91.82	91.23	91.64	91.18	86.75	75.04	93.37	90.21	78.42
#11	EVFVUNet	82.70	91.52	88.11	91.32	90.65	91.27	92.12	85.10	74.18	93.23	89.21	80.68
#12	CMU-Net	81.83	90.84	87.59	90.55	90.05	90.75	89.04	91.50	77.19	93.55	90.04	79.86
#13	DDANet	81.18	90.92	87.34	90.83	89.45	90.74	89.11	88.23	76.09	93.71	91.18	81.22
#14	MADNet	83.21	91.47	88.21	91.41	91.70	91.49	92.01	83.16	70.42	93.00	90.73	78.54
#15	Perspective-Net	80.24	91.01	87.77	90.58	91.47	90.53	88.75	90.63	75.36	93.21	89.83	78.54
#16	AutoU-Net	79.33	90.79	86.56	90.47	89.95	88.41	89.53	91.42	76.75	93.58	90.75	80.21
#17	UNet+	78.83	90.66	86.11	90.59	90.02	88.16	89.58	91.12	76.95	93.61	90.59	79.78
#18	UTNet	82.08	90.76	87.27	91.05	90.16	90.45	88.68	89.40	77.43	93.84	89.15	80.78
#19	Mobile-U-Net	83.44	91.09	87.72	91.23	91.09	90.83	89.08	87.38	75.54	93.43	88.30	79.98
#20	U-Net	79.21	90.65	86.26	90.58	89.66	88.86	89.65	91.34	76.01	93.65	90.89	79.84
#21	MT-UNet	80.25	89.99	84.17	90.61	91.54	88.94	89.39	90.11	74.06	93.03	89.08	81.84
#22	RollingNet	80.73	90.97	86.48	90.75	89.51	89.81	89.10	87.96	76.92	93.70	90.43	79.90
#23	UCTransNet	80.96	90.42	85.99	90.77	90.57	89.10	89.65	90.60	75.30	93.46	89.74	79.94
#24	MSNet	81.53	91.07	86.86	90.77	90.63	89.77	87.80	87.37	76.25	93.49	91.05	80.10
#25	TransUNet	82.09	90.61	87.40	91.01	91.80	89.46	87.83	88.81	74.81	93.20	88.47	78.96
#26	TransMUNet	81.28	90.88	87.42	90.73	88.84	89.83	88.90	86.12	76.88	93.89	89.53	81.13
#27	LGMNet	81.97	90.84	87.46	91.11	92.02	89.97	87.92	87.41	75.04	93.71	90.06	78.70
#28	CE-Net	81.77	90.61	87.22	91.34	91.38	91.49	88.93	82.90	73.73	93.65	90.99	78.14
#29	H2Former	82.21	90.85	87.53	90.80	90.72	90.04	87.89	85.68	73.86	92.81	89.21	79.21
#30	CA-Net	81.63	90.63	87.22	90.64	90.40	89.25	87.39	85.06	76.52	93.69	89.88	81.22
#31	CMU-Net	81.43	91.08	87.12	90.59	92.12	89.02	87.54	88.83	75.77	93.40	90.19	79.04
#32	D-TransUNet	79.06	90.13	85.83	90.44	91.20	89.37	88.22	88.39	76.90	93.77	88.51	80.21
#33	MedFormer	80.30	90.37	87.52	90.76	90.21	90.15	87.39	87.80	76.37	93.41	87.59	79.89
#34	FAT-Net	82.47	91.39	88.00	91.25	91.37	90.95	91.50	85.97	66.88	92.52	90.60	78.66
#35	MCA-UNet	82.00	91.17	87.80	91.14	92.57	90.26	88.87	86.08	74.13	93.34	88.80	78.86
#36	MSLAU-Net	81.44	90.53	87.75	91.05	92.93	91.20	90.67	82.98	69.95	92.46	91.53	77.16
#37	UNet++	79.84	90.17	86.93	90.47	90.80	90.01	88.32	88.71	73.74	93.11	89.15	78.51
#38	Tk-Net	82.27	91.41	88.47	91.51	90.80	90.90	87.25	83.50	66.89	93.02	87	80.30
#39	ResU-Net	80.51	90.72	87.25	90.92	90.88	90.53	87.35	86.44	73.29	92.97	88.54	78.17
#40	U-Net	80.31	90.60	87.10	90.55	91.86	90.17	87.50	86.23	73.19	92.86	88.73	77.52
#41	MSRNet	79.38	90.81	87.19	90.62	89.43	89.26	87.84	81.91	72.83	93.62	89.57	79.73
#42	ColonSegNet	77.12	87.94	83.06	90.14	90.66	88.77	87.56	90.23	77.44	93.62	89.23	79.33
#43	GH-UNet	79.67	90.63	86.80	90.44	91.88	89.72	87.38	82.54	73.28	92.48	90.06	77.37
#44	CE-Net	82.35	91.15	87.77	91.49	91.09	90.18	91.95	82.51	65.98	92.68	89.62	76.74
#45	ScnFormer	79.79	90.12	86.72	90.79	88.90	88.47	85.96	82.58	75.46	93.58	87.37	80.12
#46	DS-TransUNet	77.98	90.68	84.45	90.89	91.15	91.32	90.59	84.37	71.28	93.52	89.78	74.09
#47	DCSUNet	80.50	90.84	87.64	90.99	89.79	89.55	87.50	82.41	75.24	93.87	87.00	78.40
#48	DDS-UNet	80.69	90.56	86.49	91.11	91.06	90.03	87.78	85.11	70.18	92.69	88.82	77.15
#49	TransNorm	81.05	91.05	87.46	90.85	91.62	90.68	88.49	82.81	72.82	92.78	86.22	77.60
#50	MedKAN	80.93	91.26	87.17	90.71	90.63	90.07	87.85	80.92	73.02	93.16	87.75	79.21
#51	DoubleUNet	79.02	89.98	85.68	90.54	88.36	91.36	86.14	87.96	75.23	93.96	87.09	79.22
#52	AC-ManUSeg	79.49	90.14	86.47	90.81	90.80	89.88	86.05	88.10	79.36	92.62	87.07	77.10
#53	MMUNet	80.53	90.80	87.39	90.79	89.44	90.59	86.94	86.46	73.74	92.85	84.80	76.12
#54	U-Net	79.32	90.08	84.19	90.52	89.35	87.82	85.93	87.09	74.61	93.61	87.73	79.45
#55	HFFormer	80.44	91.02	87.46	91.28	91.83	90.93	90.68	79.62	64.16	92.30	88.73	76.68
#56	ResUNet++	78.82	89.15	84.40	90.29	90.46	86.77	87.80	88.85	76.20	93.13	86.47	77.74
#57	CASCADE	82.91	90.36	87.32	91.03	92.01	91.51	89.11	74.47	50.09	92.59	91.99	73.64
#58	CSCAUNet	80.37	90.59	87.33	90.58	90.25	90.26	87.67	82.49	44.47	92.98	89.86	76.73
#59	Tinyunet	76.51	90.12	85.53	90.18	89.77	87.14	85.77	82.86	74.27	92.94	88.56	75.55
#60	LVA-Net	79.77	90.16	85.97	91.03	91.04	90.04	89.02	78.40	63.80	92.79	88.08	77.20
#61	G-CASCADE	82.22	90.24	87.14	91.02	91.57	91.05	87.98	71.45	59.29	92.99	90.53	75.24
#62	DC-UNet	76.01	89.08	84.46	89.49	87.91	87.01	86.48	81.02	73.44	92.68	89.58	78.63
#63	ERDNet	80.04	90.11	86.39	90.40	88.54	86.39	84.58	79.42	71.16	93.29	84.22	78.49
#64	CovFormer	80.56	90.36	86.34	90.63	90.20	89.04	88.29	72.23	54.97	91.49	89.52	73.76
#65	ULite	78.02	89.32	82.87	90.27	90.58	86.39	84.69	79.06	73.50	93.30	85.37	78.87
#66	SwinUNetR	76.92	87.98	82.57	90.53	89.72	88.90	83.52	82.49	76.18	93.15	82.54	76.23
#67	SCUNet++	76.15	89.32	84.99	90.90	90.41	90.62	83.96	85.82	51.35	92.16	88.69	74.30
#68	UNetX	80.63	89.15	83.13	90.36	89.50	86.13	86.13	79.16	63.50	92.64	86.55	75.75
#69	MERT	81.82	90.81	87.30	91.21	91.49	90.95	91.25	65.38	57.56	90.41	91.17	76.63
#70	MDSA-UNet	76.69	89.89	86.65	90.72	89.86	88.44	87.31	69.68	54.87	92.26	87.78	73.95
#71	CPCANet	79.52	89.51	84.23	90.19	90.94	89.80	84.67	82.96	34.39	92.17	82.27	73.39
#72	LoViUNet	73.72	84.87	79.59	89.81	89.97	85.95	86.39	83.17	61.45	92.44	84.35	74.22
#73	DAEFormer	79.59	88.53	84.44	90.21	89.46	89.49	84.71	82.34	44.36	92.94	83.46	73.50
#74	Pranet	83.47	91.25	87.89	91.55	92.69	91.54	91.95	53.41	42.49	92.22	90.50	68.33
#75	Caranet	82.78	91.49	88.07	91.46	92.48							

2376
2377
2378
2379
2380
2381
2382
2383
2384
2385
2386
2387
2388
2389
2390
2391
2392
2393
2394
2395
2396
2397
2398
2399
2400
2401
2402
2403
2404
2405
2406
2407
2408
2409
2410
2411
2412
2413
2414
2415
2416
2417
2418
2419
2420
2421
2422
2423
2424
2425
2426
2427
2428
2429

Table 24: Average performance of 100 u-shape medical image segmentation networks with Boundary-F1. Baseline U-Net is highlighted (gray background).

Rank	Network	Ultrasound	Dermoscopy	Endoscopy	Fluoroscopy	Histopathology	Nuclear	Covidcage	X-Ray	MRI	CT	OCCT	Avg									
		BUSI	BUSI/RA	TSCU	SKC2018	Skincancer	Avast	Robust	CHASE	DRIVE	DSB2018	Glau	Monuse	Nuclear	Cell	AxCD	Promis	CF	OCCT	Avg		
#1	RVKUNet	83.64	91.50	91.40	93.77	95.85	92.59	95.28	95.70	92.10	98.74	94.59	91.17	96.96	99.49	93.37	98.67	96.99	97.24	97.39	93.13	
#2	AURA-Net	81.98	93.79	90.07	91.19	94.85	91.39	95.01	96.98	90.97	98.62	92.77	88.86	97.22	84.23	99.20	91.06	98.64	96.50	77.97	96.05	92.45
#3	UTANet	80.43	93.69	90.03	92.96	94.13	91.43	94.55	96.75	92.30	98.50	93.78	90.29	97.02	82.91	99.22	91.91	98.34	96.48	75.86	97.45	92.40
#4	MADGNet	82.87	94.23	90.53	93.28	93.93	92.77	94.76	95.18	89.19	98.51	92.99	88.55	96.89	83.07	99.25	91.83	98.47	96.77	77.74	96.93	92.39
#5	MEGANet	83.12	94.04	90.59	93.47	94.16	92.12	95.47	95.66	87.33	98.52	92.94	89.05	96.94	83.56	99.49	91.77	98.48	96.53	77.64	95.99	92.35
#6	Swin-UniNet	81.72	93.71	90.35	93.51	94.30	93.71	94.27	96.99	92.60	98.49	90.74	87.15	96.86	83.43	99.16	90.22	98.24	96.09	78.11	97.21	92.35
#7	TransResUNet	82.28	93.84	89.87	93.35	94.09	91.25	94.94	97.28	92.17	98.37	92.74	89.21	96.58	83.26	99.40	91.69	98.34	96.46	74.40	95.91	92.28
#8	DA-TransUNet	83.15	94.03	89.70	92.87	95.70	90.72	93.15	96.80	92.06	98.49	92.75	88.09	97.08	83.35	99.44	92.59	98.61	95.97	73.86	95.63	92.20
#9	EVTV-Net	81.78	94.26	90.48	93.14	93.09	92.69	95.00	95.98	91.69	98.53	91.50	90.66	96.90	83.43	99.09	92.08	98.48	96.55	71.54	97.10	92.20
#10	ESKNet	82.52	93.59	89.78	92.51	92.59	90.43	92.36	97.49	92.86	98.53	92.53	88.91	96.74	82.38	99.22	91.11	98.27	95.15	76.38	96.52	92.04
#11	DDANet	79.42	93.50	89.38	92.53	92.18	91.77	91.59	96.96	92.41	98.56	93.38	90.06	96.80	81.79	99.29	91.46	98.50	96.04	77.97	96.75	92.02
#12	FCRFermer	80.11	93.87	89.94	92.79	93.55	92.54	89.78	97.23	93.49	98.59	91.17	88.51	96.77	81.55	98.92	98.88	98.62	96.61	77.13	97.22	91.86
#13	Mobile U-ViT	83.03	93.65	90.02	93.01	93.66	91.59	91.51	96.62	92.39	98.48	90.10	89.01	96.60	82.32	99.30	90.98	98.13	95.54	76.49	96.30	91.86
#14	FAT-Net	81.64	94.08	90.61	93.49	94.01	91.96	94.62	95.63	87.26	98.68	93.32	89.93	97.31	83.46	99.31	92.17	98.70	96.35	69.34	97.27	91.96
#15	CE-Net	81.21	93.14	89.58	92.85	93.79	92.56	91.40	95.53	90.98	98.70	93.32	87.93	96.43	81.76	98.65	90.63	98.65	94.69	79.87	97.33	91.80
#16	CFFermer	83.31	92.84	90.26	93.71	94.13	92.41	94.12	96.33	91.78	98.57	92.77	88.60	97.09	82.55	99.40	90.81	97.98	96.31	67.88	96.66	91.78
#17	Perspective-UNet	78.46	93.61	89.75	92.16	93.92	90.99	91.28	97.62	91.67	98.47	92.12	87.77	96.35	81.47	99.02	90.17	98.32	96.51	78.93	97.19	91.99
#18	MSL-UNet	80.51	93.01	90.06	92.77	95.59	91.94	93.51	94.50	86.46	98.30	93.75	88.12	96.41	86.96	98.96	90.68	98.50	95.30	78.09	97.18	91.78
#19	HFermer	81.76	93.65	89.71	92.62	93.51	90.40	90.48	95.97	91.47	98.37	92.43	88.95	96.69	81.39	99.31	90.68	98.61	96.16	75.98	96.89	91.75
#20	CMU-Net	81.08	93.59	89.07	92.12	92.77	91.42	91.87	97.86	93.00	98.37	92.68	88.29	96.47	81.92	99.12	90.60	98.43	96.31	74.06	96.18	91.73
#21	MBSNet	80.37	93.74	88.84	92.53	93.31	90.12	90.21	96.61	92.34	98.44	93.26	89.09	96.43	82.15	99.30	91.11	98.23	95.78	75.50	96.79	91.71
#22	UTNet	81.35	93.24	89.32	92.79	92.76	90.55	91.22	97.20	93.06	98.59	91.33	89.55	96.88	82.03	99.24	91.11	98.06	96.04	74.18	96.68	91.71
#23	RollingUNet	78.04	93.56	88.22	92.55	92.09	90.29	91.83	96.97	92.58	98.46	92.52	88.97	96.94	82.63	99.32	90.87	97.65	95.80	75.80	96.37	91.63
#24	AutUNet	76.87	93.27	88.31	92.21	92.24	88.58	92.37	97.89	92.71	98.46	93.00	88.68	96.82	82.53	99.24	91.08	98.47	96.30	77.04	96.52	91.63
#25	TransAutNet	80.35	93.46	89.62	92.36	90.29	90.27	91.52	96.76	92.61	98.62	91.60	89.88	97.03	83.16	99.35	90.52	97.80	95.58	75.26	95.92	91.60
#26	TA-Net	81.45	94.27	90.59	93.32	93.35	91.91	95.14	95.00	97.84	98.57	92.41	89.22	96.44	83.68	98.84	91.05	97.98	96.36	67.67	96.29	91.58
#27	TransUNet	80.89	92.86	89.41	92.76	94.52	89.68	90.37	96.75	91.05	98.47	90.49	88.78	96.80	82.76	99.25	90.27	98.17	95.74	75.50	96.81	91.58
#28	LGMSNet	80.89	93.42	89.59	92.87	94.72	90.51	90.33	96.62	91.41	98.66	92.25	88.48	96.79	81.59	99.18	90.10	97.82	96.00	73.47	96.23	91.55
#29	HFermer	78.83	94.06	90.25	92.40	94.72	92.13	93.82	94.13	87.04	98.59	91.36	88.88	96.75	82.75	99.08	90.82	98.23	96.54	76.57	96.30	91.43
#30	UCTransNet	79.43	92.95	87.73	92.37	93.27	89.45	92.43	97.51	92.00	98.36	92.04	89.48	96.92	82.17	99.25	90.32	98.12	95.92	74.49	96.33	91.53
#31	UNet++	76.43	93.34	87.75	92.39	92.64	87.82	92.42	97.74	92.48	98.43	92.94	88.57	96.68	82.62	99.32	90.97	98.07	96.28	76.21	96.87	91.50
#32	CA-Net	80.74	93.95	89.06	92.14	92.04	89.69	89.81	96.38	92.39	98.58	91.55	89.03	96.94	82.69	99.13	90.13	97.68	95.42	73.39	96.18	91.44
#33	MT-UNet	78.67	92.34	85.51	92.34	94.28	89.68	92.37	97.29	93.23	98.66	91.26	90.36	96.89	81.88	99.26	90.52	97.46	95.77	74.95	97.10	91.42
#34	CE-Net	82.07	93.94	90.00	93.40	93.79	90.89	94.90	94.67	87.45	98.38	92.26	87.77	96.52	83.67	99.09	90.55	98.03	96.00	68.29	96.27	91.40
#35	U-Net	76.54	93.04	88.09	92.27	91.65	90.25	92.36	97.79	92.26	98.31	93.09	88.30	96.70	82.02	99.20	91.51	98.14	96.03	76.66	96.23	91.86
#36	D-TraUNet	77.19	92.80	87.43	91.97	93.81	90.21	90.95	96.98	92.28	98.59	90.69	89.25	96.73	81.37	99.00	90.77	97.59	95.88	76.46	96.71	91.34
#37	ReLU-KAN	79.04	93.37	89.50	92.57	92.87	91.29	90.13	96.23	90.51	98.35	90.73	87.63	96.70	81.95	98.93	90.20	97.72	96.09	76.96	96.02	91.80
#38	GH-UNet	77.03	93.88	88.50	91.97	94.52	90.05	92.35	94.42	90.58	98.17	92.23	88.84	96.44	81.54	99.03	90.23	98.30	96.15	76.50	96.17	91.47
#39	U-KAN	79.33	93.09	89.01	92.11	94.43	90.67	89.94	96.16	90.51	98.17	91.04	86.86	96.63	81.01	99.01	89.53	97.87	96.50	74.93	96.45	91.16
#40	DS-TransUNet	76.71	93.94	86.30	92.44	94.03	92.11	93.54	95.63	88.93	98.72	91.93	89.49	96.66	81.02	98.81	89.12	98.28	94.55	77.70	96.05	91.15
#41	MedFermer	79.40	92.71	89.66	92.34	92.99	90.99	89.78	97.00	91.85	98.36	89.55	88.55	96.34	81.50	98.86	89.91	97.84	96.32	71.93	96.52	91.12
#42	MSRFNet	78.06	93.21	89.24	92.13	91.65	89.54	90.34	95.74	88.96	98.59	91.78	88.52	96.38	81.55	99.11	90.73	97.70	95.77	76.05	96.50	91.08
#43	DCSUNet	79.40	93.32	89.94	92.72	92.52	90.10	90.38	95.69	91.40	98.66	89.32	88.08	96.73	82.45	98.96	90.23	97.81	95.63	71.54	96.08	91.05
#44	MCA-UNet	81.18	93.77	89.80	92.68	93.39	90.42	91.21	96.12	91.14	98.44	90.81	88.32	96.86	81.77	99.15	90.07	98.03	95.09	72.96	96.12	91.01
#45	DDS-UNet	79.17	93.21	88.51	92.93	93.72	90.53	90.33	95.54	88.94	98.16	91.15	87.53	96.55	81.44	99.17	90.28	97.24	95.97	72.99	96.74	91.02
#46	MedKAN	78.44	93.89	89.07	92.41	92.88	90.25	90.														

2430
2431
2432
2433
2434
2435
2436
2437
2438
2439
2440
2441
2442
2443
2444
2445
2446
2447
2448
2449
2450
2451
2452
2453
2454
2455
2456
2457
2458
2459
2460
2461
2462
2463
2464
2465
2466
2467
2468
2469
2470
2471
2472
2473
2474
2475
2476
2477
2478
2479
2480
2481
2482
2483

Table 25: Average performance of 100 u-shape medical image segmentation networks with HD95. Baseline U-Net is highlighted (gray background).

Rank	Network	Ultrasound			Dermoscopy		Endoscopy		Fundus		Histopathology			Nuclear	X-Ray		MRI		CT	OCI	Avg	
		BUS1	BUSB3A	TNSCT1	ISIC2018	SkinCancer	Kvasir	RoboDoc	CHASE	DRIVE	DSB2018	Glas	Monuse	Cell	Covidqrs	DCA	ACDC	PromisE	CT Synapse	OCI-Coronadiff		
#1	FAT-Net	16.80	3.87	3.90	4.11	3.63	3.88	7.00	1.60	3.82	1.08	3.08	3.51	3.81	22.26	3.04	1.83	1.19	19.91	2.04	6.45	
#2	Swin-umamba	18.98	4.11	6.79	4.05	2.79	7.22	5.15	0.96	3.16	1.20	9.78	2.28	4.22	24.75	0.28	7.02	2.15	1.30	17.32	2.32	6.64
#3	RWKV-Net	16.36	3.62	6.21	3.68	2.53	10.51	6.53	1.34	3.64	1.14	6.15	5.33	3.92	24.68	0.00	7.15	1.16	0.96	26.85	2.29	6.71
#4	AURA-Net	18.72	4.78	7.33	4.29	3.48	9.31	7.14	0.80	4.28	1.25	7.23	8.80	3.52	23.96	0.10	7.56	1.11	1.09	17.21	4.48	6.82
#5	CE-Net	19.30	3.81	7.42	3.94	4.35	10.17	5.68	1.96	5.28	1.21	7.77	9.97	3.92	23.58	0.11	5.99	1.27	1.20	15.64	3.94	6.88
#6	TA-Net	19.30	4.16	6.25	3.92	3.86	7.82	5.94	1.86	5.38	1.13	8.45	6.43	4.49	24.30	0.78	5.90	2.43	1.10	19.28	2.79	6.88
#7	MEGA-Net	17.41	4.02	6.17	3.76	4.66	10.64	2.46	1.34	6.80	1.20	8.11	8.77	3.55	24.63	0.00	6.21	1.60	1.10	23.60	3.94	6.97
#8	HFormer	24.12	3.79	6.22	3.61	3.00	8.34	9.52	2.27	5.69	1.18	7.73	7.84	3.64	22.02	0.09	7.11	1.16	1.55	17.96	5.73	7.13
#9	TransRUnet	21.50	3.84	7.47	4.51	5.34	9.81	8.30	0.70	3.42	1.18	8.35	7.67	4.07	25.10	0.05	6.11	2.35	1.26	19.97	3.37	7.22
#10	DA-TransUnet	17.18	3.94	6.99	4.50	2.72	11.15	13.67	1.13	3.60	1.18	6.99	10.01	3.47	24.07	0.04	4.87	1.10	1.38	24.39	3.17	7.29
#11	EMCAD	19.50	5.19	11.39	4.44	2.27	10.42	27.31	3.32	6.54	1.11	6.55	8.80	3.08	24.70	0.45	6.64	2.12	1.32	0.00	2.74	7.30
#12	MELU-Net	22.67	4.95	6.78	4.91	2.37	11.24	9.78	2.23	6.71	1.24	7.02	8.74	3.64	29.43	0.48	6.68	1.73	1.56	13.54	2.70	7.41
#13	UT-Net	21.77	4.04	8.36	5.12	3.49	10.10	7.64	0.82	3.43	1.62	7.34	8.05	3.36	25.25	0.09	5.73	1.76	1.27	30.90	3.47	7.68
#14	MADGNet	18.07	3.76	6.63	4.51	11.36	9.78	8.85	1.71	5.33	1.19	8.57	12.15	3.44	25.54	0.07	5.97	1.80	1.09	20.98	3.01	7.69
#15	CFFormer	14.59	5.79	6.67	3.74	3.19	9.17	4.98	1.42	3.57	1.14	6.99	8.27	2.88	25.73	0.00	7.14	1.21	1.24	43.98	2.53	7.71
#16	CE-Net	19.95	5.11	7.05	4.58	5.01	9.09	18.48	1.46	4.19	1.06	7.23	9.45	4.07	24.73	0.84	8.55	1.64	1.80	18.54	2.19	7.75
#17	DS-TransUnet	25.10	5.79	9.03	5.04	2.95	9.92	5.10	1.48	5.73	1.10	9.91	8.16	4.12	27.57	0.46	8.24	2.49	1.74	18.37	3.31	7.78
#18	MERT	18.09	3.92	6.79	4.39	3.30	9.68	7.44	4.71	7.56	1.64	7.19	6.65	4.02	27.65	0.46	7.99	6.12	1.43	23.04	3.28	7.78
#19	EVFUnet	19.65	3.71	6.61	4.34	5.12	9.37	6.72	1.36	3.71	1.20	9.56	7.64	3.32	23.37	0.44	5.91	1.88	1.17	38.69	2.78	7.83
#20	PCBFormer	21.47	4.27	6.73	4.95	2.44	9.63	18.10	0.81	2.65	0.63	10.80	9.01	4.00	26.60	0.37	8.53	1.13	1.14	23.23	2.88	7.97
#21	TransRUnet	20.36	4.77	8.36	5.11	3.98	13.31	10.18	1.44	3.16	1.16	7.07	8.09	3.27	25.99	0.07	6.48	2.65	1.46	24.85	3.99	7.84
#22	Mobile-U-ViT	17.78	3.40	6.94	4.55	4.98	10.16	13.83	1.33	3.35	1.40	13.00	8.14	3.81	26.15	0.04	6.88	1.61	1.54	27.24	3.99	8.05
#23	HFFormer	20.26	4.27	7.46	5.11	4.14	10.53	19.20	1.49	4.06	1.19	7.84	7.49	3.83	27.94	0.04	7.04	1.27	1.27	23.01	3.74	8.06
#24	TransNorm	19.25	4.55	7.14	4.84	3.10	11.84	15.84	1.45	3.12	1.32	11.87	10.01	4.34	26.09	0.19	7.29	1.89	1.23	20.03	3.54	8.07
#25	CASCADE	18.48	5.03	6.40	4.85	3.47	9.46	13.27	3.71	12.58	1.21	5.48	11.38	4.47	26.53	0.42	7.89	1.98	1.18	21.91	3.14	8.14
#26	G-CASCADE	18.37	4.79	6.70	4.83	3.99	10.05	18.24	2.51	10.27	1.12	8.46	10.37	3.65	25.10	0.55	8.15	1.20	1.62	20.31	2.59	8.20
#27	DD-Net	21.76	5.42	8.48	5.45	5.82	8.76	17.33	1.11	11.18	1.20	7.35	7.54	3.16	26.78	0.48	7.42	1.40	1.48	26.41	4.39	8.23
#28	TransUnet	21.72	5.47	7.56	5.08	3.32	14.61	16.66	1.00	4.42	1.33	12.14	8.51	4.01	24.43	0.05	8.35	2.18	1.46	19.80	2.79	8.24
#29	ResU-KAN	21.19	4.29	7.63	5.10	2.10	12.07	21.24	1.60	4.67	1.31	11.66	7.64	3.82	27.50	0.23	8.53	1.81	1.29	26.46	2.86	8.30
#30	MT-UNet	21.26	6.44	11.43	4.95	3.95	12.44	9.92	0.76	2.82	1.11	11.19	7.25	2.98	25.99	0.04	7.22	2.29	1.46	26.06	6.63	8.33
#31	ESKNet	17.25	4.96	8.20	5.24	5.37	11.40	22.93	0.62	3.16	1.16	8.47	9.89	2.99	26.95	0.11	7.50	1.29	1.46	23.52	4.33	8.34
#32	UACA-Net	18.12	3.64	6.03	4.17	3.13	9.69	3.11	11.37	21.06	1.95	10.71	7.53	3.63	22.87	0.30	9.83	1.55	1.18	18.11	5.53	8.37
#33	LGM-Net	20.06	5.03	7.43	4.66	3.06	11.15	17.35	1.33	3.85	1.19	9.58	8.50	4.15	28.55	0.26	8.09	1.84	1.36	26.02	4.11	8.38
#34	Perspective-UNet	28.51	4.33	8.29	5.68	4.32	10.36	15.57	0.67	4.24	1.21	10.70	9.25	4.36	27.48	0.35	8.84	1.46	1.21	18.95	2.48	8.41
#35	MBS-Net	20.82	4.14	9.30	4.74	4.78	10.85	28.20	1.41	3.40	1.27	6.53	8.20	3.64	28.06	0.40	6.50	2.10	1.42	21.85	6.89	8.60
#36	Car-Net	18.97	3.90	6.25	4.11	2.38	11.05	7.32	10.53	22.53	1.74	5.63	9.07	4.04	22.50	0.07	8.07	1.11	1.18	23.78	5.88	8.51
#37	PrNet	16.21	3.60	6.44	3.99	2.26	9.43	3.67	11.61	21.85	1.38	9.30	9.04	3.49	25.17	0.13	10.82	1.10	1.09	24.49	7.18	8.51
#38	CMU-Net	17.84	4.30	8.41	5.63	5.30	10.55	19.96	0.57	3.02	1.30	10.67	8.48	4.12	27.62	0.33	9.13	1.36	1.32	24.61	6.52	8.54
#39	DCAU-Net	20.16	4.39	6.79	4.80	5.00	12.83	16.32	1.38	3.79	1.12	13.88	8.53	3.34	25.93	0.11	7.59	2.10	1.45	25.74	5.49	8.54
#40	GH-Net	25.15	4.24	9.73	5.25	3.02	11.71	20.76	1.53	4.97	1.32	8.33	10.07	4.10	29.10	0.13	7.14	1.28	1.23	19.89	5.52	8.71
#41	UT-Net	20.51	4.62	7.74	4.73	4.94	12.48	20.29	0.74	2.99	1.13	10.99	9.78	3.79	26.92	0.14	6.82	1.59	1.37	28.57	6.18	8.37
#42	RollingUnet	30.04	4.19	11.15	5.17	5.76	11.08	18.23	1.11	3.27	1.29	7.89	9.28	2.93	28.02	0.04	7.67	1.69	1.49	24.80	2.59	8.88
#43	UC-TransNet	24.75	5.11	12.06	5.21	4.86	14.45	14.61	0.73	3.56	1.23	7.88	8.56	3.50	25.04	0.12	7.20	2.19	1.33	34.25	3.31	9.00
#44	DDS-UNet	19.44	4.52	8.96	4.60	4.63	11.96	25.46	1.84	3.56	2.05	11.33	9.53	4.24	26.94	0.07	7.44	2.39	1.34	25.29	2.73	9.01
#45	UK-AN	21.11	5.04	10.57	5.25	2.83	11.20	18.98	1.60	4.70	1.36	12.78	10.00	3.14	30.79	0.16	8.85	1.39	1.17	24.18	4.33	9.02
#46	MedFormer	22.86	5.35	7.46	5.62	4.93	11.65	22.12	0.86	3.78	1.50	13.91	8.28	4.41	28.17	0.43	7.93	1.97	1.27	22.94	5.57	9.06
#47	AC-ManUSeg	22.32	5.00	8.42	5.04	3.92	12.54	21.27	4.28	6.53	1.39	8.78	9.00	3.93	25.60	0.26	9.96	1.62	1.57	20.00	6.11	9.08
#48	MC-UNet	22.76	4.30	7.52	4.91	3.62	10.97	18.10	1.50	4.05	1.31	12.15	9.06	3.48	28.41	0.33	8.16	2.57	1.48	33.84	3.72	9.11
#49	MML-Net	20.19	4.41	7.35	4.96	5.85	11															

2484
2485
2486
2487
2488
2489
2490
2491
2492
2493
2494
2495
2496
2497
2498
2499
2500
2501
2502
2503
2504
2505
2506
2507
2508
2509
2510
2511
2512
2513
2514
2515
2516
2517
2518
2519
2520
2521
2522
2523
2524
2525
2526
2527
2528
2529
2530
2531
2532
2533
2534
2535
2536
2537

Table 26: GPU-Hours of variants to Achieve Optimal Performance on Different Datasets.

Network	Ultrasound			Dermoscopy		Endoscopy		Fundus		Histopathology			Nuclear		MRI		CT		OCt Cytosindhst	
	BUSI	BUSBRA	TNSUCU	ISIC2018	SkinCancer	Kvasir	RoboEndo	CHASE	DRIVE	DSB2018	Glas	Monsieac	Cell	Covidqnet	X-Ray Montgomery	DCA	ACDC	Promis		CT Synapse
AC-MambaSeg	1.27	4.96	5.65	4.06	0.23	2.06	1.38	1.35	0.16	0.42	0.25	0.45	1.55	3.95	0.98	0.53	3.30	3.37	11.64	3.60
AURA-Net	0.13	0.47	1.05	1.15	0.10	1.22	0.15	0.25	0.05	0.13	0.06	0.11	0.19	0.34	0.40	0.02	1.23	0.80	2.13	0.59
Anti-Net	0.40	1.57	2.21	0.85	0.06	1.43	0.43	0.41	0.03	0.15	0.11	0.16	0.43	0.93	0.31	0.05	1.32	0.79	1.16	1.34
BEUNet	0.30	0.70	1.59	1.10	0.15	0.91	0.33	0.28	0.04	0.11	0.11	0.17	0.43	0.69	0.86	0.12	0.46	0.97	2.45	0.72
CASCADE	0.15	0.62	1.29	0.84	0.04	1.00	0.37	0.37	0.09	0.11	0.12	0.13	0.39	1.17	0.89	0.10	0.55	0.99	2.00	0.93
CA-Net	0.40	1.18	2.74	1.90	0.08	1.28	0.39	0.51	0.06	0.33	0.11	0.24	0.52	1.57	0.87	0.12	1.59	1.01	2.74	0.76
CE-Net	0.49	0.47	1.30	3.96	0.43	1.35	1.21	1.01	0.12	0.89	0.38	0.30	1.13	5.33	0.29	0.29	3.57	4.07	9.23	2.83
CE-Net	0.24	0.83	2.54	2.69	0.05	0.58	0.53	0.75	0.13	0.30	0.18	0.34	0.86	1.89	0.72	0.14	3.19	0.98	5.32	2.00
CFFormer	0.08	0.52	2.00	1.79	0.20	1.54	0.55	0.47	0.06	0.20	0.12	0.14	0.52	0.41	0.76	0.05	1.62	1.45	1.48	1.24
CFM-UNet	0.48	1.79	3.21	1.57	0.27	1.54	0.52	0.45	0.06	0.80	0.16	0.34	0.73	1.93	0.89	0.18	2.32	1.55	4.03	1.05
CFPNet-M	0.46	0.61	1.69	1.20	0.08	1.26	0.44	0.39	0.09	0.29	0.11	0.30	0.26	1.25	0.78	0.12	1.67	1.19	2.87	0.49
CMU-NetX	0.12	0.30	1.13	0.48	0.08	1.18	0.23	0.21	0.05	0.17	0.05	0.10	0.26	0.39	0.42	0.04	0.32	0.58	1.15	0.50
CMU-Net	0.40	1.98	4.55	0.81	0.11	3.01	0.76	0.93	0.07	0.39	0.07	0.18	0.83	4.90	0.84	0.22	4.21	1.87	7.48	2.74
CPCANet	0.65	1.90	3.05	2.36	0.17	2.46	0.86	0.73	0.12	0.12	0.22	0.28	0.51	1.10	0.71	0.19	3.12	1.64	3.92	1.01
CSCAUNet	0.30	0.71	0.93	1.35	0.06	1.01	0.38	0.32	0.08	0.22	0.14	0.23	0.49	0.88	0.86	0.15	0.99	0.85	3.01	0.76
CSWin-UNet	0.40	1.45	2.73	1.85	0.19	1.34	0.36	0.05	0.08	0.75	0.14	0.23	0.56	2.11	0.93	0.06	1.11	1.15	2.23	0.87
Car-Net	0.76	2.14	3.26	2.42	0.22	1.19	0.35	0.55	0.09	0.58	0.15	0.32	0.69	1.87	0.72	0.20	2.51	0.94	5.05	1.43
ColoSegNet	0.47	0.59	2.10	1.76	0.17	1.26	0.47	0.43	0.06	0.16	0.07	0.16	0.44	1.17	0.57	0.07	1.12	1.21	2.95	1.16
ConvFormer	0.91	4.65	3.33	4.24	0.48	3.09	1.19	1.22	0.16	2.21	0.40	0.46	1.24	7.00	0.82	0.36	6.55	4.79	11.14	3.37
DAEFormer	1.29	3.28	9.74	5.54	0.47	3.18	1.12	1.09	0.13	0.61	0.34	0.78	1.98	4.23	1.01	0.36	1.91	4.37	9.72	3.01
DA-TransUNet	0.26	1.07	3.29	1.96	0.08	1.49	0.27	0.52	0.09	0.23	0.07	0.24	0.69	2.67	0.50	0.08	2.81	0.72	4.79	1.47
DCSAU-Net	0.37	1.19	2.52	1.43	0.16	1.07	0.49	0.42	0.08	0.72	0.14	0.28	0.60	1.25	0.91	0.13	1.94	1.38	3.35	1.06
DC-UNet	0.69	1.32	3.61	1.41	0.29	1.40	0.57	0.49	0.10	0.78	0.11	0.20	0.59	1.96	0.67	0.10	1.60	1.09	4.19	0.76
DDANet	0.44	0.78	2.22	1.24	0.07	1.29	0.37	0.39	0.08	0.17	0.09	0.17	0.35	1.22	0.40	0.08	1.27	0.93	2.22	0.99
DDS-UNet	0.47	1.62	3.05	4.59	0.33	2.80	1.08	0.83	0.12	0.28	0.20	0.47	0.70	1.64	0.54	0.19	2.81	1.78	2.45	2.34
DS-TransUNet	0.59	2.37	6.76	3.68	0.23	2.43	1.08	0.81	0.11	0.58	0.14	0.52	1.13	2.93	0.80	0.26	4.44	2.88	9.51	2.02
D-TransUNet	0.65	2.80	4.90	1.13	0.23	1.82	0.64	0.67	0.07	0.35	0.18	0.27	0.38	3.62	0.56	0.08	3.64	2.35	6.27	1.80
DoubleUNet	0.76	1.76	1.99	2.89	0.21	1.60	0.55	0.51	0.13	0.14	0.19	0.35	0.63	1.60	1.09	0.24	0.68	1.66	2.47	1.18
EMCAD	0.11	0.45	1.26	0.35	0.13	0.66	0.30	0.36	0.10	0.21	0.13	0.24	0.38	1.04	0.69	0.16	0.55	0.88	3.99	0.93
ERDUNet	0.31	0.83	1.83	1.52	0.09	1.00	0.34	1.52	0.07	0.45	0.09	0.19	0.50	1.04	0.78	0.12	1.25	1.25	2.82	0.72
ESKNet	0.78	3.97	6.14	3.95	0.28	2.77	0.87	1.08	0.08	0.59	0.15	0.36	0.90	2.34	0.38	0.07	3.32	3.57	2.80	2.86
EVIT-UNet	0.86	1.80	4.61	1.63	0.41	1.04	0.78	0.73	0.11	0.22	0.25	0.49	0.75	1.24	0.78	0.20	4.18	1.58	7.04	1.95
FAE-Net	0.14	0.30	0.89	1.31	0.04	0.58	0.07	0.25	0.04	0.13	0.03	0.08	0.19	0.69	0.21	0.04	0.91	0.49	2.38	0.65
FCBFormer	1.04	2.81	3.86	2.90	0.21	1.80	0.49	0.88	0.06	0.11	0.06	0.19	0.88	1.88	0.39	0.05	1.71	1.67	8.78	2.71
GH-UNet	0.95	3.08	6.25	4.40	0.30	4.03	0.54	1.23	0.15	0.59	0.39	0.56	1.81	1.55	0.68	0.17	3.77	3.42	9.85	3.52
GA-CASCADE	0.27	1.81	2.66	0.50	0.22	0.45	0.54	0.45	0.10	0.46	0.17	0.28	0.71	1.24	0.88	0.18	2.11	1.44	3.91	1.12
H2Former	0.36	1.50	2.52	1.37	0.11	1.53	0.44	0.52	0.08	0.37	0.10	0.22	0.38	0.79	0.44	0.10	2.60	1.34	4.47	1.34
Hvmmnet	0.93	1.62	2.63	1.84	0.49	2.49	0.62	0.84	0.07	0.50	0.26	0.43	1.44	1.97	0.90	0.02	1.72	2.75	6.49	2.02
HfFormer	0.12	0.25	0.65	0.23	0.13	1.02	0.27	0.28	0.08	0.11	0.05	0.15	0.28	0.59	0.33	0.07	0.82	0.57	2.08	0.67
LFU-Net	0.52	1.88	3.25	2.27	0.20	1.25	0.24	0.34	0.07	0.62	0.12	0.24	0.60	2.12	0.90	0.15	1.39	1.06	2.45	0.91
LGMsNet	0.26	0.53	1.23	0.61	0.04	1.28	0.22	0.25	0.03	0.12	0.06	0.06	0.11	0.49	0.31	0.03	1.15	0.64	0.67	0.59
LV-UNet	0.14	0.33	0.87	0.14	0.08	1.06	0.13	0.15	0.09	0.35	0.04	0.08	0.15	0.55	0.89	0.07	0.59	0.42	0.38	0.32
LEVIT-UNet	0.29	0.40	1.79	0.78	0.12	1.20	0.58	0.67	0.06	0.16	0.06	0.14	0.33	0.44	0.47	0.50	0.42	0.50	0.61	0.64
MALUNet	0.22	0.39	1.33	0.44	0.07	0.92	0.13	0.01	0.04	0.16	0.04	0.13	0.30	0.81	0.66	0.07	0.50	0.04	0.90	0.45
MBSNet	0.24	0.51	1.22	0.87	0.07	1.24	0.25	0.26	0.05	0.10	0.05	0.08	0.23	0.36	0.31	0.03	0.78	0.61	1.39	0.63
MCA-UNet	0.75	3.40	5.05	2.69	0.22	1.71	0.87	1.09	0.13	0.49	0.15	0.49	0.90	1.25	0.42	0.89	0.95	1.86	10.50	3.13
MDSA-UNet	0.72	1.67	3.72	2.52	0.31	1.75	0.48	0.57	0.11	1.09	0.18	0.45	0.87	2.38	0.94	0.18	2.87	1.48	4.89	1.50
MEGANet	0.10	0.34	1.16	1.61	0.12	1.21	0.19	0.27	0.09	0.07	0.10	0.11	0.24	0.38	0.57	0.08	0.43	0.37	1.69	0.66
MERT	0.65	1.77	7.08	0.83	0.22	1.47	0.55	0.40	0.08	0.33	0.19	0.18	0.39	1.42	0.34	0.12	1.57	1.27	7.47	1.14
MADGNet	0.15	1.44	3.33	3.87	0.21	2.72	0.48	0.92	0.12	0.90	0.19	0.39	0.98	2.05	0.53	0.18	1.60	1.13	5.91	1.51
MMUNet	0.26	1.32	2.46	1.32	0.07	1.27	0.57	0.64	0.10	0.20	0.11	0.20	1.09	1.22	0.39	0.06	1.06	1.31	5.35	1.66
MMSA-UNet	0.24	2.34	5.22	1.84	0.10	1.24	0.40	0.80	0.22	0.15	0.12	0.24	0.54	2.44	0.55	0.26	1.44	1.45	6.45	1.11
MRFNet	2.23	6.89	9.72	7.91	0.69	3.76	1.61	1.30	0.15	1.31	0.44	1.00	2.42	7.90	0.94	0.51	5.37	5.30	9.41	3.39
MT-UNet	1.76	2.67	6.79	3.97	0.39	3.81	1.34	1.20	0.14											

2538
2539
2540
2541
2542
2543
2544
2545
2546
2547
2548
2549
2550
2551
2552
2553
2554
2555
2556
2557
2558
2559
2560
2561
2562
2563
2564
2565
2566
2567
2568
2569
2570
2571
2572
2573
2574
2575
2576
2577
2578
2579
2580
2581
2582
2583
2584
2585
2586
2587
2588
2589
2590
2591

Table 27: Average zeroshot performance of 100 u-shape medical image segmentation networks with IoU. Source → Target. Baseline U-Net is highlighted (gray background), and statistical significance of p-value is highlighted: $p < 0.0001$, $p < 0.001$, $p < 0.05$, $p \leq 0.05$, and $P > 0.05$ (Not significant).

Rank	Network	BUSI → BUS	Ultrasound BUSBRA → BUS	TNSCUI → TUCC	Endoscopy Kvasir → CVC300	Endoscopy Kvasir → CVC ClinicDB	Dermoscopy ISIC2018 → PH2	Fundus CHASE → Stare	X-Ray Montgomery → NIH-test	Histopathology Monusc → Tabcmicel	Avg
#1	RWKV-Net	80.73	84.73	63.42	82.14	75.50	86.00	61.29	82.41	38.96	70.94
#2	DS-TransUNet	78.70	84.44	61.95	80.58	77.38	84.05	57.65	76.21	44.20	70.07
#3	TransResUNet	81.27	85.62	62.36	79.13	76.42	84.20	59.77	87.69	35.19	69.47
#4	CENet	82.70	86.29	62.15	78.57	73.14	84.10	53.32	71.06	43.03	69.31
#5	MADGNet	79.78	84.47	61.27	81.24	76.33	83.08	48.94	83.67	48.98	69.08
#6	G-CASCADE	82.61	85.27	65.10	77.89	74.77	85.96	48.80	78.05	46.18	68.85
#7	DA-TransUNet	82.32	84.15	61.81	71.24	70.64	82.81	56.44	85.87	54.43	68.65
#8	TA-Net	81.02	84.38	62.89	81.24	72.03	84.15	45.67	77.53	50.74	68.58
#9	MEGA-Net	81.24	86.62	64.37	78.67	75.64	84.99	45.75	88.19	38.36	68.39
#10	EMCAD	82.83	84.95	61.20	79.93	76.56	83.63	49.19	73.37	46.41	68.24
#11	CFFormer	81.12	79.53	62.34	78.56	76.18	83.04	52.38	80.49	33.32	68.09
#12	CASCADE	82.11	85.96	63.48	80.57	77.22	84.63	46.97	77.07	37.76	67.91
#13	Swin-umamba	82.91	85.02	64.00	79.96	73.57	84.62	54.52	81.96	38.39	67.86
#14	AC_MambaSeg	79.84	82.31	63.01	72.82	70.73	84.34	52.78	78.58	40.53	67.61
#15	MCAU-Net	81.88	83.28	63.78	72.00	72.00	85.49	56.89	78.50	32.40	67.60
#16	MSLAU-Net	80.96	84.90	66.15	78.24	71.49	86.52	46.51	78.69	31.46	67.20
#17	AURA-Net	78.40	84.67	61.52	79.18	73.50	83.91	51.22	81.54	31.25	67.10
#18	CSKAI-Net	78.37	84.65	63.40	77.50	74.50	84.54	49.61	73.47	36.58	67.09
#19	VMUNet	81.18	82.96	62.31	76.54	74.15	84.27	52.96	77.96	44.40	66.79
#20	FAI-Net	77.91	84.86	60.23	74.22	71.64	84.22	51.38	82.19	29.64	66.60
#21	FCBFormer	79.14	86.10	65.52	74.82	73.16	83.85	57.20	74.55	42.38	66.46
#22	Perspective-Unit	76.17	84.69	61.76	77.38	72.13	83.57	45.92	77.21	36.12	66.34
#23	Swin-umambaD	80.68	84.39	62.69	78.38	76.83	83.37	39.76	83.13	38.59	66.33
#24	LGMNet	78.45	83.34	65.16	74.57	75.91	85.00	46.58	76.02	30.87	66.06
#25	CE-Net	80.34	83.77	62.09	76.99	70.87	84.02	43.52	80.83	32.30	65.94
#26	LV-UNet	74.19	82.72	63.61	78.86	69.42	84.99	49.02	78.82	28.67	65.83
#27	GHIUNet	77.25	83.26	62.49	77.22	70.59	83.51	45.55	64.56	43.52	65.19
#28	UTANet	77.05	84.62	61.59	80.78	70.99	84.59	45.25	73.38	23.55	65.29
#29	U-KAN	77.25	83.97	62.65	72.87	69.77	83.29	46.24	69.99	38.33	65.28
#30	MMUNet	76.53	81.53	61.69	74.35	69.63	83.65	49.19	70.73	37.11	65.19
#31	MBSNet	76.37	83.08	62.45	78.22	72.68	84.65	45.63	63.98	28.80	65.15
#32	CA-Net	75.84	83.01	62.74	73.87	67.49	82.44	49.38	64.74	39.98	65.01
#33	DDS-UNet	77.36	83.49	63.09	75.43	71.24	82.18	45.03	74.29	38.82	65.01
#34	HiFormer	72.21	84.20	63.94	71.83	74.53	82.75	50.25	81.65	32.41	64.95
#35	ResU-KAN	72.73	83.11	62.79	71.81	72.61	84.22	47.60	73.55	31.51	64.82
#36	PuNet	82.13	84.19	63.59	83.31	77.39	84.58	50.31	84.58	38.53	64.81
#37	SwinUNETR	74.70	84.18	59.91	63.58	68.44	83.73	57.55	74.66	32.98	64.70
#38	H2Former	78.22	83.81	64.48	74.03	70.50	85.39	47.19	63.56	28.62	64.68
#39	EVIUNet	79.07	84.95	65.83	81.11	71.49	83.79	54.16	43.53	30.14	64.66
#40	TransFuse	80.18	83.93	61.74	79.19	72.54	84.84	35.95	81.78	32.58	64.61
#41	Caranet	81.32	84.87	64.61	79.32	73.86	84.85	26.94	86.22	33.32	64.39
#42	DAEFormer	72.80	84.02	63.12	68.10	66.69	82.81	52.57	65.70	45.16	64.36
#43	VMUNetV2	72.72	84.58	63.70	78.80	74.66	84.65	36.68	73.96	36.84	64.23
#44	MissFormer	72.82	84.76	61.39	71.99	68.27	83.88	52.27	70.49	40.61	63.99
#45	Mobile U-ViT	77.80	84.42	60.84	74.94	69.72	84.30	46.86	72.77	32.77	63.92
#46	UTNet	77.64	83.78	60.04	72.66	68.39	84.14	45.38	68.83	32.14	63.91
#47	DCAU-Net	70.88	84.08	61.95	74.88	68.86	82.77	43.94	62.76	41.48	63.81
#48	CPCANet	79.14	84.65	62.82	76.62	68.33	84.32	46.33	68.21	32.81	63.68
#49	ESKNet	76.99	84.39	63.07	77.23	73.85	83.81	40.79	71.68	36.36	63.64
#50	D-TransUNet	71.01	79.89	59.21	72.85	69.36	84.46	47.43	61.20	32.90	63.62
#51	U-Net++	76.68	85.46	66.04	73.87	75.17	83.90	28.02	77.00	32.42	63.62
#52	UCTransNet	68.11	80.41	60.58	75.06	68.57	83.54	45.90	73.57	34.93	63.51
#53	TransUNet	74.80	83.73	61.24	73.98	71.26	83.87	50.12	55.80	28.16	63.47
#54	CMU-Net	75.72	83.52	61.57	75.09	70.11	86.09	45.25	73.47	38.16	63.47
#55	SCU-Net++	73.77	82.73	59.35	71.67	67.82	82.74	47.08	68.66	35.88	63.43
#56	UNet+	70.13	80.70	60.40	75.98	69.52	83.27	49.76	73.74	29.28	63.33
#57	RollingUNet	72.58	83.70	62.34	77.36	69.26	84.97	46.98	64.60	32.75	63.08
#58	MSRFNet	69.01	81.90	58.35	72.59	73.48	83.15	55.17	58.97	21.74	62.99
#59	UACANet	80.81	84.82	62.47	81.72	74.99	85.12	25.10	81.88	26.84	62.84
#60	PolyP-PVT	81.02	85.65	65.23	73.87	75.17	83.90	28.02	77.00	32.42	62.80
#61	MERIT	80.46	83.26	66.00	81.39	74.70	85.94	38.06	73.80	43.43	62.80
#62	TransNorm	82.11	84.33	63.81	69.78	68.51	83.03	53.31	82.90	39.03	62.72
#63	DDANet	71.75	80.45	60.11	78.78	70.72	83.43	47.81	61.04	22.99	62.65
#64	ERDU-Net	76.56	84.30	62.23	72.47	69.51	83.98	52.97	60.27	34.34	62.39
#65	MedFormer	77.54	85.00	63.57	73.91	69.55	84.18	43.98	52.97	31.26	62.37
#66	U-Net	72.44	81.37	60.50	70.33	69.87	84.00	46.77	71.33	26.05	62.23
#67	TransUNet	80.27	83.90	60.54	72.24	68.20	83.39	52.10	83.03	34.36	61.87
#68	MedV-KAN	71.36	82.32	59.69	67.30	62.66	85.03	48.48	55.99	44.42	61.79
#69	TinyNet	67.40	78.61	59.50	70.89	59.72	82.99	44.68	67.16	34.12	61.73
#70	CFPNet-M	71.42	82.93	60.77	71.50	66.16	84.69	48.80	59.24	36.32	61.63
#71	AnU-Net	73.47	81.25	58.99	73.40	67.76	80.58	48.93	71.44	20.90	61.43
#72	DoubleUNet	73.47	86.51	58.48	79.92	75.72	80.70	54.56	77.45	26.88	61.37
#73	MDSA-U-Net	71.81	82.57	61.04	69.72	65.42	84.23	37.16	62.69	41.23	60.94
#74	UNetX	70.12	82.21	58.82	63.13	61.57	82.39	44.89	66.99	32.78	60.78
#75	MT-UNet	67.76	81.09	57.52	67.90	65.41	84.35	49.51	60.96	26.84	60.71
#76	UNetV2	68.88	82.84	61.87	69.68	67.73	82.38	31.55	68.47	45.32	60.24
#77	ULine	69.48	78.69	56.63	62.46	59.87	83.99	52.23	57.63	32.26	60.23
#78	CMUNetX	19.06	82.31	62.22	76.45	67.38	85.52	49.66	67.20	43.51	59.53
#79	ResUNet++	59.29	79.77	60.51	68.06	67.79	81.01	44.02	57.08	30.00	59.45
#80	MUCM-Net	70.99	82.13	58.58	54.35	50.60	83.24	45.83	76.29	32.00	59.37
#81	H-mmnet	74.93	83.30	56.18	59.46	61.00	83.55	33.00	75.52	37.65	59.28
#82	U-RWKV	66.30	81.90	61.57	58.94	59.56	84.87	44.96	59.35	26.51	59.16
#83	BEFNet	65.27	77.20	57.28	71.27	64.23	79.48	41.29	62.93	30.47	58.64
#84	ConvFormer	71.15	82.91	62.96	76.65	67.22	83.44	30.23	56.70	36.17	58.36
#85	MedT	64.12	82.59	61.63	57.05	56.94	84.14	49.33	53.30	31.27	58.27
#86	CSWin-U-Net	64.89	83.11	57.60	71.46	63.25	83.27	20.29	67.40	45.18	57.88
#87	ScalFormer	60.36	82.41	60.43	74.42	66.66	82.68	40.84	65.48	13.77	57.61
#88	DC-UNet	60.45	79.51	59.78	66.80	63.24	80.95	46.60	48.64	21.43	57.37
#89	UNETR	59.78	76.24	46.17	61.36	55.46	81.63	56.52	62.18	32.47	57.02
#90	ManU-Net	37.61	83.92	46.43	71.11	75.05	82.08	41.96	48.04	34.32	56.55
#91	Zig-R3R	57.05	81.08	53.31	65.19	61.02	84.54	33.02	68.03	27.10	56.25
#92	LeViT-UNet	58.33	70.27	53.69	60.61	61.89	81.11	32.46	66.76	38.53	55.53
#93	CFM-UNet	63.88	81.77	59.27	60.61	61.89	81.11	32.46	70.69	32.33	55.14
#94	Swin-UNet	60.42	78.35	37.59	45.60	48.58	83.05	39.79	65.60	43.81	54.06
#95	ColorSegNet	51.95	68.99	50.15	69.58	67.46	82.00	43.98	58.15	22.87	53.73
#96	MultiResNet	62.19	77.67	58.39	62.19	62.19	85.60	19.48	60.99	24.38	53.42
#97	UltraLight-VM-UNet	64.99	77.60	54.56	33						

2592
2593
2594
2595
2596
2597
2598
2599
2600
2601
2602
2603
2604
2605
2606
2607
2608
2609
2610
2611
2612
2613
2614
2615
2616
2617
2618
2619
2620
2621
2622
2623
2624
2625
2626
2627
2628
2629
2630
2631
2632
2633
2634
2635
2636
2637
2638
2639
2640
2641
2642
2643
2644
2645

Table 28: Average zeroshot performance of 100 u-shape medical image segmentation networks with U-Score. Source → Target. Baseline U-Net is highlighted (gray background), and statistical significance of p-value is highlighted: $p < 0.0001$, $p < 0.001$, $p < 0.05$, $p \leq 0.05$, and $P > 0.05$ (Not significant).

Rank	Network	BUS1 → BUS	Ultrasound BUSRA → BUS	TNSCU1 → TUCC	Endoscopy Kvasir → CV300	Endoscopy Kvasir → CVC-ClinicDB	Dermoscopy ISIC2018 → PH2	Fundus CHASE → Stare	X-Ray Montgomery → NIH-test	Histopathology Monuse → Tabcnuclei	Avg
#1	LVUNet	79.62	79.18	97.84	96.96	76.12	99.23	92.89	92.65	25.00	82.67
#2	LGMNet	84.79	78.74	90.80	76.60	89.51	90.21	80.85	78.81	39.90	78.41
#3	MBSNet	77.02	74.05	79.08	83.56	79.75	82.13	87.32	43.20	25.09	70.02
#4	CMUNet	9.41	68.19	78.86	80.54	60.39	88.85	72.94	52.42	86.90	67.85
#5	U-KAN	70.78	72.11	71.77	62.44	63.55	50.87	73.45	55.88	64.91	64.96
#6	MobileLAVT	72.22	74.93	88.24	68.02	63.51	62.62	55.00	62.65	42.28	62.51
#7	SwiUNETR	67.82	75.92	55.97	20.27	60.58	61.65	74.63	68.20	48.32	61.36
#8	RWKV-UNet	61.22	60.87	60.37	61.72	61.72	61.72	61.72	61.72	54.63	60.74
#9	CFNet-M	61.28	70.75	65.26	62.37	52.32	79.91	52.40	12.08	63.30	59.42
#10	DCSAU-Net	55.27	71.60	67.23	66.31	59.60	36.03	70.20	31.18	70.95	58.63
#11	TA-Net	58.07	56.54	55.73	58.27	55.85	52.01	54.42	54.56	58.27	55.13
#12	GCASCADE	56.29	56.29	56.29	54.38	55.53	55.26	51.75	51.75	56.29	54.82
#13	VMUNetV2	51.87	61.86	62.58	61.93	62.12	60.43	45.65	54.54	51.76	54.32
#14	MUCM-Net	66.09	70.89	46.67	9.50	9.50	57.21	72.47	43.86	60.39	54.06
#15	Tinyunet	50.36	9.52	99.89	67.78	59.52	49.25	100.00	59.94	61.09	53.68
#16	ResU-KAN	51.36	55.48	59.20	50.24	58.34	57.85	59.55	53.38	35.93	53.67
#17	Swin-umambaD	59.87	58.55	57.07	58.75	60.39	44.17	43.86	60.39	52.99	53.55
#18	MDSA-UNet	58.39	62.92	62.60	52.32	52.32	67.55	47.04	31.00	41.26	53.44
#19	CE-Net	59.07	56.04	54.75	56.67	53.28	52.07	54.55	58.87	53.60	53.05
#20	UNeXt	63.62	73.33	50.73	17.38	20.95	22.82	86.58	55.21	37.67	51.85
#21	EMCAD	53.84	53.39	46.72	53.52	53.54	43.46	48.97	46.56	53.54	50.30
#22	UTNet	56.14	55.88	45.86	50.03	47.93	53.00	55.60	44.01	37.29	49.59
#23	TransResUNet	51.29	51.29	48.14	50.68	51.29	46.72	51.29	51.29	40.76	49.19
#24	MEGANet	50.66	50.68	50.68	49.74	50.68	50.49	42.87	50.68	45.68	48.62
#25	Polyp-PVT	58.92	59.13	59.13	51.69	58.76	50.25	18.09	54.79	37.99	45.77
#26	U-RWKV	41.67	63.35	73.57	9.40	9.40	85.61	81.67	12.90	9.40	45.45
#27	TransFuse	52.09	50.27	47.84	52.41	49.82	51.90	36.28	52.76	35.76	45.42
#28	CASCADE	47.32	47.32	46.62	52.41	47.32	45.65	43.16	44.54	41.72	45.36
#29	DDA-Net	48.46	36.58	46.87	59.54	53.69	45.34	59.11	21.08	8.97	43.40
#30	ULine	60.72	9.81	11.01	11.15	9.52	79.09	90.83	9.52	50.56	33.18
#31	MissFormer	40.85	46.97	42.48	40.26	39.50	36.98	34.67	39.01	44.66	41.18
#32	MambaNet	9.21	68.85	9.21	69.26	73.10	9.21	57.45	9.21	50.76	40.81
#33	MMUNet	42.37	36.22	41.36	41.16	38.45	45.18	43.44	47.73	39.33	40.78
#34	HiFormer	39.96	45.65	47.16	46.51	46.45	27.56	25.16	46.92	32.64	40.30
#35	VMUNet	43.76	8.49	41.40	41.74	42.93	40.77	43.54	41.90	43.80	39.16
#36	AC-MambaSeg	40.27	35.88	39.76	36.26	37.55	35.84	39.49	39.49	38.76	38.75
#37	ERDUNet	46.97	48.94	47.06	43.09	8.71	44.47	42.03	16.31	38.61	38.59
#38	MedFormer	44.92	47.19	46.67	42.80	41.31	43.24	42.03	8.61	29.61	38.55
#39	CSCANet	38.73	39.51	39.38	38.79	38.79	38.48	39.97	36.01	34.81	38.02
#40	MALLUNet	66.47	61.83	42.64	9.50	9.50	9.50	9.50	72.61	79.25	37.03
#41	UNetV2	40.05	49.71	51.24	41.89	44.35	19.05	8.87	41.64	56.52	36.22
#42	U-Net++	39.73	42.08	35.74	31.99	31.99	40.71	37.85	19.88	35.15	35.15
#43	MSLAU-Net	36.48	36.46	36.58	35.91	34.44	35.58	35.30	35.50	25.44	34.61
#44	DAEFormer	34.51	37.81	38.89	29.09	31.36	25.45	35.60	27.95	39.11	33.83
#45	H2Former	37.20	36.86	38.42	35.25	35.25	35.25	32.97	32.97	31.63	33.66
#46	FAT-Net	34.91	35.96	30.98	33.42	34.12	33.85	35.59	36.12	20.71	33.09
#47	SCU-Net++	35.20	35.43	30.44	36.89	32.95	24.36	35.07	31.51	32.84	33.05
#48	UltralightVMUNet	34.82	9.42	9.42	9.42	9.42	65.92	65.92	51.07	66.00	30.98
#49	ESKNet	33.19	34.06	33.93	33.66	33.98	31.02	20.38	30.69	30.54	30.92
#50	AURA-Net	31.44	31.96	30.05	32.01	31.50	29.45	30.93	32.10	22.91	31.38
#51	MedVQA-Net	30.65	31.74	29.26	25.79	25.79	35.54	32.04	8.12	35.56	28.23
#52	CA-Net	30.40	30.03	31.19	29.64	27.55	16.65	32.10	21.63	30.55	28.05
#53	RollingUNet	28.23	30.21	30.15	30.60	28.46	23.58	30.69	22.48	7.88	26.15
#54	DDUNet	28.39	28.11	28.82	28.02	27.83	9.00	26.41	27.44	27.44	25.83
#55	DC-UNet	8.79	23.53	40.76	32.42	27.62	8.79	50.79	8.79	8.79	25.67
#56	BEFUNet	25.62	8.49	18.93	36.88	28.37	8.49	35.89	24.46	25.98	24.72
#57	LFI-UNet	9.52	9.52	9.52	9.52	9.52	9.52	42.39	33.83	42.44	24.15
#58	SimpleUNet	9.52	9.52	9.52	9.52	9.52	13.21	17.47	62.24	38.50	23.40
#59	MultiResUNet	14.92	9.10	36.43	51.70	42.92	22.06	9.10	21.57	9.10	22.60
#60	Swin-umamba	22.64	22.64	22.64	22.64	22.29	22.23	19.13	22.62	21.46	22.09
#61	CSWin-UNet	20.18	29.87	18.57	28.02	20.46	26.01	7.91	25.61	31.76	21.63
#62	SwiUNet	8.48	8.48	8.48	8.48	8.48	30.92	36.49	30.06	43.42	21.50
#63	GH-UNet	20.77	20.52	20.79	20.92	20.32	21.28	20.69	16.76	21.19	20.32
#64	MADGNet	20.32	20.29	19.44	20.48	20.48	20.48	19.97	20.48	20.43	20.23
#65	CENet	20.23	20.23	19.63	20.07	19.88	19.36	20.23	18.67	20.23	19.87
#66	LeViT-UNet	8.87	8.87	8.87	8.87	20.31	8.87	34.99	38.17	49.73	19.64
#67	Zig-RIR	8.20	29.22	8.20	21.61	12.05	35.75	27.02	29.58	9.13	19.08
#68	DoubleUNet	23.10	24.81	19.15	24.80	24.81	7.39	7.39	24.09	7.39	18.77
#69	TransAttNet	20.75	21.21	20.57	20.69	20.93	20.38	21.75	7.09	11.85	18.65
#70	DA-TransUNet	18.84	18.58	18.19	17.39	18.08	14.99	18.46	18.84	18.84	18.10
#71	U-Net	19.20	18.36	19.07	18.58	19.53	19.60	19.23	19.08	6.97	17.93
#72	UNet+	17.68	16.66	18.16	18.30	18.54	17.29	18.96	18.69	14.32	17.78
#73	TransUNet	19.63	19.34	18.31	18.43	18.18	17.67	6.86	19.72	17.62	17.53
#74	CFM-UNet	15.96	23.46	22.01	21.67	7.53	24.92	7.53	23.40	21.06	17.51
#75	CFCANet	18.42	18.51	17.34	18.28	17.27	18.07	17.12	12.24	17.66	17.55
#76	MedT	15.50	22.46	22.84	7.32	7.32	22.86	22.69	7.32	18.43	17.00
#77	UTANet	18.16	18.48	17.87	18.59	17.92	18.29	18.41	17.95	6.73	16.99
#78	Caranet	18.50	18.46	18.50	18.41	18.30	18.39	13.86	18.50	16.21	16.58
#79	AttUNet	19.41	18.17	17.43	19.50	18.74	6.97	18.78	19.07	6.97	16.50
#80	H-vonnet	22.30	22.52	7.26	7.26	16.20	21.07	13.10	22.46	21.94	16.28
#81	CMU-Net	16.06	17.06	16.85	16.97	16.74	15.29	12.65	16.69	16.74	16.26
#82	TransNorm	17.34	17.17	17.31	15.69	16.22	14.84	6.55	17.34	16.74	15.65
#83	ScribFormer	6.98	19.45	19.11	19.88	18.33	15.30	15.32	17.00	6.98	15.64
#84	ResUNet++	7.16	13.83	20.54	18.66	20.20	7.16	21.87	7.16	15.89	15.50
#85	PraNet	17.33	17.12	17.26	17.33	17.33	16.86	10.52	17.33	16.66	15.43
#86	EVTFUNet	16.03	16.16	16.18	16.18	15.75	15.31	16.18	6.38	12.62	14.70
#87	UCTransNet	13.43	12.96	14.33	14.76	14.31	14.12	14.78	14.56	14.02	14.18
#88	FCBFormer	14.49	14.61	14.55	14.22	14.43	13.96	11.84	14.15	14.52	14.14
#89	MSRFNet	14.46	15.05	13.35	15.31	15.93	14.23	16.11	6.73	6.37	13.36
#90	D-TransUNet	12.34	11.52	12.83	13.88	12.63	14.02	14.00	13.48	12.73	12.73
#91	MCA-UNet	13.39	13.39	13.37	12.75	12.86	13.39	13.39	13.14	11.88	13.09
#92	Respective-UNet	12.12	12.32	12.06	12.23	12.15	11.69	12.26	12.17	11.76	12.07
#93	LINEIT	7.08	7.08	7.08	7.08	7.08	7.08	7.08	7.08	7.08	11.64
#94	MERIT	12.52	12.28	12.56	12.56	12.51	12.56	5.73	12.16	12.51	11.63
#95	ColonSegNet	7.28	7.28	7.28	20.52	21.00	7.28	7.28	7.28	7.28	11.40
#96	DS-TransUNet	10.72	10.74	10.60	10.80	10.80	10.80	10.80	10.80	10.79	10.72
#97	UACANet	12.63	12.62	12.46	12.65	12.62	12.65	7.24	12.64	5.74	10.70
#98	ConvFormer	11.76	12								

2646
2647
2648
2649
2650
2651
2652
2653
2654
2655
2656
2657
2658
2659
2660
2661
2662
2663
2664
2665
2666
2667
2668
2669
2670
2671
2672
2673
2674
2675
2676
2677
2678
2679
2680
2681
2682
2683
2684
2685
2686
2687
2688
2689
2690
2691
2692
2693
2694
2695
2696
2697
2698
2699

Table 29: Per-dataset source ranking of 100 u-shape medical image segmentation networks with IoU

Table with 25 columns: Rank, Model, Dataset, Source, and 23 other datasets. The table lists various medical image segmentation models and their performance rankings across different source datasets.

2700
2701
2702
2703
2704
2705
2706
2707
2708
2709
2710
2711
2712
2713
2714
2715
2716
2717
2718
2719
2720
2721
2722
2723
2724
2725
2726
2727
2728
2729
2730
2731
2732
2733
2734
2735
2736
2737
2738
2739
2740
2741
2742
2743
2744
2745
2746
2747
2748
2749
2750
2751
2752
2753

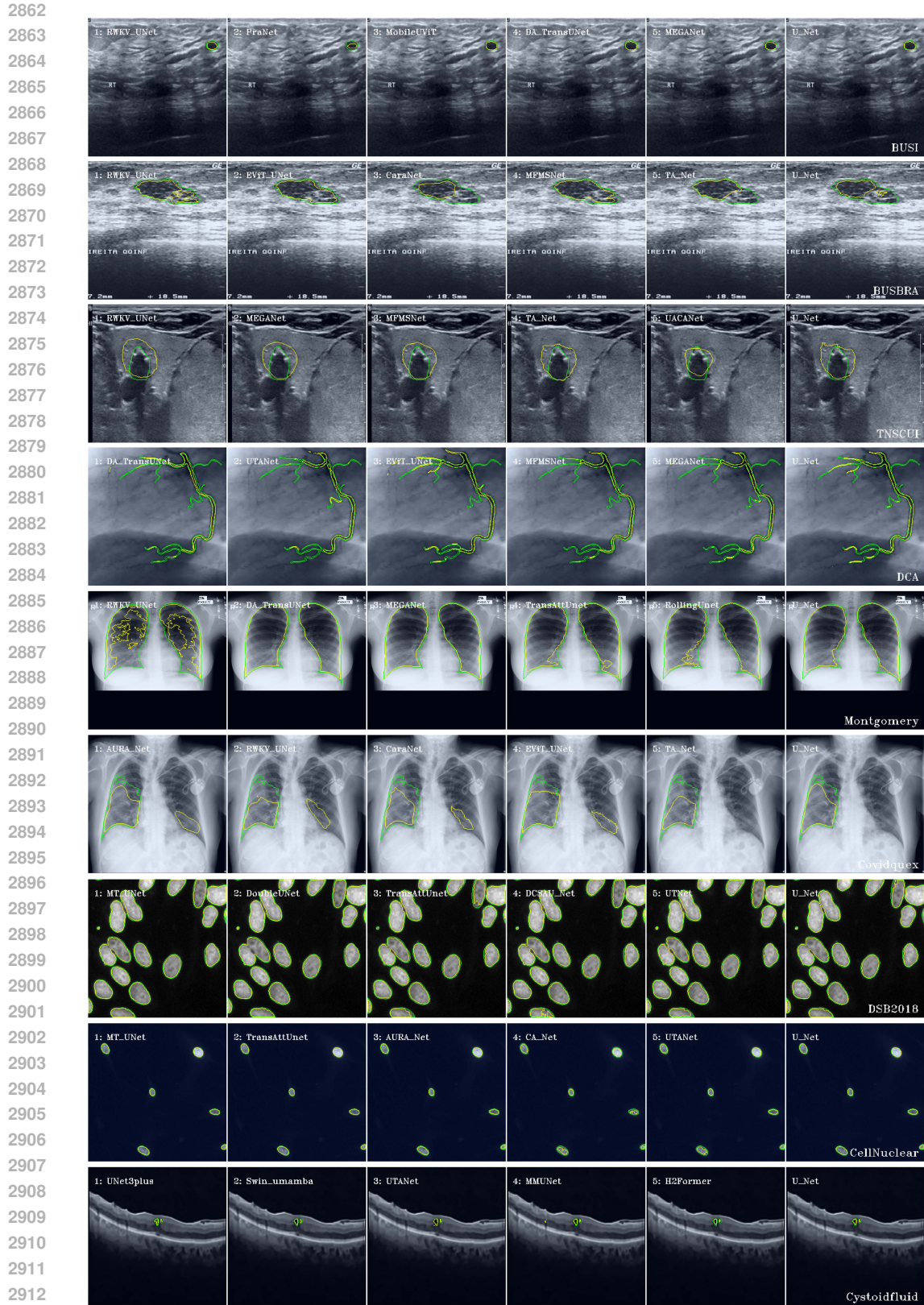
Table 30: Per-dataset target ranking of 100 u-shape medical image segmentation networks with IoU. Source → Target.

Rank	BUS1 → BUS	Ultrasound BUSRA → BUS	TNSCU1 → TUCC	Endoscopy Kvasir → CVC300	Endoscopy Kvasir → CVC-ClinicDB	Dermscopy ISIC2018 → PH2	Fundus CHASE → Stare	X-Ray Montgomery → NIH-test	Histopathology Mousse → Tabnuclei
1	Swin-umamba	MEGANet	MSLAU-Net	PraNet	PraNet	MSLAU-Net	RWKV-UNet	MEGANet	TA-Net
2	EMCAD	DoubleUNet	MERIT	RWKV-UNet	DS-TransUNet	RWKV-UNet	DS-TransUNet	TransResUNet	CE-Net
3	CE-Net	EVIT-UNet	UACANet	UACANet	G-CASCADE	G-CASCADE	SwintUNETR	CaraNet	U-Net++
4	G-CASCADE	FCBFormer	Polyp-PVT	MERIT	Swin-umambaD	MERIT	FCBFormer	DA-TransUNet	EMCAD
5	DA-TransUNet	CASCADE	LGMsNet	EMCAD	EMCAD	MMUNet	MCA-UNet	U-NetV2	G-CASCADE
6	FraNet	Polyp-PVT	G-CASCADE	TransResUNet	TransResUNet	HFFormer	UNETR	MADGNet	UNetV2
7	CASCADE	TransResUNet	CaraNet	EVIT-UNet	MADGNet	CMUNetXt	DA-TransUNet	Swin-umambaD	CSWin-UNet
8	TransNorm	U-Net++	H2Former	TA-Net	TA-Net	UACANet	UACANet	MSRFNet	TransUNet
9	MCA-UNet	MCA-UNet	MEGANet	DS-TransUNet	DoubleUNet	MADGNet	DoubleUNet	TransNorm	DA-TransUNet
10	CaraNet	G-CASCADE	Swin-umamba	CASCADE	MEGANet	MCA-UNet	Swin-umamba	RWKV-UNet	MedVkan
11	TransResUNet	Swin-umamba	Hiformer	Swin-umamba	RWKV-UNet	CFFormer	EVIT-UNet	FAT-Net	VMUNet
12	MEGANet	MedFormer	TransNorm	EMCAD	Polyp-PVT	MedVkan	CE-Net	Swin-umamba	DS-TransUNet
13	VMUNet	EMCAD	MCA-UNet	DoubleUNet	MambaNet	GH-UNet	TransNorm	MADGNet	MADGNet
14	CFFormer	EVIT-UNet	DAEFormer	TransFuse	LGMsNet	LGMsNet	ERDUNet	TransFuse	SwintUNet
15	Polyp-PVT	MSLAU-Net	VMUNetV2	AURA-Net	UACANet	MEGANet	VMUNet	Hiformer	GH-UNet
16	TA-Net	CaraNet	LV-UNet	TransResUNet	G-CASCADE	LV-UNet	AC-MambaSeg	AURA-Net	CMUNetXt
17	MSLAU-Net	FaT-Net	FraNet	CaraNet	MERIT	URWKV	DAEFormer	CE-Net	MERIT
18	UACANet	MedFormer	Hiformer	Hiformer	VMUNetV2	CaraNet	CFFormer	CFFormer	FCBFormer
19	RWKV-UNet	MisFormer	FCBFormer	LV-UNet	Hiformer	TransFuse	MisFormer	LV-UNet	DS-UNet
20	Swin-umambaD	RWKV-UNet	CASCADE	VMUNetV2	VMUNetV2	CPNet-M	MSLAU-Net	MISA-UNet	MISA-UNet
21	MERIT	Perspective-UNet	RWKV-UNet	DDANet	CaraNet	MBSNet	TransUNet	MisFormer	AC-MambaSeg
22	CE-Net	AURA-Net	CSCAU-Net	MEGANet	ESKNet	VMUNetV2	FAT-Net	G-CASCADE	AC-MambaSeg
23	TransUNet	DS-UNet	CSCAU-Net	CE-Net	Swin-umamba	CASCADE	AURA-Net	VMUNet	CA-Net
24	TransFuse	CPANet	ESKNet	CFFormer	AURA-Net	U-Net++	TransResUNet	TA-Net	TransNorm
25	AC-MambaSeg	UTANet	AC-MambaSeg	Swin-umambaD	MSRFNet	Swin-umamba	Hiformer	DoubleUNet	RWKV-UNet
26	MADGNet	VMUNetV2	ConvFormer	MSLAU-Net	FCBFormer	MSLAU-Net	TransAttUNet	Perspective-UNet	MEGANet
27	FCBFormer	MADGNet	TA-Net	MBSNet	CE-Net	CSCAU-Net	U-Net++	CASCADE	DS-UNet
28	CPANet	DS-TransUNet	ResU-KAN	G-CASCADE	MBSNet	Zig-RIR	CMUNetXt	Polyp-PVT	Swin-umambaD
29	EVIT-UNet	Mobile U-ViT	CA-Net	CSCAU-Net	ResU-KAN	MT-UNet	MT-UNet	MCA-UNet	LeViT-UNet
30	DS-TransUNet	Mobile U-ViT	Swin-umambaD	Perspective-UNet	TransFuse	ResU-KAN	TransFuse	MUCM-Net	FCBFormer
31	LGMsNet	Swin-umambaD	U-KAN	RollingUNet	Perspective-UNet	MT-UNet	MeiT	DS-TransUNet	MALUNet
32	AURA-Net	TA-Net	GH-UNet	ESKNet	TA-Net	AC-MambaSeg	EMCAD	LGMsNet	Swin-umamba
33	CSCAU-Net	TransNorm	UACANet	GH-UNet	FaT-Net	TA-Net	LV-UNet	H-vmmnet	U-KAN
34	H2Former	ERDUNet	ERDUNet	MambaNet	EVIT-UNet	CPANet	MADGNet	UTANet	CMU-Net
35	FaT-Net	Hiformer	TransResUNet	CE-Net	MSLAU-Net	VMUNet	ArtU-Net	SwintUNETR	CASCADE
36	Mobile U-ViT	PubNet	CFFormer	CPANet	TransAttUNet	MDSAU-Net	G-CASCADE	FCBFormer	CPANet
37	UTNet	SwintUNETR	RollingUNet	ConvFormer	DS-UNet	FAT-Net	CPNet-M	DS-UNet	H-vmmnet
38	MedFormer	DA-TransUNet	VMUNet	UTANet	TransResUNet	MedFormer	MedVkan	VMUNetV2	MMUNet
39	DS-UNet	DCSAU-Net	ERDUNet	CMUNetXt	CSCAU-Net	MedFormer	MedVkan	MERIT	VMUNetV2
40	GH-UNet	DAEFormer	DAEFormer	CMUNet	TransFuse	MeiT	MeiT	UCTransNet	MISCAUNet
41	U-KAN	TransFuse	CE-Net	DS-UNet	AC-MambaSeg	MeiT	DDANet	UCTransNet	ESKNet
42	UTANet	TransFuse	CE-Net	CMU-Net	DDANet	UTNet	ResU-KAN	TransU-KAN	CPNet-M
43	ESKNet	MambaNet	DCAU-Net	U-Net++	U-Net++	DCSAU-Net	DS-TransUNet	G-CASCADE	UltraLight-VM-UNet
44	U-Net++	TransFuse	DS-TransUNet	Mobile U-ViT	GH-UNet	CFM-UNet	H2Former	CMU-Net	ConvFormer
45	ERDUNet	Hiformer	UNetV2	D-TransUNet	H2Former	DS-TransUNet	SCUNet++	EMCAD	Perspective-UNet
46	MMUNet	UTNet	DA-TransUNet	FCBFormer	CMU-Net	FCBFormer	RollingUNet	EMCAD	SCUNet++
47	MBSNet	CE-Net	Perspective-UNet	DCAU-Net	U-Net	U-Net	CASCADE	Mobile U-ViT	MALUNet
48	Perspective-UNet	TransFuse	TransFuse	LGMsNet	U-KAN	ULite	Mobile U-ViT	ESKNet	UCTransNet
49	CA-Net	ScritFormer	ScritFormer	ScritFormer	MBSNet	ERDUNet	U-Net	ArtU-Net	TransUNet
50	CMU-Net	CMU-Net	MeiT	MMUNet	MedFormer	AURA-Net	DC-UNet	U-Net	ERDUNet
51	H-vmmnet	DS-UNet	UTANet	FAT-Net	U-Net++	Polyp-PVT	LGMsNet	D-TransUNet	MambaNet
52	TransAttUNet	LGMsNet	CMU-Net	H2Former	MCA-UNet	TransAttUNet	MSLAU-Net	CE-Net	TinyUNet
53	SwintUNETR	H-vmmnet	TransUNet	TransUNet	LV-UNet	Mobile U-ViT	MMUNet	MMUNet	CFFormer
54	LV-UNet	MERIT	AURA-Net	MedFormer	D-TransUNet	FCBFormer	CMU-Net	MedFormer	CaraNet
55	SCUNet++	GH-UNet	MisFormer	Polyp-PVT	RollingUNet	ESKNet	Perspective-UNet	CFM-UNet	SwintUNETR
56	ArtU-Net	CSWin-UNet	MADGNet	CA-Net	MSLAU-Net	EVIT-UNet	U-Net++	U-KAN	D-TransUNet
57	DoubleUNet	ResU-KAN	TransAttUNet	TransAttUNet	MMUNet	SwintUNETR	MUCM-Net	UTNet	UNetXt
58	MisFormer	MBSNet	EMCAD	U-KAN	UCTransNet	EMCAD	MEGANet	SimpleUNet	TransFuse
59	DAEFormer	CA-Net	MDSAU-Net	AC-MambaSeg	TransNorm	Perspective-UNet	TA-Net	SCUNet++	UNETR
60	ResU-KAN	CPNet-M	CPNet-M	UTNet	SwintUNETR	SwintUNETR	H-vmmnet	Polyp-PVT	UNETR
61	VMUNetV2	ConvFormer	UCTransNet	MSRFNet	UTNet	UCTransNet	CPANet	Zig-RIR	Hiformer
62	RollingUNet	UNetV2	TransUNet	ERDUNet	CPANet	ConvFormer	UTNet	MSLAU-Net	MCA-UNet
63	U-Net	SCUNet++	CPANet	TransUNet	MisFormer	DDANet	GH-UNet	CMUNetXt	CPM-UNet
64	Hiformer	LV-UNet	ResUNet++	MisFormer	TransUNet	TransUNet	UTANet	TinyUNet	CE-Net
65	MDSAU-Net	MeiT	U-Net	MisFormer	SCUNet++	MisFormer	DS-UNet	UNetXt	ULite
66	DDANet	MDSAU-Net	ScritFormer	U-Net++	ResUNet++	Swin-umambaD	U-RWKV	LeViT-UNet	UTNet
67	CPNet-M	ScritFormer	ScritFormer	ResU-KAN	ArtU-Net	U-KAN	U-NetXt	UltraLight-VM-UNet	MUCM-Net
68	MedVkan	MedVkan	Mobile U-ViT	CPNet-M	UNetV2	UNetV2	TinyUNet	DAEFormer	Mobile U-ViT
69	ConvFormer	AC-MambaSeg	FaT-Net	CSWin-UNet	CA-Net	CSWin-UNet	ResUNet++	SwintUNETR	ResU-KAN
70	MALUNet	CMUNetXt	DDANet	U-Net++	ColonSegNet	MUCM-Net	MedFormer	ScritFormer	MSLAU-Net
71	D-TransUNet	UNetXt	UTNet	BEFUnet	CMUNetXt	CMU-Net	ColorSegNet	MBSNet	MeiT
72	MUCM-Net	MUCM-Net	SwintUNETR	DA-TransUNet	ConvFormer	MSRFNet	DCSAU-Net	RollingUNet	MedFormer
73	DCSAU-Net	MSRFNet	DC-UNet	MultiResUNet	DAEFormer	SwintUNETR	U-Net++	GH-UNet	AURA-Net
74	UNet3+	U-RWKV	MedVkan	TinyUNet	ScritFormer	TransNorm	CE-Net	CA-Net	LU-Net
75	UNetXt	CFM-UNet	TinyUNet	U-Net	CPNet-M	TinyUNet	LFU-Net	Hiformer	LGMsNet
76	MSRFNet	MMLNet	CFM-UNet	TransNorm	U-Net++	RollingUNet	MambaNet	BEFUnet	BEFUnet
77	MSRFNet	MALUNet	CFM-UNet	MDSAU-Net	MultiResUNet	DA-TransUNet	BEFUnet	DCSAU-Net	SimpleUNet
78	UNetV2	U-Net	D-TransUNet	UNetV2	MDSAU-Net	DAEFormer	ScritFormer	MDSAU-Net	EVIT-UNet
79	UCTransNet	ArtU-Net	ArtU-Net	ColonSegNet	MT-UNet	DCSAU-Net	ESKNet	ResUNet++	ResUNet++
80	MT-UNet	MT-UNet	UNetXt	CFM-UNet	CFM-UNet	Hiformer	SimpleUNet	U-Net3+	CPANet
81	TinyUNet	Zig-RIR	MUCM-Net	DAEFormer	CSWin-UNet	SCUNet++	SwintUNETR	UNETR	FAT-Net
82	U-RWKV	UNet3+	DoubleUNet	ResUNet++	DC-UNet	ScritFormer	Swin-umambaD	U-Net++	MBSNet
83	BEFUnet	LFU-Net	MultiResUNet	MT-UNet	H-vmmnet	CA-Net	UltraLight-VM-UNet	DDANet	LV-UNet
84	UltraLight-VM-UNet	UCTransNet	MSRFNet	MedVkan	MedVkan	MultiResUNet	MERIT	MultiResUNet	Hiformer
85	CSWin-UNet	D-TransUNet	MALUNet	DC-UNet	LeViT-UNet	UNetXt	MDSAU-Net	MFTUNet	TransAttUNet
86	MeiT	ResUNet++	U-Net++	Zig-RIR	UNetXt	UNetV2	VMUNetV2	ERDUNet	Zig-RIR
87	CFM-UNet	CFFormer	CSWin-UNet	SwintUNETR	Zig-RIR	SimpleUNet	TransFuse	U-RWKV	DoubleUNet
88	MultiResUNet	DC-UNet	MF-UNet	UNetXt	CFM-UNet	DCSAU-Net	Zig-RIR	CPNet-M	MF-UNet
89	DC-UNet	ULite	BEFUnet	ULite	MambaNet	MambaNet	H-vmmnet	MSRFNet	UACANet
90	SwintUNETR	TinyUNet	ULite	UNETR	TinyUNet	ColonSegNet	LeViT-UNet	ColonSegNet	U-RWKV
91	ScritFormer	SwintUNETR	ULite	H-vmmnet	LeViT-UNet	U-RWKV	LFU-Net	ULite	U-Net
92	UNETR	MultiResUNet	UltraLight-VM-UNet	H-vmmnet	ERDUNet	MALUNet	ConvFormer	ResUNet++	MultiResUNet
93	ResUNet++	UltraLight-VM-UNet	LeViT-UNet	U-RWKV	MeiT	UNETR	CFM-UNet	ConvFormer	UTANet
94	LeViT-UNet	BEFUnet	Zig-RIR	MALUNet	UNETR	LeViT-UNet	Polyp-PVT	MedVkan	DDANet
95	Zig-RIR	LFU-Net	SimpleUNet	MALUNet	ResUNet++	ResUNet++	TransAttUNet	ColonSegNet	ColonSegNet
96	ColonSegNet	LFU-Net	SimpleUNet	SimpleUNet	SimpleUNet	DC-UNet	UACANet	RollingUNet	RollingUNet
97	LFU-Net	SimpleUNet	ColonSegNet	MUCM-Net	MUCM-Net	DoubleUNet	PraNet	MedFormer	MSRFNet
98	SimpleUNet	LeViT-UNet	MambaNet	LFU-Net	SwintUNETR	ArtU-Net	CSWin-UNet	DC-UNet	DC-UNet
99	MambaNet	ColonSegNet	VMUNet	UNetXt	SwintUNETR	UltraLight-VM-UNet	SwintUNETR	ArtU-Net	ArtU-Net
100	CMUNetXt	VMUNet	SwintUNETR	UltraLight-VM-UNet	UltraLight-VM-UNet	BEFUnet	MALUNet	EVIT-UNet	ScritFormer

2808
2809
2810
2811
2812
2813
2814
2815
2816
2817
2818
2819
2820
2821
2822
2823
2824
2825
2826
2827
2828
2829
2830
2831
2832
2833
2834
2835
2836
2837
2838
2839
2840
2841
2842
2843
2844
2845
2846
2847
2848
2849
2850
2851
2852
2853
2854
2855
2856
2857
2858
2859
2860
2861

Table 32: Per-dataset target ranking of 100 u-shape medical image segmentation networks with U-Score. Source → Target.

Rank	Source	Ultrasound	Endoscopy	Dermscopy	Fundus	X-Ray	Histopathology		
	BUS1 → BUS	BUSBRA → BUS	TNSCU1 → TUCC	Kvasir → CVC300	Kvasir → CVC-ClinicDB	ISIC2018 → PH2	CHASE → Stare	Montgomery → NIH-test	Mouse → Tabnuclei
1	LGMSNet	LV-UNet	LV-UNet	LV-UNet	LGMSNet	LV-UNet	ULite	CMUNetXt	CMUNetXt
2	LV-UNet	LGMSNet	LGMSNet	MBSNet	MBSNet	LGMSNet	LV-UNet	MUCM-Net	MALUNet
3	MBSNet	SwiatUNETR	MBSNet	CMUNetXt	CMUNetXt	SwiatUNETR	LGMSNet	MDSA-UNet	MDSA-UNet
4	Mobile U-ViT	Mobile U-ViT	CMUNetXt	LGMSNet	MambaUnet	U-RWKV	CMUNetXt	MALUNet	DCSAU-Net
5	U-KAN	MBSNet	U-KAN	MambaUnet	Mobile U-ViT	MBSNet	MUCM-Net	SwiatUNETR	SwiatUNETR
6	SwiatUNETR	UNetXt	U-KAN	Mobile U-ViT	U-KAN	CFPNet-M	CFPNet-M	Mobile U-ViT	U-KAN
7	MALLNet	U-KAN	DCSAU-Net	Tinyunet	VMUNetV2	ULite	UNetXt	SimpleUnet	SimpleUnet
8	MUCM-Net	DCSAU-Net	CFPNet-M	DCSAU-Net	RWKV-UNet	MDSA-UNet	LGMSNet	RWKV-UNet	Tinyunet
9	UNetXt	MUCM-Net	MDSA-UNet	U-KAN	SwiatUNETR	Mobile U-ViT	Tinyunet	Swiat-umambaD	TA-Net
10	CFPNet-M	CFPNet-M	VMUNetV2	CFPNet-M	Swiat-umambaD	MBSNet	ResU-KAN	UNetXt	UNetXt
11	RWKV-UNet	MambaUnet	RWKV-UNet	VMUNetV2	CMUNetXt	SwiatUNETR	U-RWKV	G-CASCADE	G-CASCADE
12	ULite	CMUNetXt	Tinyunet	RWKV-UNet	DCSAU-Net	VMUNetV2	LFU-Net	Tinyunet	RWKV-UNet
13	Swiat-umambaD	U-RWKV	ResU-KAN	DDANet	Polyp-PVT	ResU-KAN	Mobile U-ViT	UNetXt	UNetXt
14	CE-Net	MDSA-UNet	Polyp-PVT	Swiat-umambaD	TA-Net	MUCM-Net	U-KAN	Polyp-PVT	EMCAD
15	Polyp-PVT	VMUNetV2	Mobile U-ViT	TA-Net	G-CASCADE	G-CASCADE	RWKV-UNet	TA-Net	Swiat-umambaD
16	MDSA-UNet	MALUNet	Swiat-umambaD	CE-Net	TA-Net	UNet	DCSAU-Net	VMUNetV2	VMUNetV2
17	TA-Net	RWKV-UNet	G-CASCADE	G-CASCADE	DDANet	CE-Net	ResU-KAN	MambaUnet	MambaUnet
18	G-CASCADE	Polyp-PVT	SwiatUNETR	EMCAD	EMCAD	TA-Net	SimpleUnet	ULite	ULite
19	UNetXt	Swiat-umambaD	TA-Net	TransFuse	CE-Net	TransFuse	DDANet	TransFuse	LeViT-UNet
20	DCSAU-Net	TA-Net	G-CASCADE	MDSA-UNet	CFPNet-M	G-CASCADE	G-CASCADE	CMUNetXt	CMUNetXt
21	EMCAD	G-CASCADE	UNetV2	MultiResUNet	TransResUNet	MEGANet	MEGANet	MambaUnet	TransResUNet
22	TransFuse	CE-Net	UNetXt	Polyp-PVT	MEGANet	Polyp-PVT	ULite	UltraLight-VM-UNet	MEGANet
23	VMUNetV2	ULite	MEGANet	TransResUNet	TransFuse	Tinyunet	EMCAD	MEGANet	MisFormer
24	ResU-KAN	ResU-KAN	TransResUNet	ResU-KAN	UNet	TransResUNet	ERDUnet	HiFormer	VMUNet
25	TransResUNet	EMCAD	TransFuse	UTNet	CASCADE	CASCADE	TA-Net	EMCAD	SwiatUnet
26	MEGANet	HiFormer	HiFormer	MEGANet	MEGANet	DDANet	DDANet	CASCADE	LFU-Net
27	Tinyunet	MEGANet	ERDUnet	CASCADE	MDSA-UNet	MMUNet	CE-Net	UNet	Mobile U-ViT
28	DDANet	TransFuse	HiFormer	UNetV2	HiFormer	ERDUnet	UNetV2	MBSNet	U-Net++
29	CASCADE	UNetV2	EMCAD	ERDUnet	VMUNet	Swiat-umambaD	MisFormer	VMUNet	CASCADE
30	ERDUnet	EMCAD	MedFormer	MedFormer	MedFormer	MedFormer	MedFormer	TransResUNet	TransResUNet
31	MedFormer	CASCADE	MUCM-Net	UNetV2	MedFormer	MedFormer	MedFormer	AC-MambaSeg	LGMSNet
32	VMUNet	MedFormer	CASCADE	VMUNet	MisFormer	VMUNet	MEGANet	MisFormer	MMUNet
33	MMUNet	MisFormer	MisFormer	MMUNet	MMUNet	VMUNet	VMUNet	LeViT-UNet	DFAFormer
34	U-RWKV	HiFormer	MALUNet	MisFormer	AC-MambaSeg	AC-MambaSeg	CASCADE	MMUNet	AC-MambaSeg
35	MisFormer	U-Net++	MisFormer	CSCAU-Net	CSCAU-Net	CSCAU-Net	MMUNet	FAT-Net	ERDUnet
36	AC-MambaSeg	CSCAU-Net	VMUNet	SCUNet++	HiFormer	AC-MambaSeg	AC-MambaSeg	CSCAU-Net	SimpleUnet
37	UNetV2	DAEFormer	MMUNet	BEFUnet	MSLAU-Net	MisFormer	MedFormer	MSLAU-Net	Polyp-PVT
38	HiFormer	DC-UNet	AC-MambaSeg	MSLAU-Net	FAT-Net	MSLAU-Net	Swiat-umambaD	LFU-Net	CE-Net
39	U-Net++	DDANet	AC-MambaSeg	MSLAU-Net	ESKNet	DCSAU-Net	DAEFormer	AURA-Net	UTNet
40	CSCAU-Net	MSLAU-Net	CSCAU-Net	U-Net++	ESKNet++	CSCAU-Net	SCUNet++	ResU-KAN	ResU-KAN
41	H2Former	MMUNet	DAEFormer	H2Former	U-Net++	MedVKAN	SCUNet++	DCSAU-Net	TransFuse
42	MSLAU-Net	FAT-Net	HiFormer	ESKNet	AURA-Net	FAT-Net	U-Net++	MDSA-UNet	MedVKAN
43	SCUNet++	MSLAU-Net	MSLAU-Net	FAT-Net	ESKNet	MDSA-UNet	MDSA-UNet	ESKNet	CSCAU-Net
44	FAT-Net	SCUNet++	MultiResUNet	DC-UNet	RollingUnet	SwiatUnet	H2Former	SwiatUnet	SCUNet++
45	UltraLight-VM-UNet	ESKNet	ESKNet	AURA-Net	BEFUnet	AURA-Net	FAT-Net	Zig-RIR	HiFormer
46	DAEFormer	AURA-Net	CA-Net	RollingUnet	DDANet	DDANet	BEFUnet	DAEFormer	CSWin-UNet
47	ESKNet	MedVKAN	FAT-Net	CA-Net	DC-UNet	CSWin-UNet	MedVKAN	DDANet	CA-Net
48	AURA-Net	RollingUnet	SCUNet++	DAEFormer	CA-Net	DAEFormer	MSLAU-Net	CSWin-UNet	ESKNet
49	MedVKAN	CA-Net	AURA-Net	DDANet	DDANet	SwiatUnet	SwiatUnet	BEFUnet	BEFUnet
50	CA-Net	CSWin-UNet	AURA-Net	CSWin-UNet	Swiat-umamba	SCUNet++	AURA-Net	DoubleUnet	DDANet
51	DDANet	Zig-RIR	MedVKAN	MedVKAN	ColonsSegNet	CA-Net	AURA-Net	HiFormer	DDANet
52	RollingUnet	DDANet	DDANet	DoubleUnet	UNetXt	MedT	VMUNetV2	CFM-UNet	CFM-UNet
53	BEFUnet	DoubleUnet	U-Net++	TransUnet	TransUnet	TransUnet	UNetXt	Swiat-umamba	MBSNet
54	DoubleUnet	MedT	CFM-UNet	MDAGNet	Swiat-umamba	MDAGNet	ESKNet	RollingUnet	LV-UNet
55	Swiat-umamba	CFM-UNet	Swiat-umamba	Zig-RIR	CSWin-UNet	MultiResUNet	DDANet	H-vminet	AURA-Net
56	H-vminet	Swiat-umamba	CFM-UNet	GH-UNet	GH-UNet	GH-UNet	TransFuse	CA-Net	H-vminet
57	GH-UNet	H-vminet	GH-UNet	TransArtUnet	LeViT-UNet	LeViT-UNet	DoubleUnet	MultiResUNet	Swiat-umamba
58	TransArtUnet	MedT	TransArtUnet	ColonsSegNet	RestUnet++	MADGNet	MedT	DDANet	GH-UNet
59	MADGNet	TransArtUnet	RestUnet++	MADGNet	MedVKAN	TransArtUnet	Swiat-umamba	MADGNet	CFM-UNet
60	CENet	GH-UNet	CENet	SwiatUNETR	CENet	UNet	Swiat-umamba	U-Net++	FAT-Net
61	CSWin-UNet	MADGNet	MADGNet	CENet	UNet	CENet	ColonsSegNet	TransUnet	MADGNet
62	TransUnet	CENet	DoubleUnet	ScribFormer	Anti-Net	UNetV2	TransArtUnet	TransUnet	CE-Net
63	Anti-Net	ScribFormer	ScribFormer	Anti-Net	UNetXt	HiFormer	RestUnet++	DA-TransUnet	DA-TransUnet
64	DA-TransUnet	UNet	TransUnet	ResUnet++	ScribFormer	UNet	CENet	DA-TransUnet	MedT
65	Caranet	CPCANet	BEFUnet	UTANet	Caranet	CPCANet	Anti-Net	UNet3+	UNet3+
66	CPCANet	CPCANet	CSWin-UNet	UNet	TransUnet	TransUnet	GH-UNet	CPCANet	CPCANet
67	UTANet	UTANet	Caranet	TransUnet	DA-TransUnet	UNet3+	MADGNet	Caranet	HiFormer
68	UTANet	Caranet	Caranet	Caranet	UTANet	Pranet	UNet	UTANet	TransUnet
69	UNet3+	UNet	DA-TransUnet	UNet3+	Pranet	CA-Net	TransUnet	TransNorm	CMU-Net
70	TransNorm	Anti-Net	UNet3+	CPCANet	CPCANet	EViT-UNet	UNet3+	Pranet	TransNorm
71	Pranet	TransNorm	UTANet	DA-TransUnet	CMU-Net	ScribFormer	DA-TransUnet	ScribFormer	Pranet
72	CMU-Net	Pranet	Anti-Net	UNetXt	TransNorm	CMU-Net	ScribFormer	GH-UNet	Caranet
73	EViT-UNet	CMU-Net	CPCANet	Pranet	H-vminet	DA-TransUnet	CPCANet	CMU-Net	ResUnet++
74	CFM-UNet	UNet3+	TransNorm	CPCANet	MSRFNet	TransNorm	UTANet	ERDUnet	FCBFormer
75	MedT	EViT-UNet	Pranet	EViT-UNet	EViT-UNet	MSRFNet	TransNorm	UNet3+	UNet3+
76	MultiResUNet	RestUnet++	CMU-Net	TransNorm	FCBFormer	UCTransNet	CMU-Net	UCTransNet	UCTransNet
77	FCBFormer	MSRFNet	EViT-UNet	MSRFNet	UCTransNet	D-TraITUnet	EViT-UNet	FCBFormer	D-TraITUnet
78	MSRFNet	FCBFormer	FCBFormer	UCTransNet	D-TraITUnet	FCBFormer	MSRFNet	D-TraITUnet	EViT-UNet
79	UCTransNet	MCA-UNet	UCTransNet	FCBFormer	MCA-UNet	FCBFormer	UCTransNet	CPCANet	CPCANet
80	MCA-UNet	UCTransNet	MCA-UNet	D-TraITUnet	UCANet	SimpleUnet	UCTransNet	MCA-UNet	MCA-UNet
81	D-TraITUnet	UCANet	MSRFNet	MCA-UNet	MERIT	UCANet	D-TraITUnet	U-RWKV	ConvFormer
82	UCANet	Perspective-UNet	D-TraITUnet	UCANet	MERIT	MCA-UNet	MCA-UNet	UCANet	TransArtUnet
83	Perspective-UNet	MERIT	Perspective-UNet	MERIT	Perspective-UNet	Zig-RIR	Perspective-UNet	Perspective-UNet	Perspective-UNet
84	Perspective-UNet	ConvFormer	UCANet	ConvFormer	ConvFormer	ConvFormer	MERIT	MERIT	DS-TransUnet
85	ConvFormer	D-TraITUnet	ConvFormer	Perspective-UNet	DS-TransUnet	DS-TransUnet	DS-TransUnet	CFPNet-M	CFPNet-M
86	DS-TransUnet	DS-TransUnet	Perspective-UNet	Perspective-UNet	ULite	CFFormer	DS-TransUnet	DS-TransUnet	U-RWKV
87	CFFormer	ULite	DS-TransUnet	ULite	DS-TransUnet	LFU-Net	CFFormer	CFFormer	Zig-RIR
88	LFU-Net	DS-TransUnet	DS-TransUnet	ULite	CFFormer	SimpleUnet	ULite	ULite	MultiResUNet
89	SimpleUnet	DS-TransUnet	DS-TransUnet	CFFormer	SimpleUnet	SimpleUnet	UltraLight-VM-UNet	MambaUnet	MambaUnet
90	CMUNetXt	Tinyunet	LFU-Net	SimpleUnet	Tinyunet	ULite	MultiResUNet	DC-UNet	DC-UNet
91	MambaUnet	UltraLight-VM-UNet	SimpleUnet	MALUNet	MALUNet	MambaUnet	Polyp-PVT	MedFormer	RollingUnet
92	LeViT-UNet	MultiResUNet	UltraLight-VM-UNet	MUCM-Net	MUCM-Net	MambaUnet	DDANet	MedVKAN	DoubleUnet
93	DC-UNet	MT-UNet	MambaUnet	UltraLight-VM-UNet	UltraLight-VM-UNet	LeViT-UNet	LeViT-UNet	ColonsSegNet	ColonsSegNet
94	MT-UNet	LeViT-UNet	LeViT-UNet	U-RWKV	U-RWKV	DC-UNet	H-vminet	MT-UNet	ScribFormer
95	SwiatUnet	SwiatUnet	LeViT-UNet	LeViT-UNet	LeViT-UNet	MT-UNet	ColonsSegNet	U-Net	U-Net
96	Zig-RIR	VMUNet	Zig-RIR	MT-UNet	ERDUnet	DoubleUnet	CFM-UNet	ResUnet++	Anti-Net
97	ColonsSegNet	SwiatUnet	MT-UNet	SwiatUnet	SwiatUnet	ColonsSegNet	Caranet	TransArtUnet	UTANet
98	ResUnet++	CFFormer	ColonsSegNet	MoT	CFM-UNet	ResUnet++	Pranet	MSRFNet	MSRFNet
99	UNETR	ColonsSegNet	ColonsSegNet	H-vminet	MoT	ResUnet++	UCANet	EViT-UNet	UCANet
100	ScribFormer	UNETR	UNETR	UNETR	UNETR	Anti-Net	ConvFormer	ConvFormer	MT-UNet



2914 Figure 15: Segmentation results of the Top 5 models and U-Net, where the green curve represents
 2915 the ground truth and the yellow curve represents the model prediction.

2916
 2917
 2918
 2919
 2920
 2921
 2922
 2923
 2924
 2925
 2926
 2927
 2928
 2929
 2930
 2931
 2932
 2933
 2934
 2935
 2936
 2937
 2938
 2939
 2940
 2941
 2942
 2943
 2944
 2945
 2946
 2947
 2948
 2949
 2950
 2951
 2952
 2953
 2954
 2955
 2956
 2957
 2958
 2959
 2960
 2961
 2962
 2963
 2964
 2965
 2966
 2967
 2968
 2969

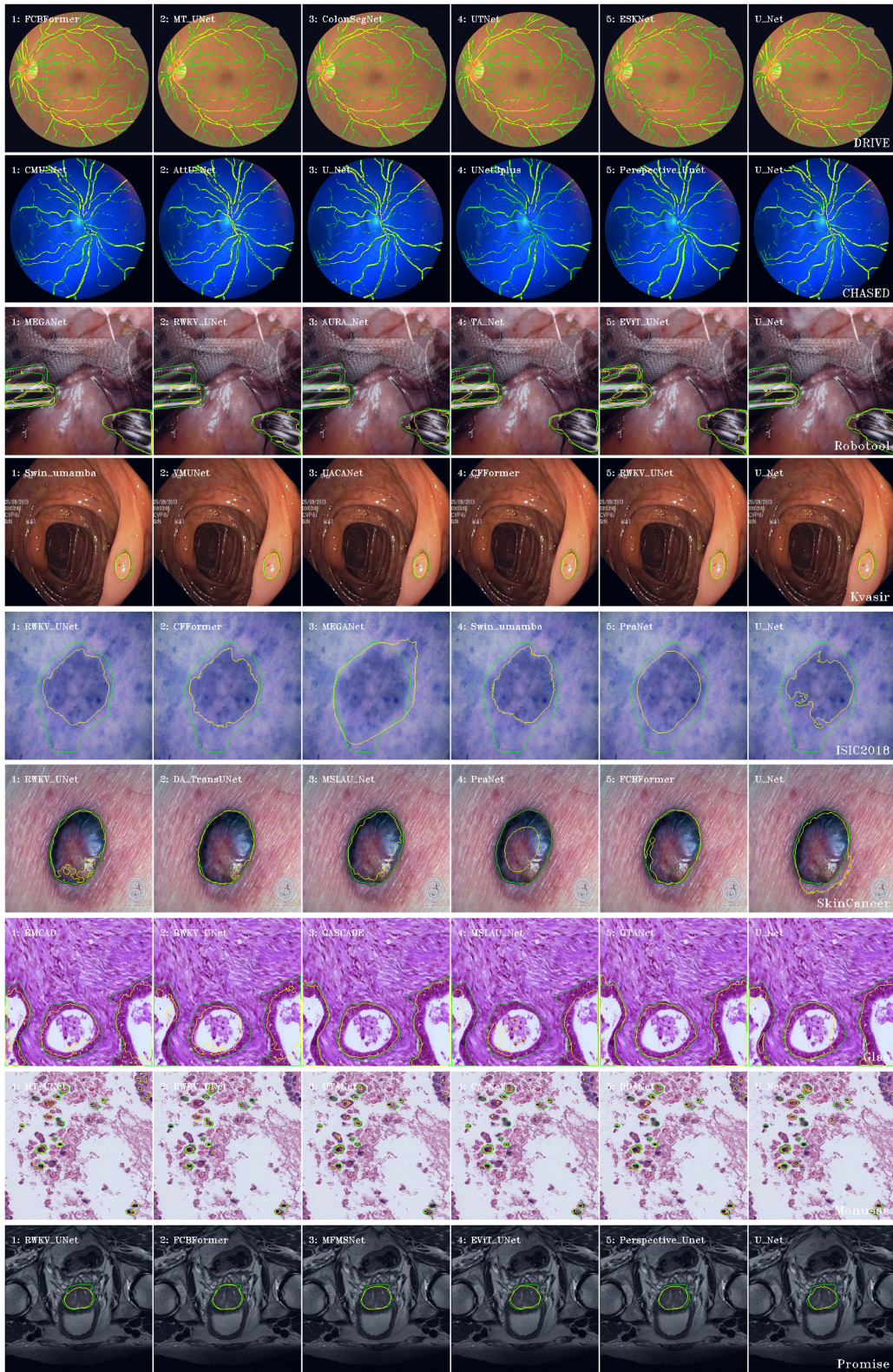


Figure 16: Segmentation results of the Top 5 models and U-Net, where the green curve represents the ground truth and the yellow curve represents the model prediction.